Title: Antibiotics of the future are prone to resistance in Gram-negative pathogens

Authors: Lejla Daruka[1,2]†, Márton Simon Czikkely[1,3]†, Petra Szili[1,3]†, Zoltán Farkas[1]†, Dávid Balogh[1], Elvin Maharramov[1,2], Thu-Hien Vu[1], Levente Sipos[1], Botond Dávid Vincze[1], Gábor Grézal[1,4], Szilvia Juhász[1], Anett Dunai[1], Andreea Daraba[1], Mónika Számel[1], Tóbiás Sári[1,2], Tamás Stirling[1,2], Bálint Márk Vásárhelyi[1], Eszter Ari[4,1,5], Chryso Christodoulou[1], Máté Manczinger[1,6,7], Márton Zsolt Enyedi[8], Gábor Jaksa[9], Stineke van Houte[10], Elizabeth Pursey[10], Csaba Gergő Papp[11,12], Zóra Szilovics[11,12,2], Lajos Pintér[9], Lajos Haracska[13], Attila Gácser[11,12], Bálint Kintses[1,14,15]*, Balázs Papp[1,4,16]* & Csaba Pál[1]*

Affiliations:

[1]Synthetic and Systems Biology Unit, Institute of Biochemistry, Biological Research Centre, National Laboratory of Biotechnology, Eötvös Loránd Research Network (ELKH); Szeged, HU-6726, Hungary
[2]Doctoral School of Biology, University of Szeged; Szeged, HU-6726, Hungary
[3]Doctoral School of Multidisciplinary Medical Sciences, University of Szeged; Szeged, HU-6722, Hungary
[4]HCEMM-BRC Metabolic Systems Biology Lab; Szeged, HU-6726, Hungary
[5]Department of Genetics, ELTE Eötvös Loránd University; Budapest, HU- 1117, Hungary
[6]HCEMM-BRC Systems Immunology Research Group; Szeged, HU-6726, Hungary
[7]Department of Dermatology and Allergology, University of Szeged; Szeged, HU-6722, Hungary
[8]Single Cell Omics Advanced Core Facility, Hungarian Centre of Excellence for Molecular Medicine; Szeged, HU-6728, Hungary
[9]Delta Bio 2000 Ltd.; Szeged, HU-6726, Hungary
[10]Environment and Sustainability Institute & Centre for Ecology and Conservation, Biosciences, University of Exeter; Penryn, TR10 9FE, Cornwall, United Kingdom
[11]HCEMM-USZ Fungal Pathogens Research Group, Department of Microbiology, University of Szeged; Szeged, HU-6726, Hungary
[12]ELKH-USZ Fungal Pathomechanisms Research Group, Faculty of Science and Informatics, University of Szeged; Szeged, HU-6726, Hungary
[13]Mutagenesis and Carcinogenesis Research Group, Institute of Genetics, Biological Research Centre, Eötvös Loránd Research Network (ELKH); Szeged, HU-6726, Hungary
[14]HCEMM-BRC Translational Microbiology Research Group; Szeged, HU-6726, Hungary
[15]Department of Biochemistry and Molecular Biology, Faculty of Science and Informatics, University of Szeged; Szeged, HU-6726, Hungary
[16]National Laboratory for Health Security, Biological Research Centre, Eötvös Loránd Research Network; Szeged, HU-6726, Hungary
† These authors contributed equally.
* Corresponding authors. Email: kintses.balint@brc.hu, pappb@brc.hu & cpal@brc.hu

Abstract: Despite the ongoing development of new antibiotics, the future evolution of bacterial resistance may render them ineffective. We demonstrate that antibiotic candidates currently under development are as prone to resistance evolution in Gram-negative pathogens as clinically employed antibiotics. Resistance generally stems from both genomic mutations and the transfer of antibiotic resistance genes from microbiomes associated with humans, both factors carrying equal significance. The molecular mechanisms of resistance overlap with those found in commonly used antibiotics. Therefore, these mechanisms are already prevalent in natural populations of pathogens, indicating that resistance can rapidly emerge through selection of pre-existing bacterial variants. Additionally, resistance to new peptide-based antibiotics enhances bacterial virulence, raising concerns. However, certain combinations of antibiotics and bacterial strains are less prone to developing resistance, emphasizing the potential of narrow-spectrum antibacterial therapies that could remain effective. Our comprehensive framework allows for predicting future health risks associated with bacterial resistance to new antibiotics.

Main Text:

Multi-drug resistant bacterial infections have been recognized as a major public health concern, and are responsible for a significant proportion of deaths worldwide[1]. Alarmingly, the O'Neill report[2] estimated that the mortality of drug-resistant bacterial infections might exceed that of malignant tumors by 2050, unless the current trends are reversed. Paradoxically, however, many pharmaceutical companies have discontinued their antibiotic research programs[3]. This is partly due to the rapid spread of multi-drug resistant bacteria, which makes the commercial success of new antimicrobial drugs unpredictable[4,5].

The danger of wasting considerable time, effort, and funding on antibiotic candidates prone to resistance deter companies from developing new antibiotics. Of many examples, GlaxoSmithKline (GSK) spent 15 million USD to acquire the GSK2251052 molecule and invested considerable further money in its development. However, the project was later cancelled due to the rapid emergence of resistance against GSK2251052[6]. Antibiotics launched to the market can also lose utility and revenues in only a few years due to fast emerging resistance. A recent example is dalbavancin, one of the few treatments available to patients infected with methicillin-resistant *S. aureus* (MRSA)[7,8]. Approximately 10 years of research and funding was jeopardised, as resistance emerged after merely two years of commercialization.

Therefore, it is imperative to predict the possible evolutionary routes toward resistance, especially at an early stage of antibacterial drug discovery. However, identification of antibacterial compounds with limited resistance is a complex problem for three main reasons: i) the variety of molecular mechanisms contributing to antimicrobial resistance, ii) the numerous pathogenic bacteria to be considered, and iii) the number of potential antibacterial compounds to be tested. Specifically, bacteria can acquire resistance through diverse genetic mechanisms, including point mutations, amplification of genomic segments, and horizontal transfer of resistance genes[9].
Based on the 2021 WHO pipeline report[10] and recent reviews on the subject[11–13], we selected new antimicrobial compounds which have been introduced into clinical practice recently (after 2017) or are currently in development (i.e., 'recent' antibiotics, see Table 1). The selected compounds are generally small molecules, directly target Gram-negative bacteria, and are planned to be employed as monotherapies, mostly as intravenous or oral applications, but prior knowledge on de novo emergence of resistance is limited (Supplementary Table 4, for selection criteria, see Supplementary Table 1, and Supplementary Note). Our study includes four new antibacterial compounds that permeabilize the bacterial outer membrane (Supplementary Fig. 1), although their exact modes of action differ (Supplementary Note). Our main goal was to compare the resistance profiles of these 'recent' antibiotics to clinically employed antibiotics (i.e., 'control'). The 'control' antibiotics belong to distinct major classes of antibiotics, and all of them have been in clinical usage for many years (Supplementary Table 1). To systematically characterize the bacterial capacity for resistance and the underlying molecular mechanisms, we combined laboratory evolution, functional metagenomic screens, and targeted mutagenesis. To explore potential clinical relevance of our findings, we examined whether the identified resistance mutations and antibiotic resistance genes can be found in natural bacterial isolates and in human associated microbiomes (Fig. 1). Finally, by focusing on peptide-based antibiotics, we examined the side-effects of resistance on bacterial virulence.

Results

Overlap in naturally occurring resistance between control and recent antibiotics

We first selected 40 representative strains from four Gram-negative bacterial pathogens, including *Escherichia coli*, *Klebsiella pneumoniae*, *Acinetobacter baumannii* and *Pseudomonas aeruginosa* (Supplementary Table 2), and measured their susceptibilities to 22 'control' and 13 'recent' antibiotics (Supplementary Table 3). Several strains with clinical origins were confirmed to be extensively drug resistant (XDR), as the MICs of nearly all clinically recommended antibiotics were above the established clinical breakpoints (Supplementary Fig. 2, Supplementary Fig. 3, Supplementary Fig. 4). On this panel of bacterial strains, only cefiderocol and eravacycline displayed a substantially expanded spectrum of antibacterial activities compared to the respective control antibiotics with similar modes of action (Fig. 2A). Indeed, hierarchical clustering based on the heatmap of antibiotic susceptibility profiles have revealed that 'control' and 'recent' antibiotics with related modes of action cluster together (Fig. 2B). Moreover, bacterial strains resistant to multiple 'control' antibiotics tend to be resistant to 'recent' antibiotics as well (Fig. 2C). Together, these results indicate an overlap in resistance mechanisms between the two antibiotic groups.

Rapid species-specific evolution of resistance in the laboratory

Next, we asked whether resistance can readily evolve in bacterial pathogens, rendering these compounds less effective in the long-term. Prior laboratory evolution studies generally focused on only a single species, and frequently on non-pathogens. Here we selected one MDR and one sensitive strain of *E. coli*, *K. pneumoniae*, *A. baumannii* and *P. aeruginosa*, respectively (Supplementary Table 2). 32% of all antibiotic-strain combinations were excluded from the analysis due to high initial resistance level (i.e., MIC > 4 μg/ml) (Supplementary Table 3).

To explore first-step resistance, we used a standard protocol for spontaneous frequency-of-resistance analysis (FoR assay)[14–17] at multiple concentrations of each antibiotic. Approximately 10^{10} bacterial cells were exposed to one of each antibiotic on agar plates for two days at concentrations where the given strain is susceptible (Supplementary Table 3). Mutants with decreased antibiotic susceptibility were detected in 49.8% of the populations (i.e. at least four-fold MIC-fold change). Although clinical breakpoint is generally unknown, recommended intravenous usage is available for most of the studied 'recent' antibiotics. Therefore, data on the highest available peak plasma concentration of the drug (measured at intravenous administration) were used as a proxy to estimate potential clinical relevance of the MIC changes in the mutants (Supplementary Table 1). In spite of the short time-scale of the screens, the MICs were either equal to or above the peak plasma concentration in as high as 18.7% of the mutant lines (Fig. 3A and Supplementary Table 5).

The above data demonstrates that clinically relevant resistance to 'recent' antibiotics frequently arises in a matter of days. However, the underlying FoR assays cannot detect very rare mutations and combinations thereof[18], and hence underestimate bacterial potential for resistance. Using the same set of eight starting strain (Supplementary Table 2), we next initiated adaptive laboratory evolution with the aim to maximize the level of antibiotic resistance in the populations achieved during a longer, but fixed time period (for up to ~120 generations, see methods). 10 parallel evolving populations were exposed to increasing concentrations of one of each 'recent' or 'control'

antibiotics. The level of resistance was estimated by comparing the MICs of the evolved lines and the corresponding ancestor strains (Fig. 3B).

In general, the evolution of resistance was a rapid process (Supplementary Table 5); the median antibiotic resistance level in the evolved lines was ~64 times higher compared to the ancestor. The MIC levels were either equal to or above the peak plasma concentration in 87% of all studied populations, indicating their potential clinical relevance. On average, 'recent' and 'control' antibiotics were equally prone to bacterial resistance (Supplementary Fig. 5, paired T-test, P = 0.37). Alarmingly, high levels of resistance readily emerged against 'recent' antibiotics with potent antibacterial activities against a wide-range of MDR and XDR clinical isolates (Supplementary Fig 6).

However, there was a large heterogeneity in the relative level of resistance (i.e., MIC fold-change) across antibiotic-strain combinations, spanning a 65 000-fold range between the observed minimum and maximum values (Fig. 3C). Using multiple linear regression, we examined the global impact of these two features (antibiotic and the strain's genetic background) on the resistance level reached while also accounting for the resistance level of the ancestor (Fig. 3D). Additively, the antibiotic and the genetic background explain ~39% of the variation. Importantly, a model that allows an interaction term between genetic background and antibiotic combination explains an additional ~31% of variation in final resistance (Fig. 3D). Together, these results indicate that the initial genetic make-up of the bacterial population has a large impact on resistance evolution, mainly in an antibiotic specific manner. Supplementary Fig 7 shows examples on antibiotics with especially high variation in the capacity to evolve resistance across bacterial species.

Overlap in mutational profiles across antibiotic treatments

To identify mutational events underlying resistance, resistant lines derived from laboratory evolution (n=332) and frequency-of-resistance (n=135) assays were subjected to whole-genome sequencing (Supplementary Table 6). We implemented an established computational pipeline to identify mutations relative to the corresponding ancestral genomes. 10 evolved lines accumulated exceptionally large numbers of mutations, many of which are likely to be functionally irrelevant (Supplementary Fig. 8). These lines exert elevated genomic mutation rates due to mutations in methyl-directed mismatch repair (*mutS*, *mutL* or *mutY*). Indeed, such mutator bacteria frequently arise in response to antibiotic stress in clinical and laboratory settings[19]. For the remaining 457 lines, we identified 1664 unique mutational events, including 1103 single nucleotide polymorphisms (SNPs) and 561 insertions or deletions (indels) (Supplementary Fig. 9). We found a significant excess of non-synonymous over synonymous mutations, indicating that the accumulation of the SNPs in protein-coding regions was largely driven by selection towards increased resistance (Supplementary Fig 10). 19.6% of the observed mutations generated in-frame stop codons or frameshifts or disruption of the start codon, which were most likely to yield result loss-of protein function (Supplementary Fig 11). This result is consistent with prior studies on the role of inactivating mutations in antibiotic resistance[20]. In total, 578 mutated protein coding genes were detected, of which 174 mutated in at least two independently evolved lines per species (Supplementary Table 7). Remarkably, 66% of all parallel mutated genes carried mutation in lines adapted to different antibiotics (Supplementary Table 7). These results indicate that despite substantial differences in antibiotic treatments, there is a significant overlap in the set of mutated

genes (Fig. 4A, Fig. 4B, Supplementary Table 7). This pattern was far from being random; the overlap was especially high when antibiotics with related modes of action were considered (Wilcoxon two-sample test, $P < 0.0005$). Additionally, many of the genes detected in multiple antibiotic screens are involved in multidrug resistance (for examples, see Supplementary Table 8).

Resistance mutations are prevalent in nature

The above results indicate an overlap in the molecular mechanisms of resistance between clinically employed antibiotics and new antibiotic candidates (Fig. 4A, Fig. 4B). Therefore, we hypothesized that the laboratory observed mutations may be already present in environmental and clinical bacterial isolates, indicating their potential clinical relevance.

To investigate this hypothesis, we analysed the prevalence of the observed mutations from laboratory evolved *E. coli* and *A. baumannii* lines in a catalogue of genomes derived from natural isolates of *E. coli* (n=20,786) and *A. baumannii* (n=15,431) (Fig. 4C). For simplicity, the analysis focused on non-synonymous mutations in protein coding sequences, and estimated their frequencies in the genomes of environmental isolates in these two species. In case of *E. coli*, as high as 30.5% of the 220 laboratory observed non-synonymous mutations were identified in at least one of the investigated genomes, while the same figure is 28% of 207 mutations for *A. baumannii*. While the majority of the mutations found in *E. coli* were found to be relatively rare (i.e., typically found in less than 1% of the isolates, Supplementary Table 9), they were specifically enriched among pathogenic isolates than in other natural isolates (Fisher's test, $P < 2.2\times10^{-16}$, odds ratio = 3.16). Several adaptive mutations were equal or even more abundant than canonical antibiotic resistance mutations in clinical isolates (Supplementary Fig 12).

To explore cross-resistance explicitly, we performed deep-scanning mutagenesis in the target genes of moxifloxacin, an established topoisomerase inhibitor. The quinolone resistance-determining regions (QRDR)[21] of the gyrA and parC genes were subjected to a single round of mutagenesis using DIvERGE[22] in *E. coli* and *K. pneumoniae*. The mutant libraries were subsequently exposed to moxifloxacin stress, resulting in an up to 128-fold increment in resistance levels (Supplementary Fig. 13). 20 mutant clones for each species were isolated; the moxifloxacin MIC level reached or was above the clinical breakpoint (0.25 μg/ml) in all cases. Targeted sequencing of QRDR revealed 1 to 3 mutations per clone. In total, 33 different combinations of mutations involving 44 distinct mutations were found (Supplementary Table 10). Moxifloxacin resistance-conferring mutation combinations reduced susceptibility to topoisomerase inhibitors under clinical development, including delafloxacin and gepotidacin (Supplementary Fig. 13 and Supplementary Table 10). Remarkably, 52% of the 44 mutations have been previously implicated in resistance to topoisomerase inhibitors or are present in the genomes of environmental *E. coli* isolates (Supplementary Fig. 14). Furthermore, natural strains carry some of the specific mutational combinations identified by DIvERGE (Supplementary Fig. 14).

Mobile resistance genes are diverse and present in human-related environments

Laboratory evolution can identify resistance mutations only, and thus it ignores the impact of horizontally transferable resistance mechanisms. Therefore, we next explored the abundance of mobile antibiotic resistance genes from environmental and clinical resistomes. We previously created metagenomic libraries from (i) river sediment and soil samples at 7 antibiotic polluted

industrial sites in the close vicinity of antibiotic production plants in India (that is, anthropogenic soil microbiome), (ii) the stool samples of 10 European individuals who had not taken any antibiotics for at least one year before sample donation (that is, gut microbiome), and (iii) samples from a pool of 68 multi-drug resistant bacteria isolated in healthcare facilities or obtained from strain collections (that is, clinical microbiome)[23] (Supplementary Table 11). Each library contained up to 5 million DNA fragments (contigs), corresponding to a total coverage of 25 Gb (i.e., the size of ~5,000 bacterial genomes). Established functional metagenomic protocols was used to detect small DNA fragments in these libraries (~1.7 KB long on average) that confer resistance in intrinsically susceptible clinical *E. coli* and *K. pneumoniae* strains[23].
690 independent DNA fragments emerged against the tested 'recent' and 'control' antibiotics, resulting in an up to 256-fold increment in resistance level of the bacterial hosts (Supplementary Table 12, Supplementary Fig. 15). The overall numbers of contigs are statistically the same for the two antibiotic groups (paired T-test, $t = -1.3286$, $df = 12$, $P = 0.2$, Fig. 5A). However, no resistance conferring DNA fragment was detected to tridecaptin M152-P3 in any of the metagenomic libraries and host species (Fig. 5A). Alarmingly, the clinical microbiome was an especially rich source of antibiotic resistance conferring DNA segments (Fig. 5A).

The screens also revealed an overlap in the set of resistance conferring DNA fragments across 'recent' and 'control' antibiotics (Fig. 5B). This pattern holds for antibiotic pairs with different modes of action, such as topoisomerase inhibitors and tetracyclines. For example, 136 resistance contigs were detected overall against moxifloxacin, a clinically employed topoisomerase inhibitor and omadacycline, a new tetracycline antibiotic, and as high as 50% of those contigs overlap between the two antibiotics.

In total, 642 non-redundant open reading frames (ORFs) were detected, many of which were present in multiple DNA fragments (Supplementary Table 12). 77% of the 690 DNA fragments displayed close sequence similarity to known resistance genes (i.e., ARG) in relevant databases (Supplementary Table 12). These ARGs are involved in antibiotic inactivation, antibiotic efflux or protect the antibiotic targets (Supplementary Fig. 18), and their phylogenetic origin is diverse (Supplementary Fig. 17). Notably, many of them encode transcription factors involved in the regulation of efflux pumps and membrane stress (Supplementary Fig. 18, Supplementary Table 12). For example, the gene RamA was detected in multiple screens; it is a transcriptional activator found in *Enterobacter aerogenes* and *K. pneumoniae*, but not in *E. coli*. The introduction of RamA induces an MDR phenotype in drug-susceptible *E. coli* through elevating the activity of the *acrAB* efflux pumps and decreasing porin production[24].

Next, we evaluated whether the detected putative ARGs could pose threats to public health by considering gene mobility and presence in bacteria isolated from human hosts. We first asked whether they have recently been subjected to horizontal gene transfer (HGT) in nature. For this purpose, we used a previously generated catalogue based on pairwise alignment of 2794 genomes of phylogenetically diverse human-related bacterial species. The aim was to identify genes with near perfect sequence identity shared by distantly related bacterial genomes. This dataset was extended with putative ARGs present on natural plasmids derived from diverse environments[23]. Using the above two criteria, 20.7% of the putative ARGs were found to be carried by plasmids or have been subjected to recent horizontal gene transfer events (Fig. 5A; Supplementary Table 12).

We also studied the phylogenetic and ecological distribution of the putative ARGs across *E. coli* natural isolates, which occupy a wide range of ecological niches, and display highly variable genomic contents[25]. Specifically, we used genomic data on 16,000 *E. coli* strains that have been categorized into three habitats of isolation (agriculture, human or wild animals hosts) and 11 phylogenetic groups[26]. Overall, 48 putative ARGs have close homologs in the studied E. coli genomes (Supplementary Table 12). These genes are generally present in less than 10% of the investigated genomes, suggesting that they are part of a mobile subset of the *E. coli* pangenome (Supplementary Fig. 19). Additionally, they are detectable in the genomes of bacteria isolated from multiple habitats (Fig. 5C). Notably, natural *E. coli* genomes with at least one putative ARG against certain 'recent' antibiotics (such as cefiderocol, ceftobiprole and omadacycline) are frequent in all three main habitats considered (Fig. 5D, Supplementary Fig. 20). These patterns are not due to exceptionally successful colonisation of particular clones, as these putative ARGs are present in *E. coli* genomes belonging to multiple phylogroups (Supplementary Fig. 21) and were isolated from diverse geographical locations (Supplementary Fig. 22).

Resistance to peptide-based antibiotics enhances bacterial virulence

Numerous factors influence the rise and maintenance of antibiotic resistance in natural bacterial populations. So far, our analysis focused on two main factors: the rate at which resistance genes and mutations arise and the level of resistance conferred by these genetic changes. Another factor to be considered is how resistance shapes bacterial fitness and virulence. Here we mainly focus on two peptide-based antibiotic candidates SPR206 and POL7306); therapeutic use of such peptide-based antibiotics is a major concern[27,28], as it may simultaneously select for mutants with enhanced virulence. Accordingly, we studied representative *K. pneumoniae* lines all of which were adapted to SPR206 or POL7306, respectively, and displayed cross-resistance to other peptide-based antibiotics, including the last-resort antibiotic colistin (Supplementary Fig. 23, Supplementary Table 13). Of note, SPR206-resistant lines bear only a minor fitness cost *in vitro* (Supplementary Fig. 24, Supplementary Table 13), and display invasive disease phenotype in mice (Supplementary Fig. 25, Supplementary Table 13).

The impact of SPR206 and POL7306 resistance on virulence was investigated in a greater wax moth larva model (*Galleria mellonella*). The employed infection model is rapidly gaining popularity for testing bacterial infectivity due to the great reproducibility of test results[29]. Crucially, the tested mutants showed significantly increased killing of larvae as compared to the corresponding ancestral strain (Fig. 6A, Supplementary Fig. 26, Supplementary Fig. 27, Supplementary Table 13). Additionally, infection with SPR206 resistant lines frequently led to SPR206 treatment failure (Fig. 6B, Supplementary Table 13). These results indicate that elevated virulence can evolve as a side-effect of selection for resistance against peptide-based antibiotics.

Although *K. pneumoniae* is generally considered to be an extracellular pathogen, internalisation of clinical isolates into epithelial cells in the human gut have been described[30]. Indeed, *K. pneumoniae* infections frequently originate from the gastrointestinal reservoir by penetrating the intestinal barrier[31]. Internalisation of antibiotic sensitive and SPR206-resistant *K. pneumoniae* lines was studied here in a Caco-2 cells, a model system of the intestinal epithelial barrier. Standard gentamicin-based invasion assays showed that SPR206-resistant lines invaded Caco-2 cells far more efficiently than the corresponding ancestor (Fig. 6C). In particular, the number of intracellular bacteria was markedly increased in populations of SPR206-resistant lines (Fig. 6D).

Moreover, primocin-based clonogenic survival assays showed that the SPR206-resistant lines caused enhanced cytotoxicity in these human cells (Fig. 6E).

Mechanistic understanding of the above patterns requires future in-depth molecular analysis. However, we note that laboratory evolved SPR206 resistance was driven by mutations in the BasS/BasR two-component system (Supplementary Fig. 28): several mutations in this system detected in the laboratory are already present in natural *E. coli* isolates (Supplementary Fig. 29). Remarkably, the BasS/BasR system shapes resistance to cationic peptides by controlling the production of positively charged lipopolysaccharide molecules of the outer bacterial membrane[32]. Additionally, these genes play a central role in bacterial virulence in mice, and are necessary for bacterial invasion of macrophages[33].

Discussion

Our work showed that bacterial resistance generally evolves rapidly against new antibacterial compounds in the laboratory, frequently in a matter of days. The non-synonymous mutations that accumulated during the course of laboratory evolution could be clinically relevant, as they were overrepresented in the genomes of clinical bacterial isolates. These results predict that resistance to new antibiotics will arise through selection for pre-existing resistant strains in genetically heterogenous populations, in addition to *de novo* mutations. Additionally, functional metagenomics have revealed a range of ARGs in the environment that could provide resistance to new antibacterial compounds when transferred into susceptible bacterial hosts. Many of these ARGs could be potential future health risks, for three reasons. First, the clinical microbiome was an especially rich source of antibiotic resistance conferring DNA segments. Second, the ARGs have been subjected to horizontal gene transfer or are carried by plasmids. Third, several ARGs are already present in the genomes of *E. coli* strains isolated from diverse habitats, including human, wild-animals and agriculture. These patterns generally hold for compounds that have novel or dual modes of action and have been previously suggested to be relatively immune to bacterial resistance in the laboratory. These results raise the question why the resistance genes and mutations to antibiotic candidates which have not reached the market yet are already present in the environment.

One possibility is that due to overlap in resistance mechanisms, prolonged antibiotic exposure in clinics and in agriculture have selected for resistance mechanisms that simultaneously reduce susceptibility to antibacterial compounds still in development. Several lines of evidence support this scenario. First, there is a strong positive correlation between the frequency of resistance to new antibacterial compounds and that of established antibiotics across pathogenic isolates. Second, several genes mutated repeatedly across different antibiotic treatments in the evolved lines. Third, metagenomics screens revealed an overlap in the set of resistance conferring DNA fragments between new antibacterial compounds and clinically employed antibiotics. This pattern also holds for antibiotic pairs with different modes of action, such as topoisomerase inhibitors and tetracyclines. Finally, deep-scanning mutagenesis established specific mutational combinations that provide cross-resistance between established and novel topoisomerase inhibitors.

Ideal antibiotic candidates with limited susceptibility to resistance should fulfil multiple criteria: i) resistance by genomic mutations should provide only a limited resistance level, ii) mobile antibiotic resistance genes should be rare, and iii) the associated resistance mechanisms should not

be prevalent in human associated microbiomes and bacterial pathogens. Unfortunately, none of the compounds studied in this work fulfil all these criteria simultaneously (Fig 7). Some relevant examples are highlighted below.

Tridecaptin M152-P3 (TRD) is a non-ribosomally synthesised lipopeptide antibiotic candidate that binds Lipid II and it thereby causes disruption of the bacterial membrane potential[34]. The essential bacterial membrane-anchored cell-wall precursor Lipid II has been considered a promising target for antibiotics with limited resistance[35]. Indeed, no resistance conferring DNA fragment was detected to tridecaptin M152-P3 in any of the metagenomic libraries and host species (Fig. 7). However, tridecaptin M152-P3 was particularly prone to resistance by genomic mutations: up to 128-fold increments in resistance levels were detected in laboratory evolved lines. These lines carry mutations which are also detectable in natural *E. coli* isolates (Fig 4C).

Eravacycline (ERA) was specifically designed to overcome resistance to common tetracycline-specific efflux and ribosomal protection mechanisms[36]. Although eravacycline has a relatively broad antimicrobial spectrum, resistance to this compound evolves rapidly in the laboratory through modification or the regulation or activity of efflux pumps (Fig 3A, 3B, Supplementary Table 6, Supplementary Table 8). Similarly, sulopenem (SUO) is a broad-spectrum thiopenem β-lactam antibiotic that is being developed for the treatment of infections caused by multidrug-resistant and cephalosporin-resistant bacteria belonging to the *Enterobacteriales* group[37]. However, it was prone to resistance in multiple screens. In particular, functional metagenomics identified several DNA fragments carrying New-Delhi-metallo (NDM)- β-lactamase genes (Supplementary Table 8, Supplementary Table 12).

Resistance to new peptide-based antibiotics (e.g., SPR206) readily emerged by genomic mutations. SPR206 is in clinical trials with potent activity against a wide-range of multidrug resistant bacteria[38]. However, an increase in resistance level as high as 128-fold emerged in *K. pneumoniae* as a result of single mutations in the two-component BasS/BasR regulatory system. Even more worryingly, SPR206 resistant *K. pneumoniae* mutants displayed elevated virulence in an invertebrate bacterial infection assay and in human cell culture invasion models. These results suggest that elevated virulence may evolve as a side-effect of selection for resistance against peptide-based antibiotics in clinical development[28,39].

Our work highlights the concern that antibiotic selection is currently dependent solely on susceptibility indicators in various bacterial pathogens. Future application of the same antibiotic to initially susceptible pathogens can have different outcomes depending on their capacity to evolve resistance[40,41]. Indeed, we have found that the level of resistance achieved during adaptive laboratory evolution was highly contingent upon the bacterial species and strains studied. By focusing on a single bacterial species or on evolution by genomic mutations only, there could be a danger that antibiotic development programs waste considerable resources on resistance prone antibiotic candidates. Future works should study the impact of antibiotic resistance on bacterial fitness and virulence systematically, resistance against Gram-positive specific antibiotic candidates and new antibiotic combination therapies.

In sum, the framework provided in this work highlights the importance of testing resistance evolution and the underlying mechanisms rigorously with complementary methods and in multiple

relevant bacterial species. Application of such a framework is feasible and advisable to new antibiotics before acceptance for clinical usage.

Methods

Strains, antibiotics and media

This study focused on multiple bacterial strains, as follows. We tested the activity spectrum of the antibiotics in this study on a set of 40 clinically relevant pathogenic strains of four species (*E. coli*, *K. pneumoniae*, *A. baumannii*, and *P. aeruginosa*, see the whole list of pathogens in Supplementary Table 2). For the FoR and ALE experiments, 2 strains per species were chosen: *E. coli* ATCC 25922, *K. pneumoniae* ATCC 10031, *A. baumannii* ATCC 17978, and *P. aeruginosa* ATCC BAA-3107 as sensitive (SEN) strains, and *E. coli* NCTC13846, *K. pneumoniae* ATCC 700603, *A. baumannii* ATCC BAA-1605 and *P. aeruginosa* LESB58 as multi-drug resistant (MDR) strains. In the case of *E. coli*, we chose the ATCC25922 strain as sensitive strain, due to its widespread usage in the literature, and an MCR-1 carrying *NCTC 13846* as the MDR strain, due to the high interests in the impact of this mobile resistance gene on colistin resistance[42]. For the other 3 species, sensitive and MDR strains were selected based on the highest number of control antibiotics they showed sensitivity or resistance to, respectively, with an additional criterion for MDR strains, that they should be part of an official strain collection (Supplementary Fig 2). Functional metagenomic screens were performed with *E. coli* ATCC 25922 and *K. pneumoniae* ATCC 10031 strains. Deep-scanning mutagenesis (DIvERGE) was performed with *E. coli* K-12 MG 1655 and *K. pneumoniae* ATCC 10031 strains.

Nineteen antibiotics were applied in this study from six different antibiotic families, thirteen newly developed ('recent') antibiotics, which are in different phases of clinical trials and six conventional ('contol') antibiotics with long clinical history, from each antibiotic family. For name, abbreviation and further details see Table 1 and Tabel S1. Antibiotics were custom synthesized or were purchased from several distributors (Supplementary Table 1). Upon preparation, each antibiotic stock solution was filter-sterilized and kept at −20 °C until usage. For more details on 'recent' and 'control' antibiotics, see Supplementary Note, Table 1 and Supplementary Table 1. For data on clinical breakpoints and peak plasma concentrations, see Supplementary Table 1.

Unless otherwise indicated, cation-adjusted Mueller-Hinton Broth 2 (MHB , Millipore) medium was used throughout the study, except for cefiderocol (CID) and a folate biosynthesis inhibitor, SCH79797 (SCH). Following EUCAST recommendation on cefiderocol, iron-depleted MHB media was used[43]. To maximize antibacterial activity of SCH, based on prior experience with folate biosynthesis inhibitor antibiotics[44], Minimal Salt (MS) medium was used (1 g/L (NH4)2SO4, 3 g/L KH2PO4 and 7 g/L K2HPO4) supplemented with 1.2 mM NA3C6H5O7 × 2H2O, 0.4 mM MgSO4, 0.54 μg/mL FeCl3, 1 μg/mL thiamine hydrochloride, 0.2% Casamino-acids and 0.2% glucose).

Bacterial membrane integrity assay

The ability of antibiotics to permeabilize the outer membrane of *E. coli* ATCC 25922 was determined using the fluorescent probe 1-N-phenylnaphthylamine (NPN)[45]. Cells were grown overnight in MHB then 200 μL of the overnight culture was used to inoculate 20 mL of MHB and the cells were grown to mid-logarithmic phase (OD_{600} 0.4–0.6). Bacterial cultures were harvested by centrifugation at 1,100 × *g* for 10 min. Next, cells were washed and resuspended to an OD_{600} of 0.4-0.6 in the buffer, containing 5 m*M* of HEPES (pH 7.0), 5 m*M* of glucose. Bacterial suspension

(100 µl) with a sub-MIC concentration of the tested antibiotics was added to the wells of a black 96-well plate and mixed with freshly prepared NPN solution (50 µl) and HEPES buffer (50 µl). Next, the mixture was left to equilibrate at room temperature for 15 min. Fluorescence was read immediately using a fluorescence plate reader ($\lambda_{ex} = 350$ nm, $\lambda_{em} = 410$ nm). Fluorescence value of the untreated *E. coli* ATCC 25922 strain was used as control, to estimate changes in membrane integrity in response to antibiotic stress.

High-throughput MIC measurements

A standard serial broth microdilution technique[46] was used to determine MICs, as suggested by the Clinical and Laboratory Standards Institute (CLSI) guidelines. A robotic liquid handling system was used to automatically prepare 11 to 16-step serial dilution in 384-well microtiter plates. 5×10^5 bacterial cells per mL were inoculated into each well containing 60 µl medium. Bacterial cultures were incubated at 37°C with continuous shaking (300 RPM) for 18 hours (2 replicates from each). Cell growth was monitored by measuring the optical density (OD_{600} values, using Biotek Synergy microplate reader). MIC was defined as the antibiotic concentration of complete growth inhibition (i.e., $OD_{600} < 0.05$). The same protocol was used to estimate antibiotic susceptibility of laboratory evolved lineages. Relative MIC was calculated as follows: relative $MIC = MIC_{evolved} / MIC_{ancestor}$.

Frequency-of-resistance assays

To estimate the frequency of spontaneous mutations that confer resistance in a microbial population, frequency of resistance (FoR) assay was used. Using standard protocols[14–17], approximately 10^{10} cells from stationary-phase cultures were plated to antibiotic-containing MHB broth plates. Before plating, bacteria were grown overnight in MHB medium at 37 °C, 250 RPM, collected by centrifugation, and washed once in equal volumes of MHB broth. From this concentrated bacteria suspension ~10^{10} cells were plated to agar plates containing the selective drug at the desired concentration (i.e., 2×, 4×, 8× and 20× MIC of each given antibiotic). Unless otherwise indicated (see the section above on high-throughput MIC measurements), MHB agar medium was used throughout the study. All experiments were performed in 3 replicates. Plates were grown at 37 °C for 48 hours. Total colony forming units (CFUs) were determined simultaneously in each experiment by plating appropriate dilutions to antibiotic-free MHB agar plates. Resistance frequencies for each bacterial strain were calculated by dividing the number of formed colonies by the initial viable cell count. We aimed to perform both frequency-of-resistance (FoR) and laboratory evolution (ALE) assays with all selected 8 bacterial strains, however, 34% of all antibiotic-strain combinations (N = 52) were excluded from further experiments due to high intrinsic resistance (i.e., MIC > 4 µg/ml) (Supplementary Table 3). For each remaining antibiotic-strain pair, 10 bacterial colonies from the highest antibiotic concentration were selected for further MIC measurements and whole genome sequence analysis.

High-throughput laboratory evolution

A previously established protocol[47,48] was employed for laboratory evolution, with the aim to ensure that populations with the highest level of resistance were propagated further. Starting with antibiotic concentration resulting in ~50% growth inhibition, 10 parallel populations per antibiotic-ancestor strain combination were grown for 72 h, at 37 °C and continuous shaking (300 RPM). As rapid degradation has been observed for *β*-lactams and cephalosporins in liquid laboratory media[49],

ceftobiprole, cefiderocol and cefepime were not subjected to adaptive laboratory evolution. Unless otherwise indicated, MHB broth medium was used. After each incubation period, 20 µl of 370 of each bacterial culture was transferred to four new independent wells containing freshly prepared medium containing different antibiotic concentrations (0.5×, 1×, 1.5×, and 2.5× the concentration of the previous step). A chess-board layout was used on the plate to monitor potential cross-contamination events. Cell growth was monitored prior to each transfer by measuring the optical density at 600 nm (OD_{600} value, Biotek Synergy 2 microplate reader). Only populations with the highest drug concentration (and reaching $OD_{600} > 0.2$) were selected for further transfer. The evolution experiment was generally continued for 20 transfers, resulting in a total of 728 evolved lines (78 lines were omitted because of limited growth).

Whole genome sequencing

To identify potential antibiotic resistance conferring mutations, we generally selected 2 to 5 lines from frequency-of-resistance (FoR) and laboratory evolution (ALE) experiments, respectively, for whole genome sequencing. Resistant populations were grown overnight in antibiotic-free medium. DNA isolation from overnight cultures was performed with GenElute Bacterial Genomic DNA Kit (Sigma), according to the manufacturer's instructions. DNA was eluted 120 µl RNAse free sterile water, in 2 elution steps. 60 µl of the eluted DNA was then concentrated by DNA Clean and Concentrator Kit (Zymo), according to the manufacturer's instructions. Final DNA concentration was measured with a Qubit Fluorometer and concentration was set to 1 ng/ml in each sample. Sequencing libraries from isolated genomic DNA were prepared with Nextera XT DNA library preparation kit (Illumina) following the manufacturer's instructions. The sequencing libraries were sequenced on an Illumina NextSeq 500 sequencer using 2*150 PE mid or high output flow cells to generate 2 × 150 bp paired-end reads.

To determine and annotate the variants, we mapped the sequencing reads to their corresponding reference genomes using an established method (Burrows-Wheeler Aligner)[50]. From the aligned reads, PCR duplicates were removed with the Picard Mark Duplicates tool (see http://broadinstitute.github.io/picard/). We removed every read that has been aligned with more than 6 mismatches (disregarding insertions and deletions). The SNPs and INDELs were called with Freebayes[51] with the following parameters: -p 5--min-base-quality 28. The identified variants were filtered by the vcffilter tool from vcflib[52] using the following parameters –f 'QUAL > 100'. To avoid missing rare but valid hits, we did not set a lower limit for the prevalence of rare variants. If necessary, mutations were also manually inspected within the aligned reads using IGV[53] to reduce BWA alignment or freebayes artefacts. Finally, the variants were annotated with SnpEf, and kept only those that were not present in the ancestor. We filtered out mutations that appeared in more than nine lines, as these variants are likely already present in the ancestor as well. Furthermore, mutations that appeared in less than nine but more than six lines were manually inspected to exclude sequencing artefacts. We also excluded mutations that affect 40 bp or longer repetitive regions, resulting in a filtered set of mutations. Lines containing mutations in the mutL, mutS or mutY genes, or lines with more than 19 mutations, defined by outlier filtering (Q3 + 3*IQR), were considered hypermutators and were subsequently discarded.

To analyze the presence / absence of mutations across genes and strain backgrounds, we first complemented existing gene functional annotation for the 8 bacterial strain backgrounds as follows. Nucleotide sequence and annotation files of 6 strains (*E. coli* ATCC 25922, *K. pneumoniae* ATCC 10031, *A. baumannii* ATCC 17978, *P. aeruginosa* ATCC BAA-3107, *K.*

pneumoniae ATCC 700603, and *A. baumannii* ATCC BAA-1605) were downloaded from the ATCC database (https://www.atcc.org/). For *P. aeruginosa* LESB 58 and *E. coli* NCTC13846 strains, genomic data was downloaded from NCBI Nucleotide (accession numbers FM209186.1 and NZ_UFZG00000000.1). Next, all genes in the GeneBank files, including hypothetical ones, were functionally annotated using PANNZER2[54,55]. To compare the sets of mutated genes across strain backgrounds, we determined genes that are shared across different strains by identifying groups of orthologous genes using OrthoFinder (version:2.5.4)[56,57].

Comparison of variants to public genomes of bacterial isolates

We assessed whether amino acid substitutions occurring in the FoR and ALE samples are present in natural populations of *E. coli* and *A. baumannii* as follows. We compiled a comprehensive genomic dataset for *E. coli* strains by downloading assembled genome sequences or un-assembled reads, and metadata, from four sources: i) the JGI Integrated Microbial Genomes & Microbiomes (IMG) database[58] on 29 Jan 2020, ii) the NCBI RefSeq prokaryotic collection [Available from: https://www.ncbi.nlm.nih.gov/refseq/] on 29 Jan 2020; iii) genomes that were analyzed in the study of Moradigaravand et al.[59]; and iv) genomes that were analyzed in the study of Johnson et al.[60].

After trimming the adapters with the Cutadapt v3.2 program[61], we de novo assembled the next-generation sequencing short reads (downloaded from the Sequence Read Archive (SRA) database[62]) of genomes of source iii) and iv) using the SPAdes v3.14.1 software[63]. Then, we applied the BUSCO v5.0.0. workflow[64] to exclude genome sequences with less than 95% of the BUSCO genes, indicating inadequate completeness / quality. When multiple genome sequences belonged to the same BioSample ID, only the one with the highest BUSCO score, longest sequence and fewest contigs were kept, while all metadata of the original sequences were merged. This resulted in 20,786 *E. coli* genomes (Data S1) for which gene prediction was performed using Prodigal (Version: 2.6.3,[65]) to obtain protein coding gene annotations that are consistent across the genomes. ORFs with less than 100 AAs were filtered out. Strains were classified as pathogens and non-pathogens based on their genomic metadata. For *A. baumannii* strains, we downloaded all available assembled genome sequences from the NCBI RefSeq prokaryotic genome collection (Available from: https://www.ncbi.nlm.nih.gov/refseq/) on 12 Sep 2022. Then we applied genome filtering with 95 percentage completeness using BUSCO v5.4.6. and protein prediction using Prodigal as described above for *E. coli*. This resulted in 15,185 *A. baumannii* genomes (Data S1).

Next, we searched for the presence of each amino acid changing SNP across the *E. coli* and Acinetobacter genome collections as follows. First, we performed sequence similarity search of each gene carrying a given variant using DIAMOND blast (version 2.0.2,[66]) using an e-value of 0.00001 with 90% coverage and 90% identity to identify homologs among the genomes. In the next step, we performed multiple sequence alignment using MAFFT with the --retree 2 option (version: 7.475,[67]). Then, we analyzed the amino acid frequency across the alignments in all mutated positions. All *E. coli* and *A. baumannii* variants that were present in the corresponding species' genome collection and appeared more than once in our FoR and ALE samples were selected for further analysis.

Functional metagenomic screens

Resistance conferring DNA fragments in the environment were identified by functional selection of metagenomic libraries. In a previous work[23], we created metagenomic libraries to obtain environmental and clinical resistomes, including i) river sediment and soil samples from seven antibiotic polluted industrial sites in the close vicinity of antibiotic production plants in India[68] (anthropogenic soil microbiome), ii) fecal samples from 10 European individuals who had not taken any antibiotics for at least 1 year before sample donation (that is, gut microbiome) and iii) samples from a pool of 68 multi-drug resistant bacteria isolated in healthcare facilities or obtained from strain collections (see Supplementary Table 11). For full details on library construction, see Apjok and colleagues[23].

Briefly, environmental and genomic DNA was isolated using the DNeasy PowerSoil Kit (Qiagen) and the GenElute Bacterial Genomic DNA Kit (Sigma), respectively. Environmental and genomic DNA was enzymatically fragmented followed by the size selection of 1.5-5 kb long fragments. Metagenomic inserts were cloned into a medium-copy-number plasmid, containing 10-10 nt long barcodes flanking the insert (uptag and downtag). Library sizes ranged from 2-6 million clones with an average insert size of 2 kb.

Libraries were introduced into *K. pneumoniae* ATCC 10031 and *E. coli* ATCC 25922 by bacteriophage transduction (DEEPMINE)[23] and electroporation, respectively. DEEPMINE employs hybrid T7 bacteriophage transducing particles to alter phage host-specificity and efficiency for functional metagenomics in target clinical bacterial strains.

In the current study, we followed previously described protocols with two minor modifications. First, transducing hybrid phages were generated with a T7 phage lacking the gp11-gp12-gp17 genes, constructed as previously[69]. Second, we used a new phage tail donor plasmid for complementing the deleted phage tail genes. This plasmid was cloned using the ΦSG-JL2 phage tail coding genes, the packaging signal region of T7 phage and the pK19 plasmid backbone based on a previous work[70].

Functional selections for antibiotic resistance were performed on MHB agar plates containing a concentration gradient of the antimicrobial compounds[71,72]. Cells containing the metagenomic libraries were plated in a cell number covering at least 10 times the size of the corresponding metagenomic library. Plates were incubated at 37°C for 24 h. For each functional selection, a control plate was prepared with the same number of cells containing the metagenomic plasmid without a cloned DNA fragment in its multi-cloning site. These control plates showed the inhibitory zone of the antimicrobial compound. To isolate the resistant clones from the libraries, sporadic colonies were identified above the inhibitory zone based on the control plate by visual inspection. Colonies were then collected for plasmid isolation (Thermo Scientific GeneJET Plasmid Miniprep Kit). Metagenomic inserts in the resistant hits were sequenced by two complementary sequencing methods. First, random 10 nt barcodes flanking the metagenomic inserts on the resistant plasmids from each selection experiment were PCR amplified. For this, we used primers that contain 2x8 nt long barcodes specific for each selection experiment. Amplicons were pooled, size selected on agarose gel and sequenced by Illumina. Second, metagenomic inserts and their flanking 10 nt uptag and downtag barcodes were sequenced by Nanopore.

Annotation of antibiotic resistance genes (ARGs)

Consensus insert sequences from Nanopore sequencing were matched with the respective selection experiment using the data from Illumina sequencing. First, sequencing reads from Illumina sequencing were demultiplexed using the 2x8 nt long barcodes specific to the selection experiment, and then the demultiplexed reads were matched with the consensus insert sequences using the random 10 nt long barcodes specific to the metagenomic inserts. To reduce redundancy and spurious matches, the list of metagenomic contigs were filtered 1) to unique barcodes, keeping barcodes with the highest nanopore read count and 2) to contigs that were supported by at least 8 nanopore reads and 5 illumina reads. Prediction of ARGs within these contigs was based on ORF prediction using Prodigal v2.6.3,[65], followed by searching the annotated ORFs within the CARD and ResFinder databases[73,74]. Searches were performed using blastx from NCBI BLAST v2.12.0[75] with 10^{-5} E-value threshold and otherwise default settings. ORFs were clustered at 95% identity and coverage using CD-HIT v4.8.1,[76] and only one representative ORF was kept for each cluster. The inserts were classified based on whether or not any ARGs were found in them, and whether or not at least one of these ARGs was associated with the antibiotic being tested in that particular selection experiment. Close orthologues of the host-specific proteins were excluded from further analyses, by performing a blastp search of each ORFs on host proteomes (https://www.uniprot.org/proteomes/UP000001734, https://www.uniprot.org/proteomes/UP000029103, downloaded on 2022.11.24.) and removing each ORFs with higher than 80% sequence similarity. The potential origin of the inserts was assessed by searching the Nanopore contigs within the NCBI Prokaryotic RefSeq Genomes database[77] using blastn from NCBI BLAST v2.12.0 with default settings and resolving taxids to hierarchical classifications using R[78] and the taxizedb package[79–81].

Catalogue of mobile ARGs

A mobile gene catalogue (that is, a database of recently transferred DNA sequences between bacterial species[82]) was created previously[23]. Briefly, 1377 genomes of diverse human-related bacterial species from Integrated Microbial Genomes and Microbiomes database[82] and 1417 genomes of Gram negative ESKAPE pathogens from NCBI RefSeq database were downloaded. Using NCBI blastn 2.10.1+,[75] we searched the nucleotide sequences shared between genomes belonging to different species. The parameters for filtering the NCBI blastn 2.10.1+ blast results were the following: minimum percentage of identity, 99%; minimum alignment length, 500; maximum alignment length, 20,000. Then, to generate the mobile gene catalogue, we compared them with the merged CARD 3.1.0[73] and ResFinder (d48a0fe) databases[74] using diamond v2.0.4.142[66]. Natural plasmid sequences were identified by downloading 27,939 complete plasmid sequences from the PLSDB database (version 2020-11-19,[83]). Then, the representative sequences of the isolated 114 ARG clusters were BLASTN searched both in the mobile gene catalogue and in natural plasmid sequences with an identity and coverage threshold of 90%. Those ARGs were considered as mobile which were present in the mobile gene catalogue and/or in natural plasmid sequences.

Detecting ARGs across E. coli phylogroups, host species types and geographic regions

Host type, geographic location and phylogroup were determined for a dataset of 16,272 E. coli genomes in previous work[26]. In brief, the initial complete dataset of 26,881 E. coli genomes was retrieved from the NCBI RefSeq database in February 2022, and filtered for genomes with complete metadata. Clermont phylogrouping[84] was performed in silico using the EzClermont command-line tool[85], while host and location metadata were retrieved and categorised using the

Bio.Entrez utilities from Biopython v1.77. All genomes were sorted into the following host species categories: 'Human', 'Agricultural/Domestic animals', and 'Wild animals'. This was achieved using regular expressions constructed by manually reviewing text in the 'host' field of the biosample data for each accession number. Geographic locations were split into 20 subregions according to Natural Earth data[86]. A local blastp search was performed for this collection of *E. coli* genomes against a database of the predicted ARG ORFs identified in functional metagenomic screens, using default parameters. ARGs with both 90% amino acid identity and 90% query coverage per subject, and present in no more than 10% of the examined *E. coli* genomes were analyzed further.

DIvERGE mutagenesis

We performed deep-scanning mutagenesis in the target genes of moxifloxacin, an established topoisomerase inhibitor. The quinolone resistance-determining regions (QRDR)[21] of the gyrA and parC genes were subjected to a single round of mutagenesis using DIvERGE in *E. coli* K-12 MG 1655 and *K. pneumoniae* ATCC 10031. A previously described workflow[22] was employed with minor modifications. Briefly, cells carrying pORTMAGE311B plasmid (Addgene no. 120418) were inoculated into 2 ml LB medium plus 50 µg/ml kanamycin and were grown at 37°C and continuous shaking (250 RPM) for 12 hours. From this starter culture, 500 µl stationary-phase culture was propagated in 50 ml of the same fresh medium under identical conditions. Induction was initiated at a fixed population density (OD_{600} =0.4) by adding 50 µl of 1 M *m*-toluic acid (dissolved in 96% ethyl alcohol; Sigma-Aldrich) for 30 to 45 minutes at 37°C. After induction, cells were cooled on ice for 15 minutes. Next, cells were washed three times with sterile ice-cold ultrapure distilled water. Finally, the cell pellet was resuspended in 800 µl sterile ultrapure distilled water and kept on ice until electroporation.

To perform DIvERGE mutagenesis, the corresponding *gyrA* QRDR- and *parC* QRDR-targeting oligonucleotides were equimolarly mixed. 2 µl of the 500 µl oligonucleotide mixture was added to 40 µl electrocompetent cells in 5 parallel samples. The used oligonucleotides are listed in Supplementary Table 10. Following electroporation, the parallel samples were pooled and were suspended into 25 ml fresh LB medium to allow for cell recovery (37°C and 250 RPM). After 60 minutes of recovery period, an additional 25 ml LB medium was added, and cells were grown for an additional 24 hours.

To select clones with reduced susceptibility to moxifloxacin, 500 µl of each mutant cell libraries were spread onto moxifloxacin-containing MHB agar plates. The plates were incubated at 37°C for 48 h. Finally, 20-20 antibiotic resistant clones were selected randomly and analyzed further by capillary sequencing.

In vitro growth measurements

We observed the growth phenotype of bacterial populations with available whole genome sequencing data by assessing their growth at 37 °C in antibiotic-free MHB medium following established protocols[87]. We inoculated 5×10^4 cells from early stationary-phase cultures (prepared in MHB medium) into 60 µL of MHB medium in a 384-well microtiter plate and monitored bacterial growth for approximately 24 hours. Bacterial growth was estimated by the optical density of the culture (OD_{600}). These measurements were carried out every 5 minutes using BioTek Synergy HL1 microplate reader while bacterial cultures were grown at 37 °C under continuous

shaking. Each bacterial variant and their corresponding wild types were measured in at least 9 replicates. Finally, growth rates were calculated from the obtained growth curves according to a previously described procedure. Fitness was approximated by calculating the area under curve (AUC)[88,89]. AUC has been previously used as a proxy for fitness because it has the advantage of integrating multiple fitness parameters, such as the slope of the exponential phase (i.e., growth rate) and the final biomass[90].

In vivo bacterial infections

Galleria mellonella caterpillars were obtained in bulk from local supplier company TerraPlaza (Vál, Hungary) and stored at 15 °C in absence of food. The KP-SEN ancestral bacterial strains and the corresponding mutant lineages that display resistance to SPR206, POL7306, Polymyxin B, respectively, were grown overnight in MHB broth and washed twice in sterile phosphate buffered saline (PBS). Bacterial suspensions were injected into the hemocoels of the larvae via the first left proleg using 10 µl Hamilton syringes (Reno, Nevada, U.S.A.). Larvae were incubated in petri dishes lined with filter paper at 37 °C for 48 h and survival was documented every 6 hours. Insects were considered dead if they failed to respond to touch[91]. To establish the bacterial inoculum size required to kill *G. mellonella* over 48 hours for KP-SEN, 10 larvae were inoculated with 10 µl of bacterial suspensions in PBS containing 10^4 to 10^8 bacterial cells per animal. Bacterial colony forming unit (CFU) number was verified by viable bacterial counts on MHB agar. Based on this preliminary experiment, 10^7 per animal for KP-SEN was determined as the ideal inoculum size to kill *G. mellonella* larvae.

Antibiotic treatments were injected in the second right proleg using 10 µl Hamilton syringes (Reno, Nevada, U.S.A.). Antibiotic toxicity was determined by injecting 10–10 larvae with 5, 10, 20, 50 and 100 mg per body weight kg of SPR206, and no toxicity was observed at these dosages. SPR206 monotherapy was tested by first injecting the larvae with the appropriate Kp-SEN strain or laboratory evolved lineage, then the SPR206 treatment dosage. Monotherapies were tested with 5, 10, 20, 50 and 100 mg per body weight kg doses. SPR206 at 50 mg per body weight kg improved survival by approximately 50% at the 48 hour mark, therefore this treatment dosage had been chosen for the *in vivo* resistance experiment. All experimental data were visualized with Kaplan-Meier survival curves, utilizing R version 4.2.2 and compatible packages survival, survminer and ggsurvplot.

Bacterial invasion assay

To test bacterial invasion capacity, a previously described protocol was used with minor modifications[92]. Caco-2 cells were cultured in DMEM (Capricorn) supplemented with 10% v/v FBS, 1% v/v NEAA, 100 µg/mL penicillin, and 100 U/mL streptomycin and maintained at 37°C in a 5% CO_2 incubator. Contamination of *Mycoplasma* spp. were excluded using the Lonza MycoAlert® Detection Kit.

KP-SEN as ancestor, SPR206 resistant lines (KP-SEN SPR FoR #1 and KP-SEN SPR FoR #3) were inoculated in 5 ml of LB medium and incubated overnight at 37 °C in a shaking incubator. To infect human cells, the overnight inoculum was centrifuged and washed with 1xPBS, than diluted to 0.5 OD in infection medium (DMEM supplemented with 10% v/v FBS and + 10 mM HEPES). Human cells were incubated with bacteria for 3 h at 37°C in a 5% CO_2 incubator. Infection medium was then aspirated and cells were washed with 1xPBS and treated with culture

medium containing 100 µg/ml gentamicin (to eliminate the extracellular bacteria) or 100 µg/ml primocin (to eliminate the intra- and extracellular bacteria) or fixed with 3% w/v PFA solution for further examinations.

The infected human cells were treated with 100 µg/ml gentamicin culturing medium for 24 hours to kill extracellular bacteria. After incubation the human cells were washed with 1x PBS. Human cell cultures were washed with 0.5% v/v Triton X-100 and 0.25% trypsin to lysed human cells and resolve them from the bottom of Petri dishes. The lysates were transfer microcentrifuge tubes and were sonicated in 40 KHz frequency 2s (VEVOR 10L Ultrasonic Cleaner Machine). Colony forming units (CFU) of invasive bacterial cells were determined by plating 1x, 10x, 100x and 1000x dilutions to MHB agar plates.

Clonogenic survival assay

The infected human cells were treated with 100 µg/ml primocin containing a culturing medium for 24 hours. Cells were then washed with 1xPBS, plated into 10 cm diameter Petri dishes and incubated for 14 days. The obtained colonies were fixed with ice cold methanol:acetic acid (3:1) and stained with 0.1% crystal violet. The fraction of the surviving cells were calculated and normalized to non-infected control cells[93].

Immunofluorescence

Human cells were plated onto glass coverslips and infected with bacterial cells. The cell mixtures were then washed with 1xPBS and fixed with 3% w/v PFA for 10 minutes, permeabilized with 0.5% v/v Triton X-100 in PBS for 10 minutes and incubated in blocking buffer (3% BSA, 0.1% v/v Triton X-100 in PBS) for 1h at room temperature. Samples were incubated in primary antibodies (mouse gH2AX, rabbit ZO-1) diluted in blocking buffer overnight at 4°C. Cells were washed three times with 0.1% v/v Triton X-100 in PBS and incubated with fluorescently-tagged secondary antibodies (anti-mouse Alexa Fluor 488 and anti-rabbit Alexa Fluor 555) diluted in blocking buffer at room temperature for 1h in the dark. Cells were washed twice with 0.1% v/v Triton X-100 in PBS and counterstained with Hoechst (1 µg/mL in PBS) for 10 minutes.

Z-stacks of images were acquired on a LSM800 confocal setup with a 63x/1.4 Oil DIC M27 objective, and controlled by the ZEN 2.3 software. Fluorescence excitation was performed using diode lasers at 405, 488 and 561 nm. Images were analyzed after generating the maximum intensity projections of the Z-stacks. The raw images were analyzed in Fiji (ImageJ) after generating the maximum intensity projections of Z-stacks.

In vivo infection of mice musculus gastrocnemius and bacterial CFU

Drug-resistant *K. pneumoniae* is frequently responsible for wound and systemic infections; therefore, we benchmarked the *in vivo* effects of reduced susceptibility to SPR206 in a murine thigh infection model[94–96] with minor modifications. Bacterial inoculums of the parental *K. pneumoniae* (KP-SEN) and the generated SPR206-resistant lines (KP-SEN SPR FoR #1 and KP-SEN SPR FoR #3) were prepared by inoculating single bacterial colonies into 5 ml of MHB broth and were incubated at 37°C for 16 h under constant agitation (250 RPM). Next, ½ volume of a 50% (vol/vol) glycerol-water mixture was added to each culture, and 550 µl of these cell suspensions was frozen at −80°C. 2 days before infection, 50 µl of bacterial stock from -80°C were inoculated into 5 ml MHB broth and incubated at 37°C for 16 h under constant agitation (250

RPM). To synchronise the 3 bacterial strains, on the next day, 50 µl of the bacterial suspension were inoculated into fresh MHB broth and incubated again at 37°C for 16 h under constant agitation (250 RPM). On the day of infection bacterial cells were washed with phosphate-buffered saline (pH 7.4) (PBS) 3 times, then cell counts for each *K. pneumoniae* strain were determined with Bürker-chamber and the bacterial concentration were adjusted appropriately (see below). For determination of the virulence of the parental and generated *Klebsiella pneumoniae* strains, 8- to 9-week-old female specific-pathogen-free BALB/c (Animalab Hungary, Vác, Hungary) mice were infected via both the left and right *musculus gastrocnemius* with 5×10^6 bacterial cells in 40 µl PBS ($N \geq 7$ per *K. pneumoniae* strain) (0.4 ml bacterial suspension / *musculus gastrocnemius*). 24-hours post infection, animals were humanely euthanized with CO_2 asphyxiation, and both left and right calf were collected surgically, weighed, and homogenized in 2 ml PBS with an Ultra-Turrax T25 homogenizer (Sigma). Organ homogenates were 10-fold diluted and 0.1 ml diluted homogenates were plated to Brain-Heart Infusion agar (BHI agar), and the numbers of colony-forming units (CFU per gram tissue) were determined after 24-h incubation of the plates at 30°C. As calf muscles from both hind legs of all animals were utilized for the experiment, there are 2 data points indicated for each animal ($N \geq 14$ per infection group).

Ethics statement

All aspects of this work, including housing, experimentation, and animal disposal were performed according to the Hungarian national (1998. XXVIII; 40/2013) and European (2010/63/EU) animal ethical guidelines. All experiments were performed under animal biosafety level 2 (ABSL2) conditions. Procedures were licensed by the Animal Experimentation and Ethics Committee of the Biological Research Centre of the Hungarian Academy of Sciences and the Hungarian National Animal Experimentation and Ethics Board (clearance number XVI./03521/2011) with the University of Szeged granting permission XII./00455/2011 and XVI./3652/2016 to work with mice.

Tables

Antibiotic	Abbreviation	Antibiotic class	Generation	Date of approval/clinical phase
Omadacycline	OMA	tetracyclines	recent	2018
Eravacycline	ERA		recent	2018
Doxycycline	DOX		control	1967
Ceftobiprole	CTO	cephalosporins	recent	2019
Cefiderocol	CID		recent	2019
Cefepime	CEP		control	1994
Delafloxacin*	DEL	topoisomerase inhibitors	recent	2017
Gepotidacin*	GEP		recent	Phase 3
Zoliflodacin	ZOL		recent	Phase 3
Moxifloxacin*	MOX		control	1999
Apramycin	APR	aminoglycosides	recent	Phase 1
Gentamicin	GEN		control	1964
Sulopenem	SUO	carbapenems	recent	Phase 3
Meropenem	MER		control	1996
Tridecaptin M152-P3	TRD	membrane targetings	recent	pre-clinical
POL-7306*	POL		recent	pre-clinical
SCH79797*	SCH		recent	pre-clinical
SPR-206	SPR		recent	Phase 1
Polymyxin B	PMB		control	1964

Table 1 - Antibiotics employed in this study. The table shows the antibiotics used in this study, including 'control' (blue) and 'recent' (orange) antibiotics. Some of the recent antibiotics are derivatives of established antibiotic classes and are supposed to address problems associated with class-specific resistance mechanisms. When it comes to compounds with novel molecular targets (or novel mode of action against a known target), the antibiotic pipeline is thin [10]. In this group, we considered lead compounds in clinical trials or at least established efficacy against Gram-negative ESKAPE pathogens in mouse infections models. The list includes multi-targeting compounds (indicated by asterisks, *), which are considered to be less prone to resistance [97,98]. Similarly, compounds that attack essential components of the outer cell membrane have been previously suggested to be immune to bacterial resistance [11,99], as potential resistance mutations to these drugs would seriously compromise normal cellular functioning. Four new antibacterial compounds in our study permeabilized the bacterial outer membrane through various mechanisms (Supplementary Fig. 1). APS has been utilized in veterinary medicine for more than ten years, its current focus lies in clinical trials for the treatment of systemic Gram-negative infections in human patients. As the evolutionary dynamics of resistance against antibiotic combinations can be very different from that of monotherapies, we study recent advances in adjuvant therapies (e.g. β-lactamase inhibitors) in a separate study. Similarly, Gram-positive specific antibiotic candidates, such as teixobactin, will be studied elsewhere. For more information on antibiotic choice, see Supplementary Note.

Figures

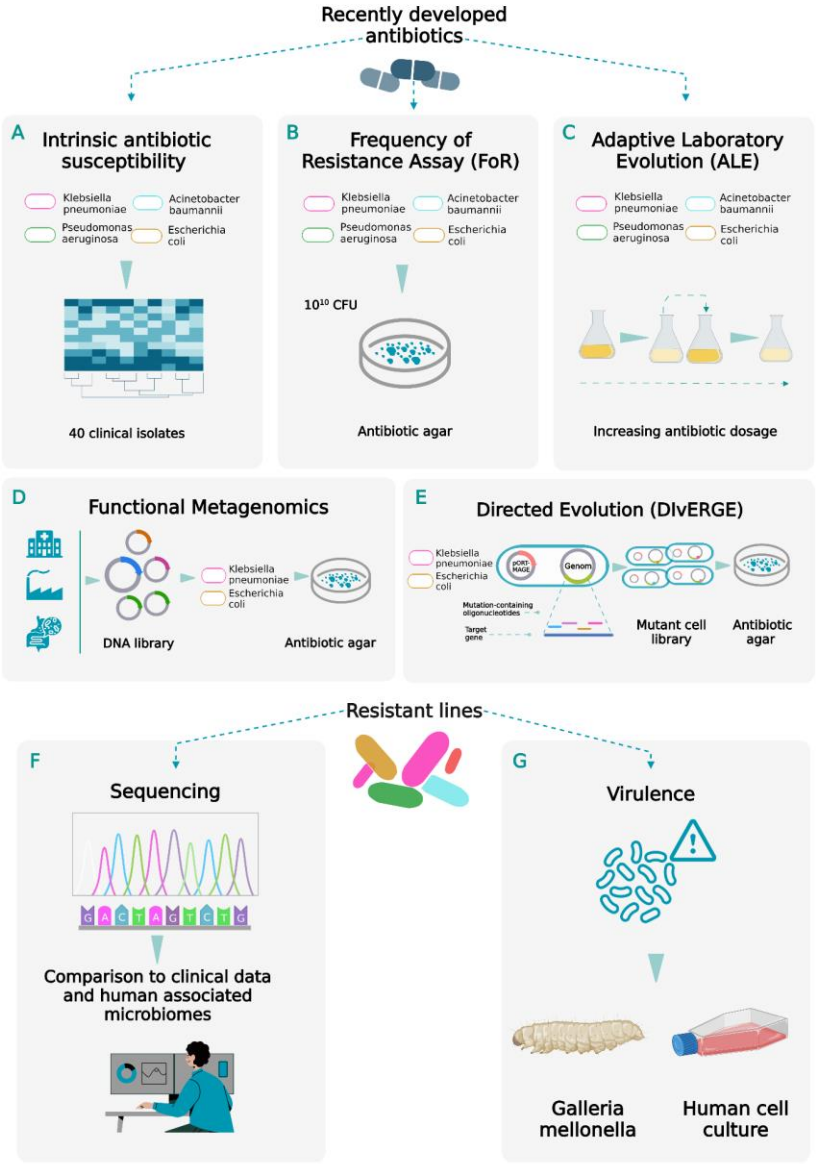

Fig. 1. Deep analysis of resistance evolution. Evolution of resistance to 13 recently developed antibiotics was studied. To this aim we selected new antimicrobial compounds which are currently under development or have reached the market recently. To systematically study the possible routes of resistance evolution and the underlying molecular mechanisms, we combined multiple methods shown in gray boxes. We used multiple clinically relevant Gram-negative bacterial species as indicated in each box. **A)** Intrinsic antibiotic susceptibility testing was performed using clinical isolates of *E. coli*, *K. pneumoniae*, *A. baumannii* and *P. aeruginosa*. **B-C)** Standard frequency of resistance assays (FoR) with 10^{10} cells and adaptive laboratory evolution (ALE) experiments were performed using a sensitive and MDR strain of *E. coli*, *K. pneumoniae*, *A. baumannii* and *P. aeruginosa*. **D)** Functional metagenomic screens for antibiotic resistance genes from three metagenomic DNA libraries (soil and gut microbiomes and clinical genomes) were

performed in *E. coli* and *K. pneumoniae.* **E)** The directed evolution method called DIvERGE was used in *E. coli* and *K. pneumoniae* to test cross-resistance between recent and established topoisomerase inhibitors. **F)** We sequenced the complete genomes of 457 resistant lines to decipher the underlying molecular mechanisms of resistance and explore the prevalence of these mutations in the genomes of naturally occurring clinical isolates. **G)** Using the invertebrate model organism *Galleria mellonella* and human cell culture assays, we identified antibiotic resistant lines with increased virulence.

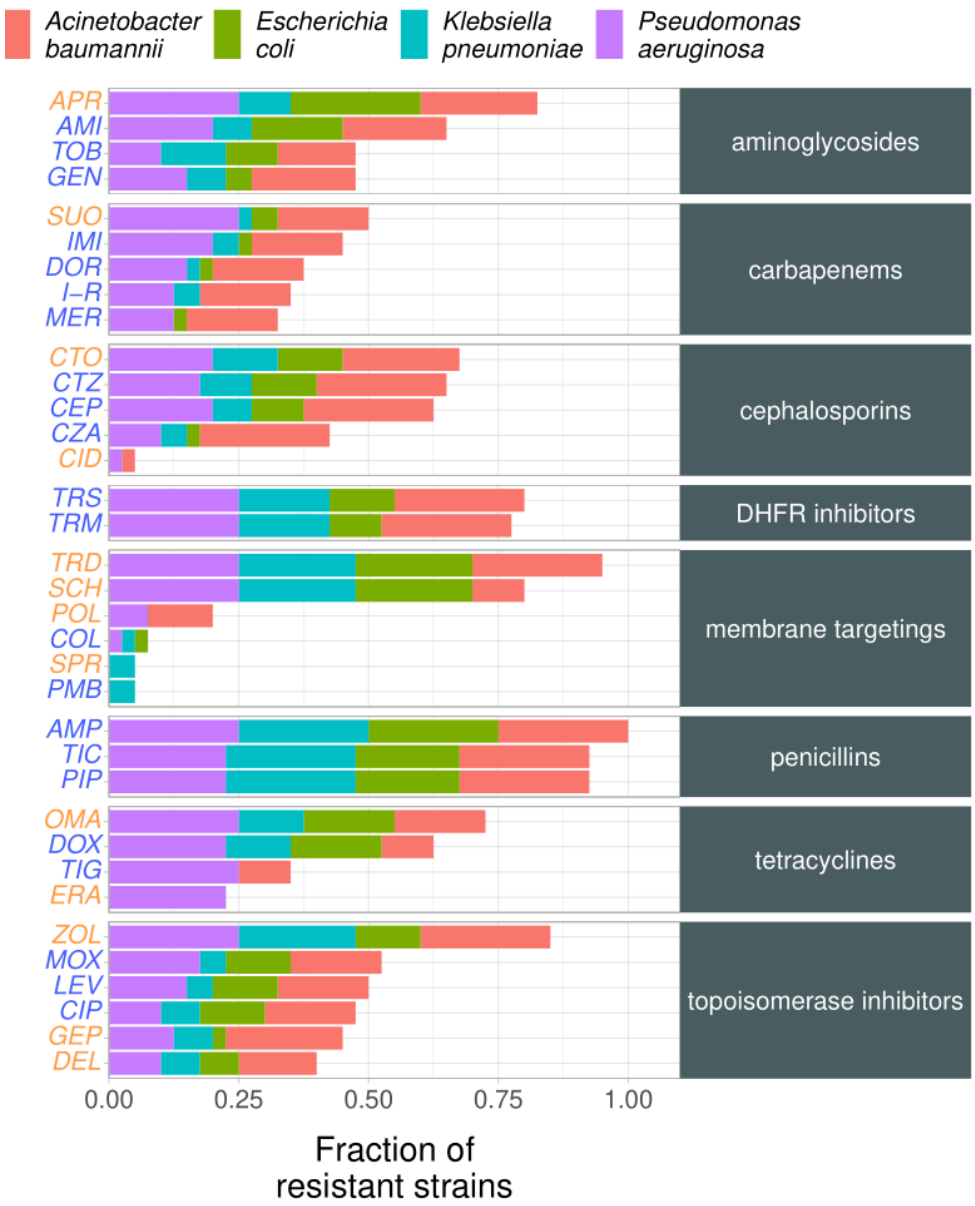

Fig. 2A. The barplot shows the fraction of strains resistant to 'recent' or 'control' antibiotics, indicated by orange and blue labels, respectively. The colors of the bars indicate the 4 bacterial species studied. Due to the shortage of information on clinical breakpoints for 'recent' antibiotics, resistance was defined by an MIC threshold (4 µg/ml, for further details, see Supplementary Table 1, Supplementary Table 3 and Supplementary Fig. 4). The fraction of resistant strains was estimated by normalizing the number of resistant strains to the total number of tested strains. For antibiotic abbreviations, see Table 1.

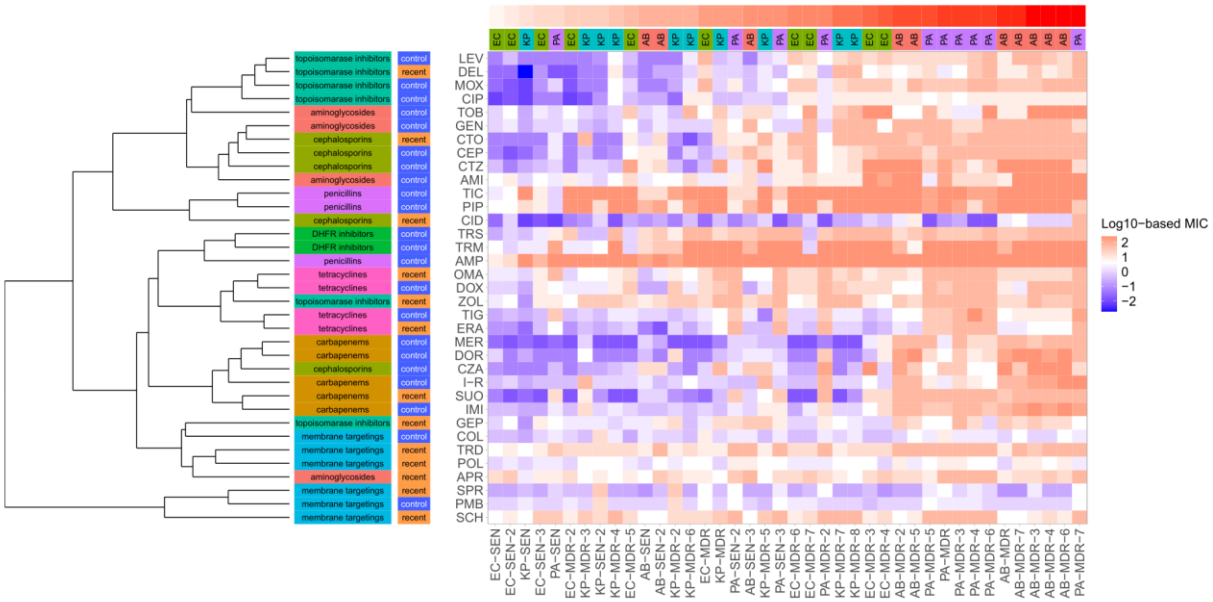

Fig. 2B. The heatmap shows the antibiotic susceptibility profiles of bacterial strains belonging to four bacterial species, including *Escherichia coli* (EC), *Klebsiella pneumoniae* (KP), *Acinetobacter baumannii* (AB) and *Pseudomonas aeruginosa* (PA). The antibiotic panel consists of 22 'control' (blue) and 13 'recent' (orange) antibiotics. Antibiotic generations and classes are indicated on the left panels. Antibiotic clustering was based on calculating Spearman's correlation of MIC values and using the complete hierarchical clustering method. The bacterial strains are ordered by the fraction of 'control' antibiotics (top panel) they are resistant to (defined by the corresponding species-specific clinical breakpoint values). For abbreviations, see Table 1 and Supplementary Table 2.

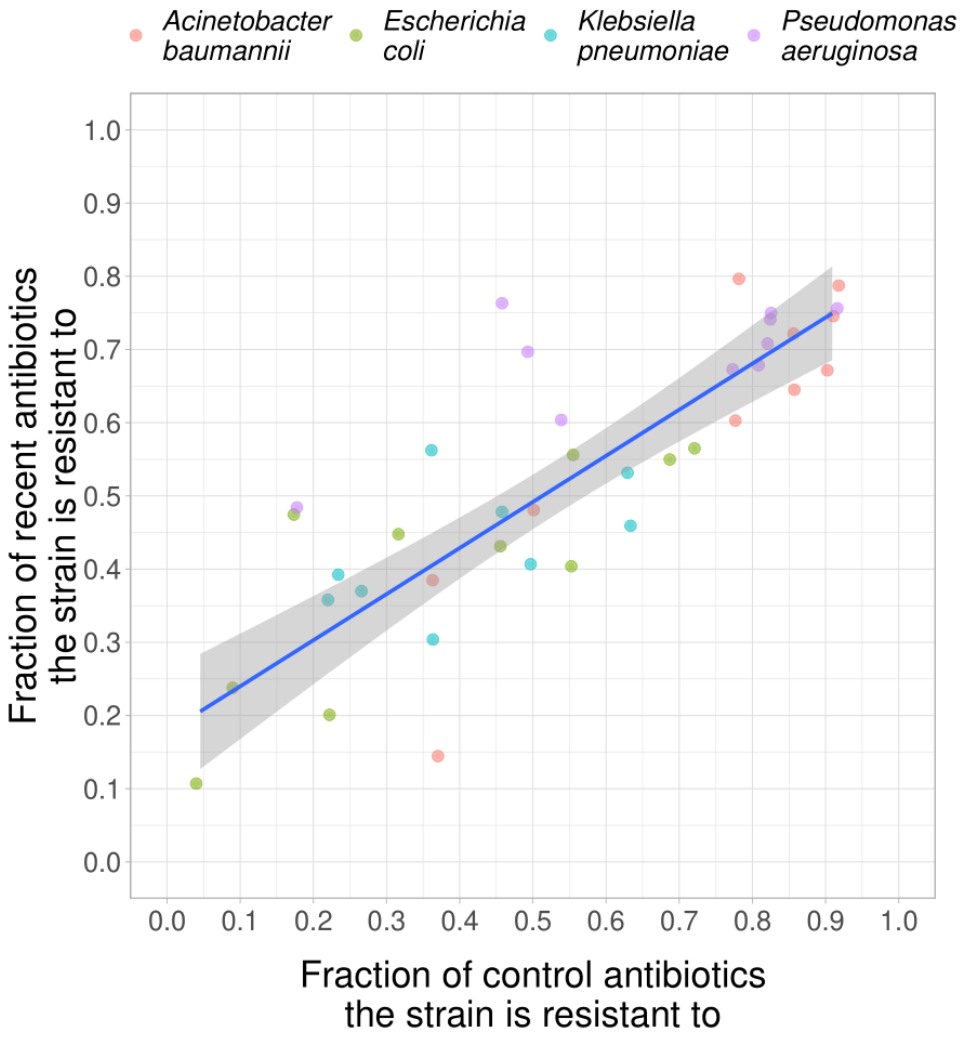

Fig. 2C. The scatterplot shows the fractions of 'recent' and 'control' antibiotics a bacterial strain is resistant to. For each strain, the fractions were calculated by dividing the number of antibiotics with resistance to the total number of antibiotics tested. The estimated two fractions show a strong positive correlation to each other (Spearman's rho = 0.83, $P < 0.001$). Bacterial resistance was defined by an arbitrary MIC cutoff (4 µg/ml). For abbreviations, see Supplementary Table 2.

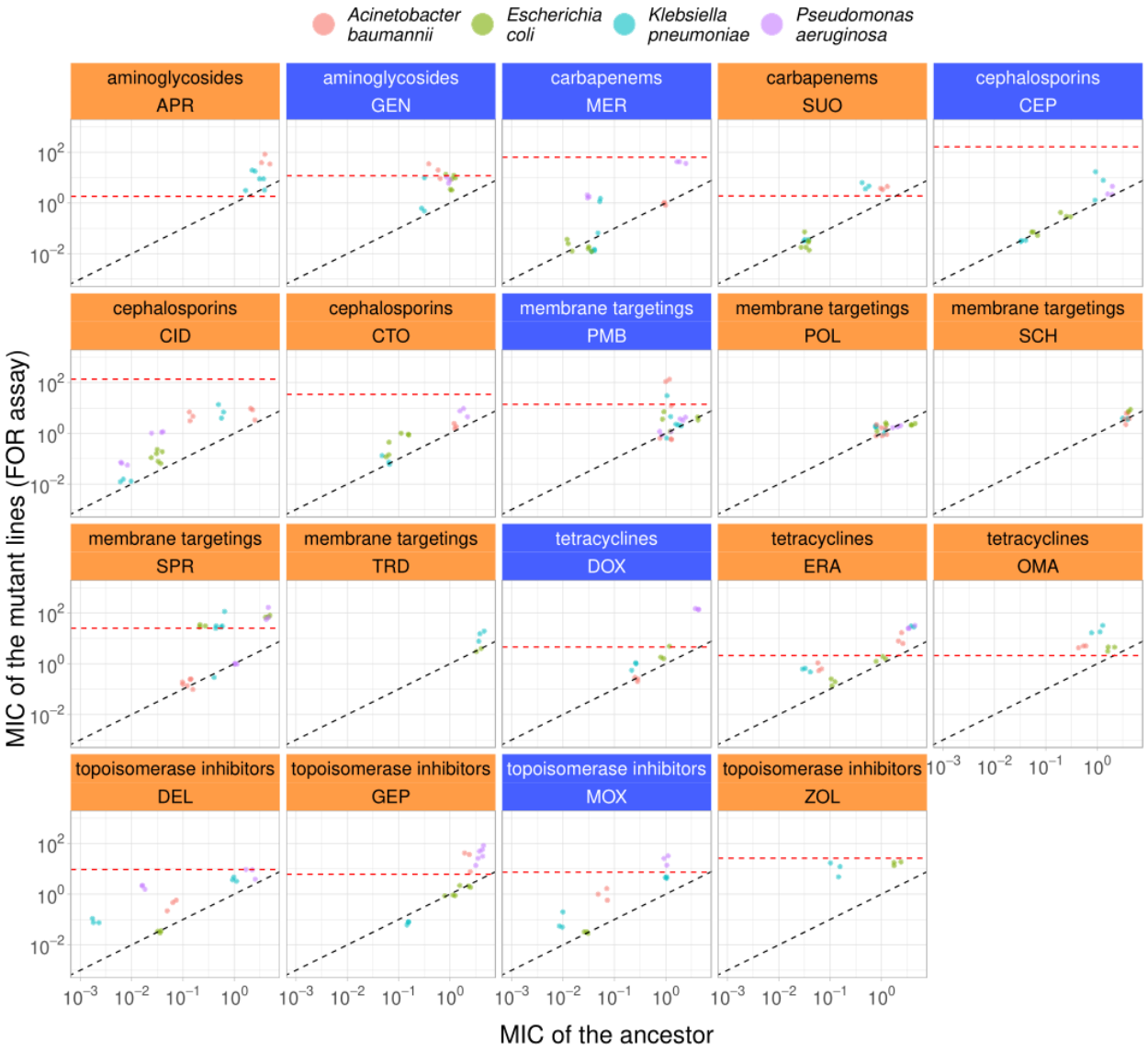

Fig. 3A. Changes in minimum inhibitory concentrations in mutants isolated in frequency-of-resistance (FoR) assays. Each point represents the MICs of a mutant line and the corresponding ancestor (log10 scale). Control and recent antibiotics are indicated by blue and orange panels, respectively. The color of the data points represents the bacterial species. The black dashed line indicated y = x (i.e. no changes in MIC in the mutants), whereas the red dashed line shows the antibiotic specific peak plasma concentration (Supplementary Table 1). For abbreviations, see Table 1.

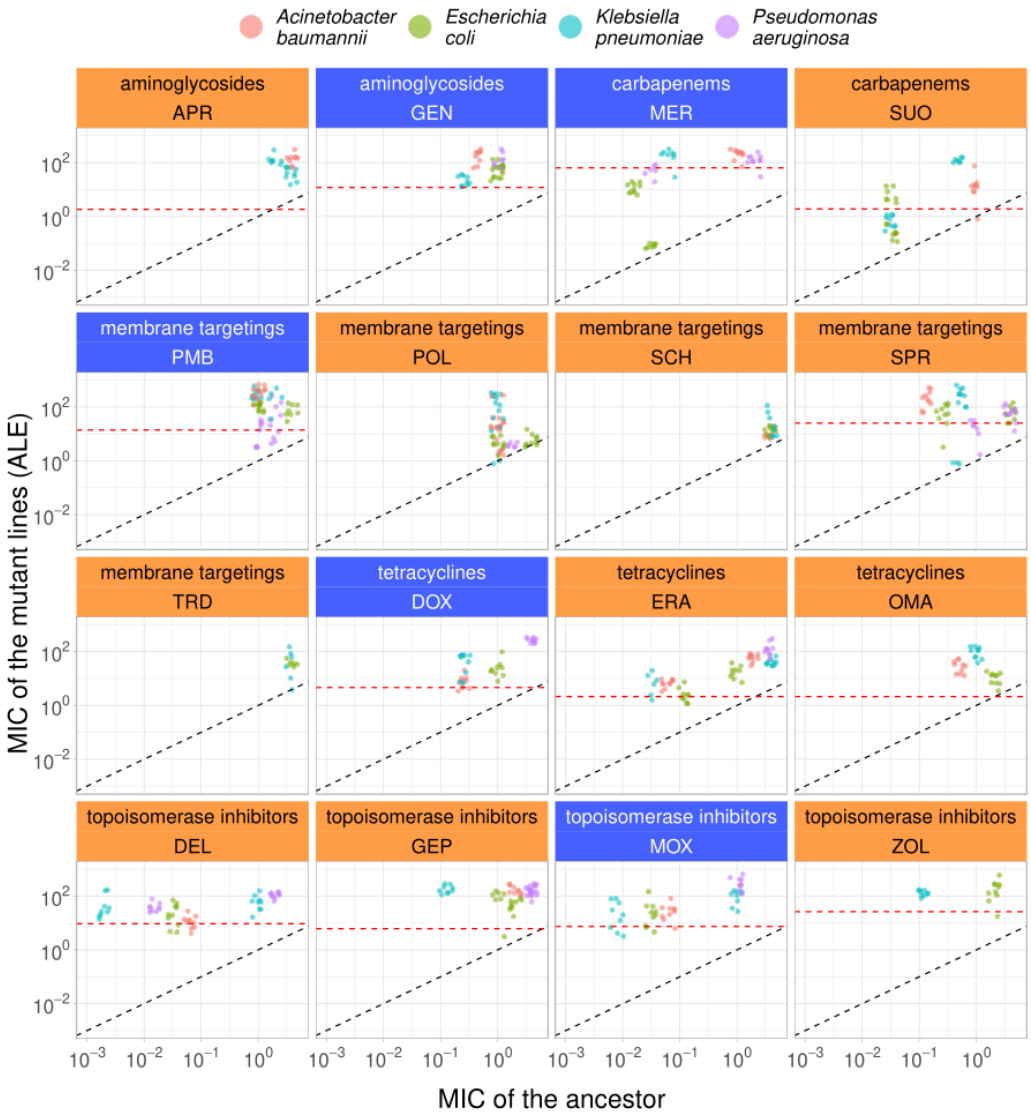

Fig. 3B. Changes in minimum inhibitory concentrations (MIC) after adaptive laboratory evolution (ALE). Each point represents the MICs of a laboratory evolved line and the corresponding ancestor (log10 scale). 'Control' and 'recent' antibiotics are indicated by blue and orange panels, respectively. The color of the data points represents the bacterial species. The black dashed line indicated y = x (i.e. no changes in MIC during the course of laboratory evolution), whereas the red dashed line shows the antibiotic specific peak plasma concentration. For abbreviations, see Table 1. Due to low stability in the liquid laboratory medium employed, cephaslosoporin antibiotics were not subjected to ALE.

Fig. 3C. **Relative MIC of laboratory evolved lines across all antibiotic-ancestor strain combinations.** Relative MIC is the MIC of the evolved line divided by the MIC of the corresponding ancestor. Each point is a laboratory evolved line, the colors indicate the bacterial species. The boxplots show the median, first and third quartiles, with whiskers showing the 5th and 95th percentiles. There is a highly significant heterogeneity in relative MIC across antibiotic-strain combinations (Kruskal-Wallis chi-squared = 630.43, df = 80, P < 2.2e-16). For antibiotic and bacterial strain abbreviations, see Table 1 and Supplementary Table 2.

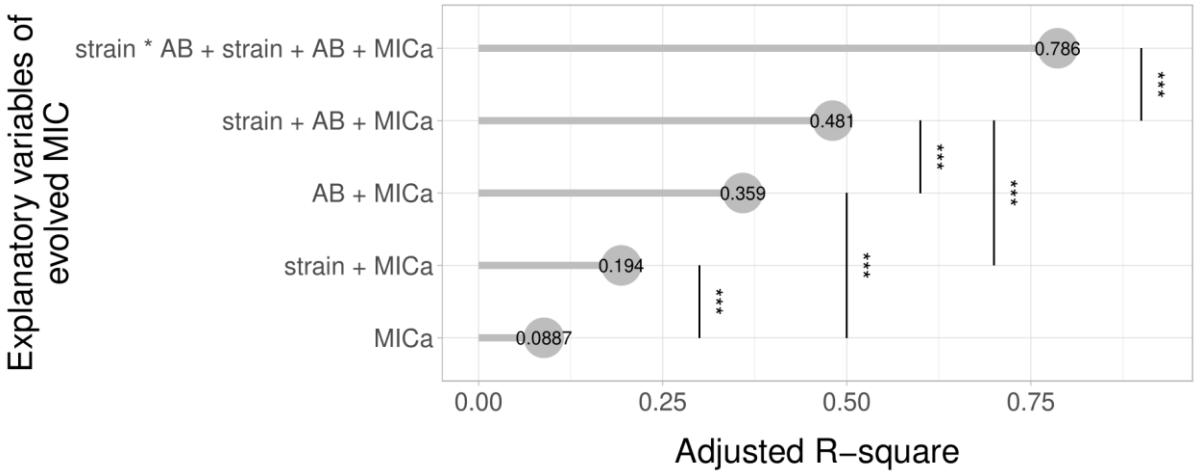

Fig. 3D. Multiple linear regression (MLR) analysis on features shaping the resistance level reached during evolution. The analysis focused on three main features i) the MIC level of the ancestor strain (MICa), ii) the antibiotic employed (AB) and the iii) genetic background (strain). The adjusted coefficient of determination (adjusted R-square) was used as a statistical metric to measure how much of the variation in evolved log-2 MIC can be explained by the variation in these features and combinations thereof, while adjusting for the number of parameters used in the fitted model. Additivity and interaction between explanatory variables are denoted with sign **+** and sign ***, respectively. We found a significant increase in adjusted R-square in all cases when a more complex model was compared to a simpler one (ANOVA, $P < 0.0001$).

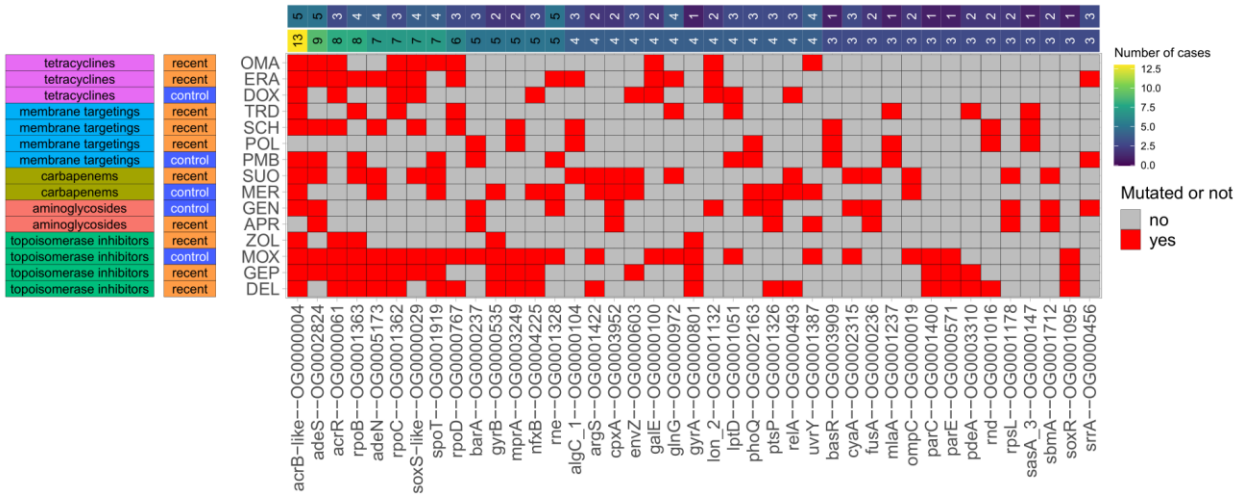

Fig. 4A. Repeatedly mutated genes during laboratory evolution across different antibiotics. The heatmap shows commonly mutated genes (and the corresponding orthogroups) across the tested antibiotics after adaptive laboratory evolution (ALE). Genes were considered commonly mutated if they accumulated non-synonymous mutations in response to at least three different antibiotic treatments. Panels on the left denote the class and the generation of the given antibiotics. Panels from top to bottom correspond to the number of antibiotic classes and the number of antibiotics a given orthogroup is mutated against. For further details, see Supplementary Table 7.

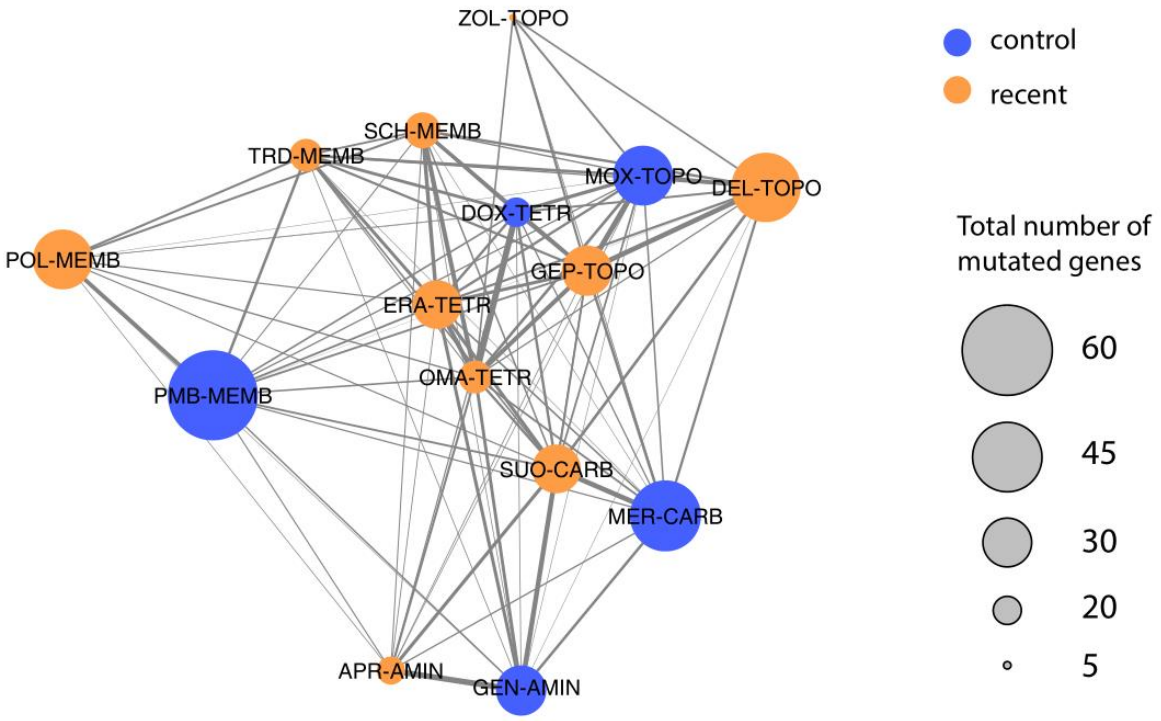

Fig. 4B. Mutation profile similarity across antibiotics. Each node represents a recent (orange) or control (blue) antibiotic. Links indicate an overlap in the set of mutated genes (or corresponding orthogroups) detected after adaptive laboratory evolution. Only non-synonymous mutations in protein coding genes were considered. The thickness of the links indicates the extent of overlap (calculated by Jaccard similarity) between antibiotic treatments. Abbreviations: TOPO: topoisomerase inhibitors, TETR: tetracyclines, AMIN: aminoglycosides, CARB: carbapenems, CEPH: cephalosporins, MEMB: membrane targeting antibiotics.

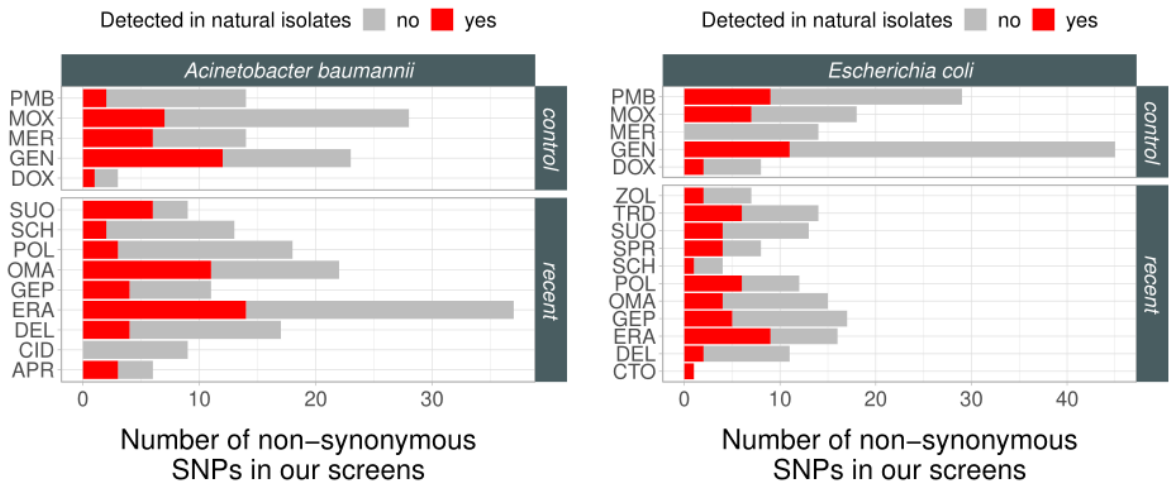

Fig. 4C. Non-synonymous mutations shared by laboratory evolved lines and natural isolates of *E. coli* and *A. baumannii.* The barplots show the number of non-synonymous mutations found in laboratory evolved *A. baumannii* (left panel) or *E. coli* (right panel) adapted to different antibiotics. Mutations also detected in the genomes of natural isolates of the same species are marked with red, whereas those that remained undetected are marked with gray. No significant difference was found in the fraction of non-synonymous mutations shared by natural strains between control and recent antibiotics (binomial regression model, P = 0.171). For abbreviations, see Table 1.

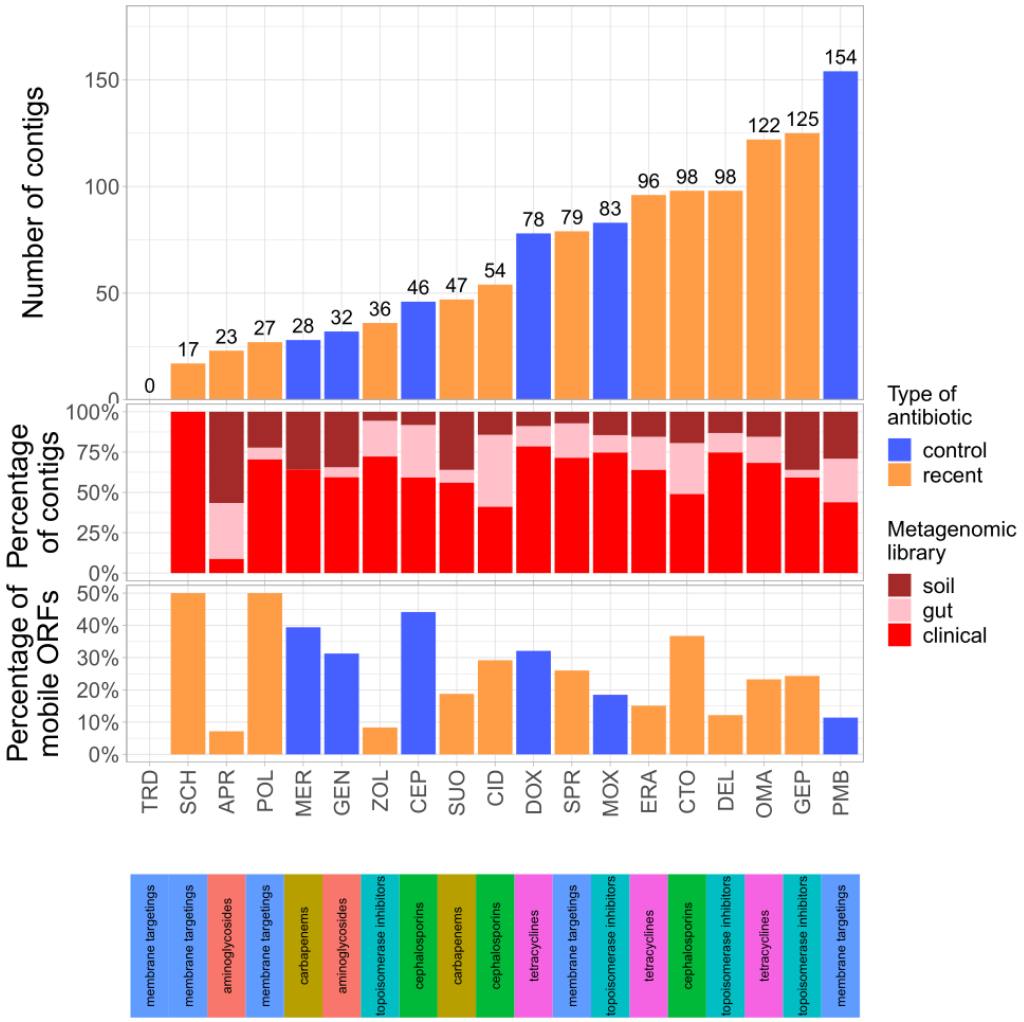

Fig. 5A. Functional selection of metagenomic libraries with 18 antibiotics resulted in numerous distinct resistance-conferring DNA contigs, with the only exception of tridecaptin M152-P3 (TRD). The barplot on the top shows the number of unique DNA fragments (contigs) that confer resistance to control (blue) and recent (orange) antibiotics, respectively, whereas the barplots at the bottom show the distribution of the identified resistance conferring contigs across metagenomic libraries and the percentage of mobile ORFs per antibiotic, respectively. ORF mobility was defined by evidence for recent horizontal gene transfer events or presence on mobile plasmids (see Methods). We observed no significant difference in the number of contigs against recent antibiotics and their corresponding control antibiotic (paired T-test, $t = -1.3286$, $df = 12$, $P = 0.2$). The same pattern is true for the percentage of mobile ORFs (paired T-test, $t = -0.31067$, $df = 12$, $P = 0.76$). For abbreviations, see Table 1.

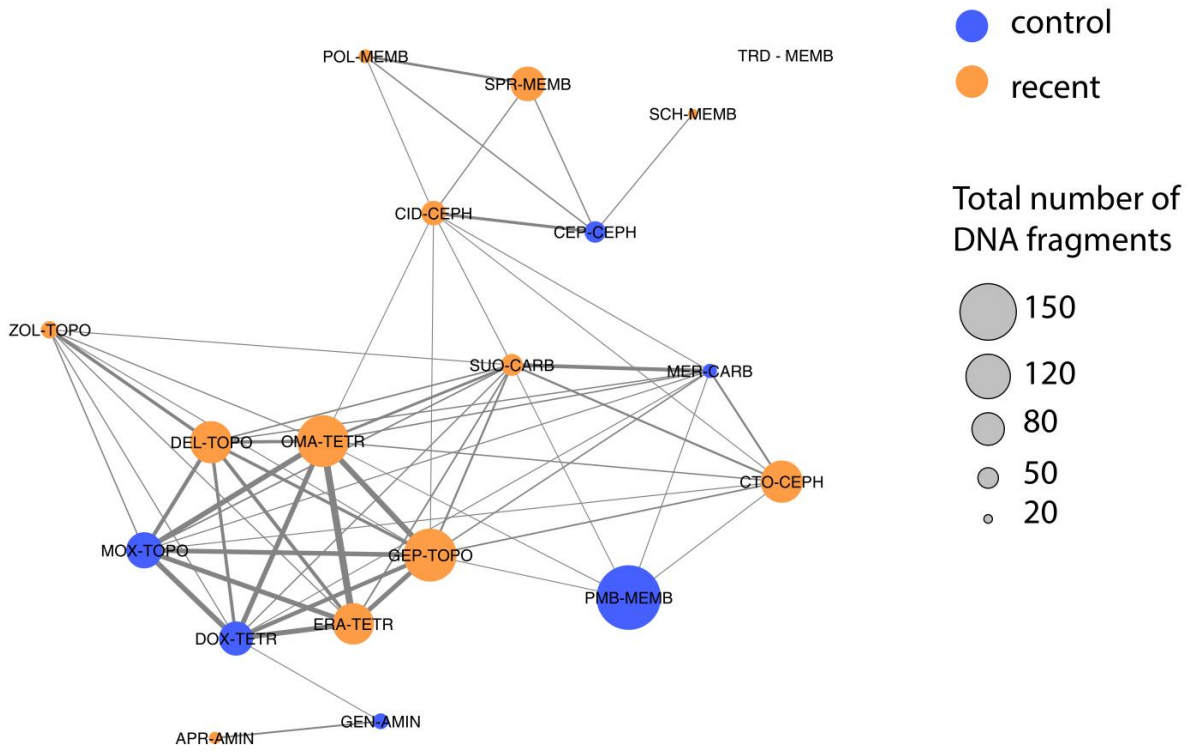

Fig 5B. Overlap in the set of resistance conferring DNA-fragments (contigs) across antibiotics. Each node represents a recent (orange) or control (blue) antibiotic, while links indicate overlap in the resistance conferring DNA contigs identified in functional metagenomic screens. The thickness of the link indicates the extent of overlap (calculated by Jaccard similarity) between antibiotic treatments. The size of the nodes corresponds to the total number of detected DNA fragments per antibiotic. The class a given antibiotic belongs to is also indicated (TOPO: topoisomerase inhibitors, TETR: tetracyclines, AMIN: aminoglycosides, CARB: carbapenems, CEPH: cephalosporins, MEMB: membrane targeting antibiotics). For abbreviations, see Table 1.

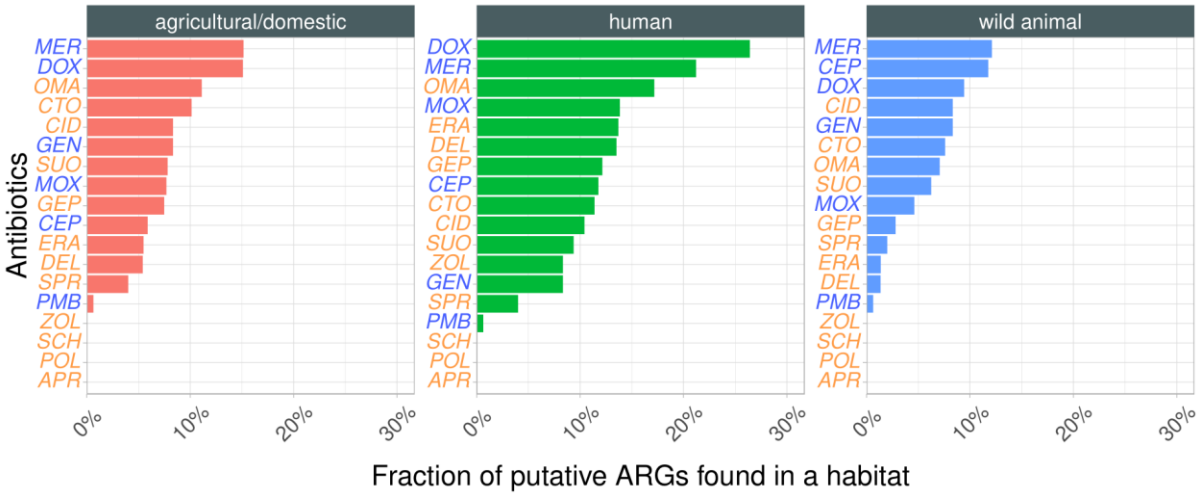

Fig 5C. Putative ARGs against various antibiotics are present in natural *E. coli* genomes. The barplot shows the fraction of putative ARGs detected in natural genomes of *E. coli* in a given habitat across control (blue labels) or recent (orange labels) antibiotics. For each habitat, no significant difference was found between the fraction of putative ARGs conferring resistance to control and recent antibiotics (binomial regression model, P = 0.786/0.608/0.302 for agricultural/domestic, human and wild animal, respectively). For abbreviations, see Table 1.

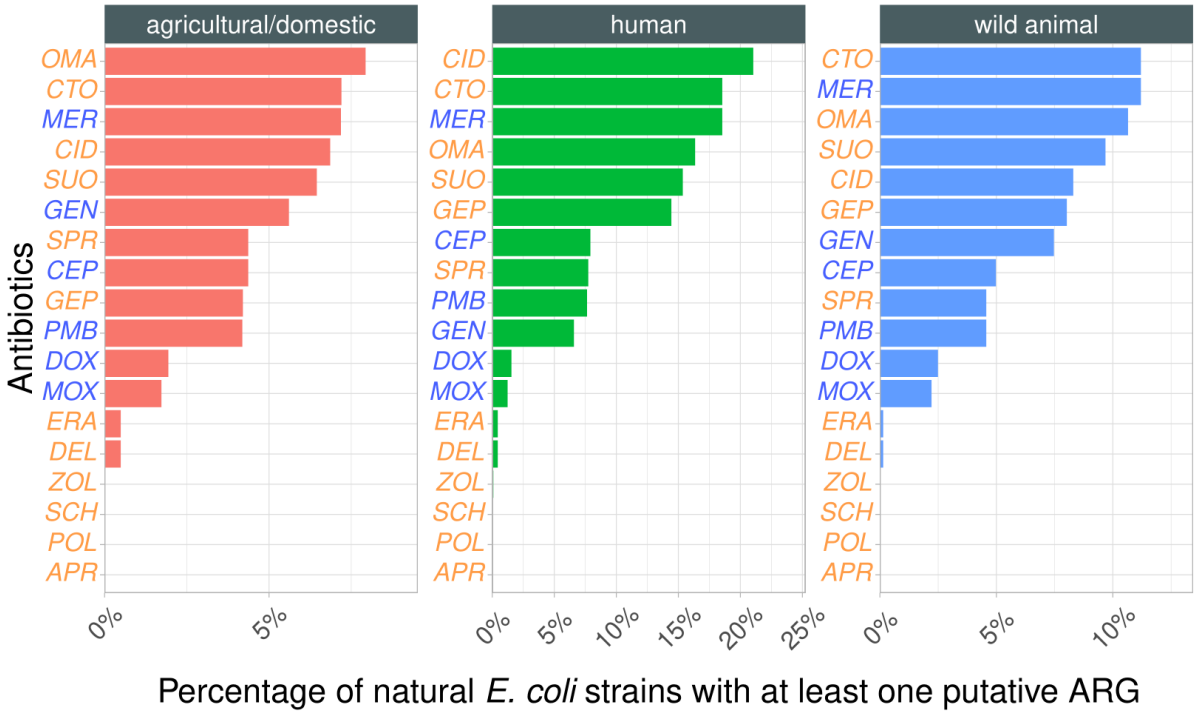

Fig 5D. Natural *E. coli* genomes with at least one putative ARG against specific recent antibiotics. The barplot shows the fraction of natural *E. coli* genomes with at least one putative ARGs (present in less than 10% of the investigated genomes) against control (blue label) and recent (red label) antibiotics. For each habitat, we found significant differences between the percentage of natural *E. coli* strains with at least one such putative ARGs that confer resistance to control and recent antibiotics (binomial regression model, $P < 0.01$). For abbreviations, see Table 1.

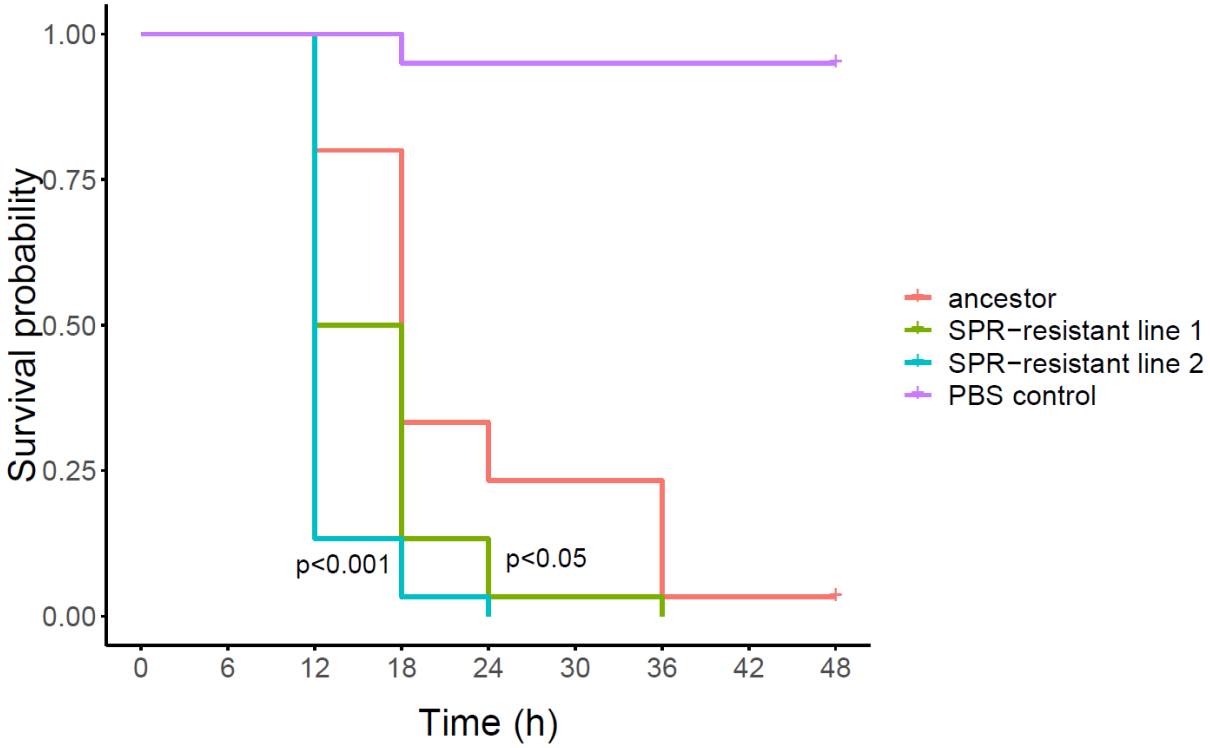

Fig. 6A. *In vivo* virulence of SPR206-resistant lines in a *Galleria mellonella* infection model. Kaplan-Meier survival curve depicts the survival probabilities for animals infected with the ancestor (KP-SEN, that is *K. pneumoniae* ATCC 10031) and the corresponding SPR206-resistant lines (resistant line 1, i.e., KP-SEN SPR FoR #1 and resistant line 2, i.e., KP-SEN SPR FoR #3). The phosphate buffered saline (PBS) control group received one injection of sterile phosphate buffered saline. The resistant lines display significantly elevated virulence compared to the ancestor ($P < 0.05$ for line #1 and $P < 0.001$ for line #3, respectively). P-values were calculated using standard log-rank tests. Experiments were performed in three biological replicates, with 10 animals per treatment group, hence each curve represents 30 animals. For abbreviations, see Supplementary Table 2.

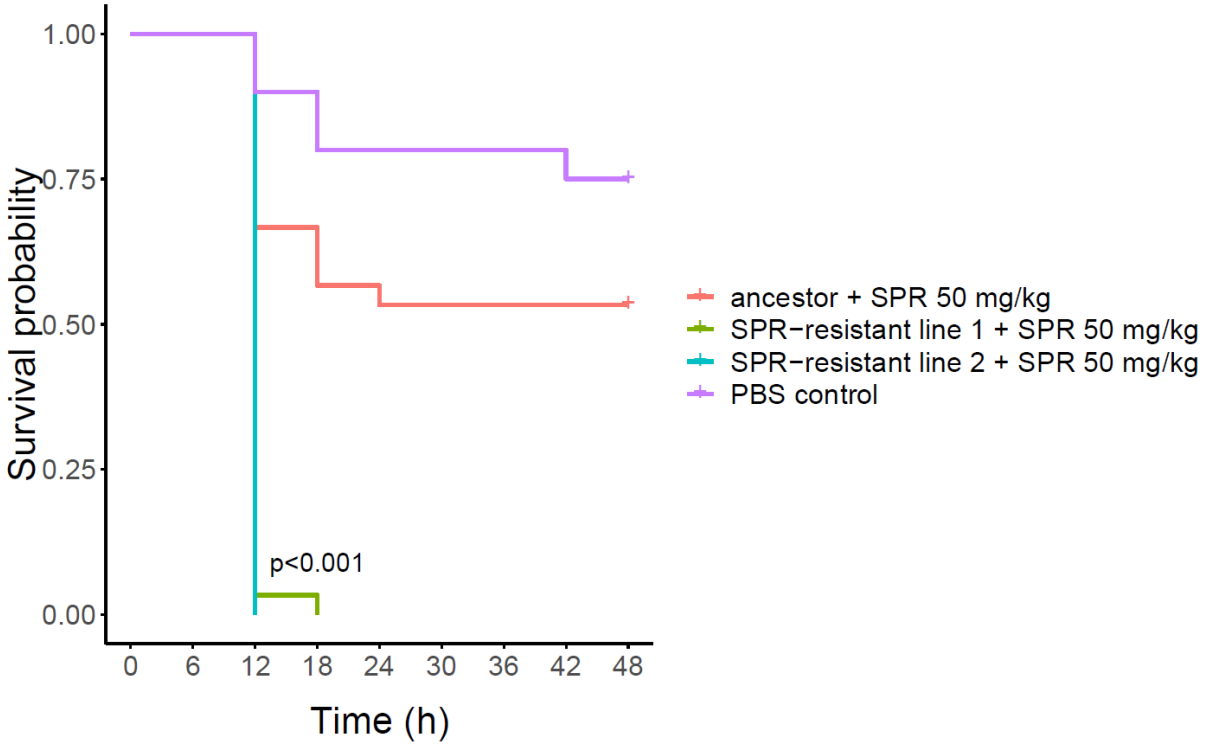

Fig. 6B. Infection of *Galleria mellonella* with SPR206-resistant lines leads to antibiotic treatment failure. Kaplan-Meier survival curve depicting the survival probabilities for animals infected with the ancestor (KP-SEN, that is *K. pneumoniae* ATCC 1031) and two corresponding SPR206-resistant lines (resistant line 1, i.e., KP-SEN SPR FoR #1 and resistant line 2, i.e., KP-SEN SPR FoR #3). Each animal received a one-time dose of 50 mg/(body weight kg) SPR206 via injection to the hemocoel within 2 hours of bacterial injection. The phosphate buffered saline (PBS) control group received one injection of sterile phosphate buffered saline. While animals injected with the wild type bacteria had approximately 60% survival at the termination of the experiment, 100% of the animals infected with the SPR206-resistant lines perished within 18 hours despite the antibiotic treatment ($P < 0.001$ for both lines #1 and #3, P-values were calculated using standard log-rank test.) Experiments were performed in three biological replicates, with 10 animals per treatment group, hence each curve represents 30 animals. For abbreviations, see Supplementary Table 2.

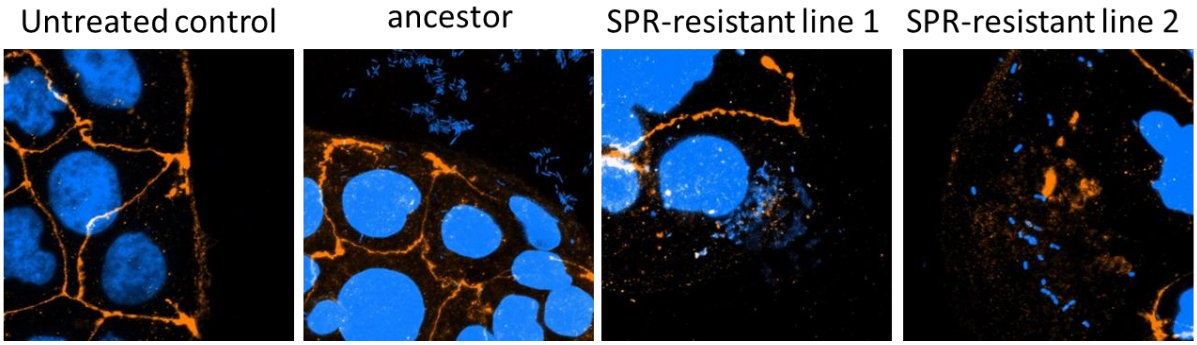

Fig. 6C. *K. pneumoniae* SPR206-resistant lines show increased penetration into human cells. Representative images showing bacterial invasion into Caco-2 human epithelial cells compared to uninfected cells (untreated control). The strains studied are the antibiotic sensitive ancestor (KP-SEN, i.e. *K.pneumoniae* ATCC 10031) and two corresponding SPR206-resistant lines (resistant line 1, i.e., KP-SEN SPR FoR #1 and resistant line 2, i.e., KP-SEN SPR FoR #3). The membrane of Caco-2 cells is fluorescently labeled by ZO-1 (orange color). ZO-1 stabilizes the tight junction solute barrier through coupling to the perijunctional cytoskeleton. In addition, the nuclei of Caco-2 cells and bacteria are stained by Hoechst dye (blue color). The ZO-1 signal indicates that bacterial cells can penetrate through the human cell membrane. For abbreviations, see Supplementary Table 2.

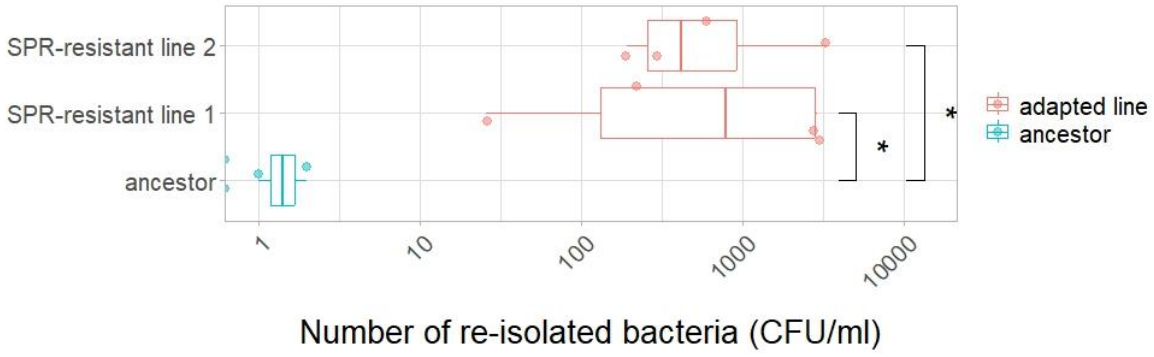

Fig. 6D. Bacterial invasion assay with antibiotic sensitive and SPR206-resistant *K. pneumoniae* lines The strains studied are the antibiotic sensitive ancestor (KP-SEN, i.e. *K.pneumoniae* ATCC 10031) and two corresponding SPR206-resistant lines (resistant line 1, i.e., KP-SEN SPR FoR #1 and resistant line 2, i.e., KP-SEN SPR FoR #3). After 3h infection, extracellular bacteria were eliminated by 24h gentamicin treatment. Bacterial invasion of Caco-2 cells was quantified by determining the number of colony-forming units (CFU). Experiments were performed in 4 biological replicates. Boxplots show the median, first and third quartiles, with whiskers showing the 5th and 95th percentiles. P-values were calculated using the Wilcoxon rank sum test (* indicates $P < 0.05$). For abbreviations, see Supplementary Table 2.

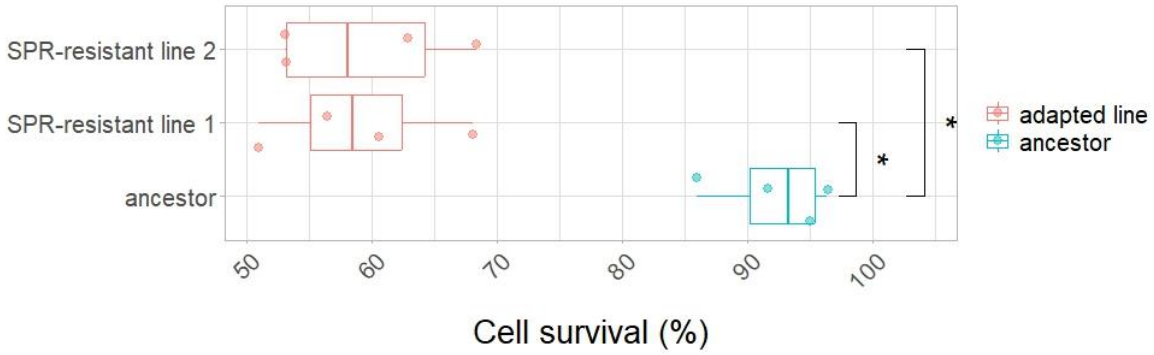

Fig. 6E. SPR206-resistant KP-SEN lines display elevated cytotoxicity in Caco-2 cells. The figure shows the results of a clonogenic cell-survival survival assay. The strains studied are the antibiotic sensitive ancestor (KP-SEN, i.e. *K.pneumoniae* ATCC 10031) and two corresponding SPR206-resistant lines (resistant line 1, i.e., KP-SEN SPR FoR #1 and resistant line 2, i.e., KP-SEN SPR FoR #3). After 3h infection, intra- and extracellular bacteria were eliminated by 24h primocin treatment, and the fraction of surviving Caco-2 cells was calculated using standard protocols. Experiments were performed in 4 biological replicates. Boxplots show the median, first and third quartiles, with whiskers showing the 5th and 95th percentiles. P-values were calculated using the Wilcoxon rank sum test (* indicates $P < 0.05$). For abbreviations, see Supplementary Table 2.

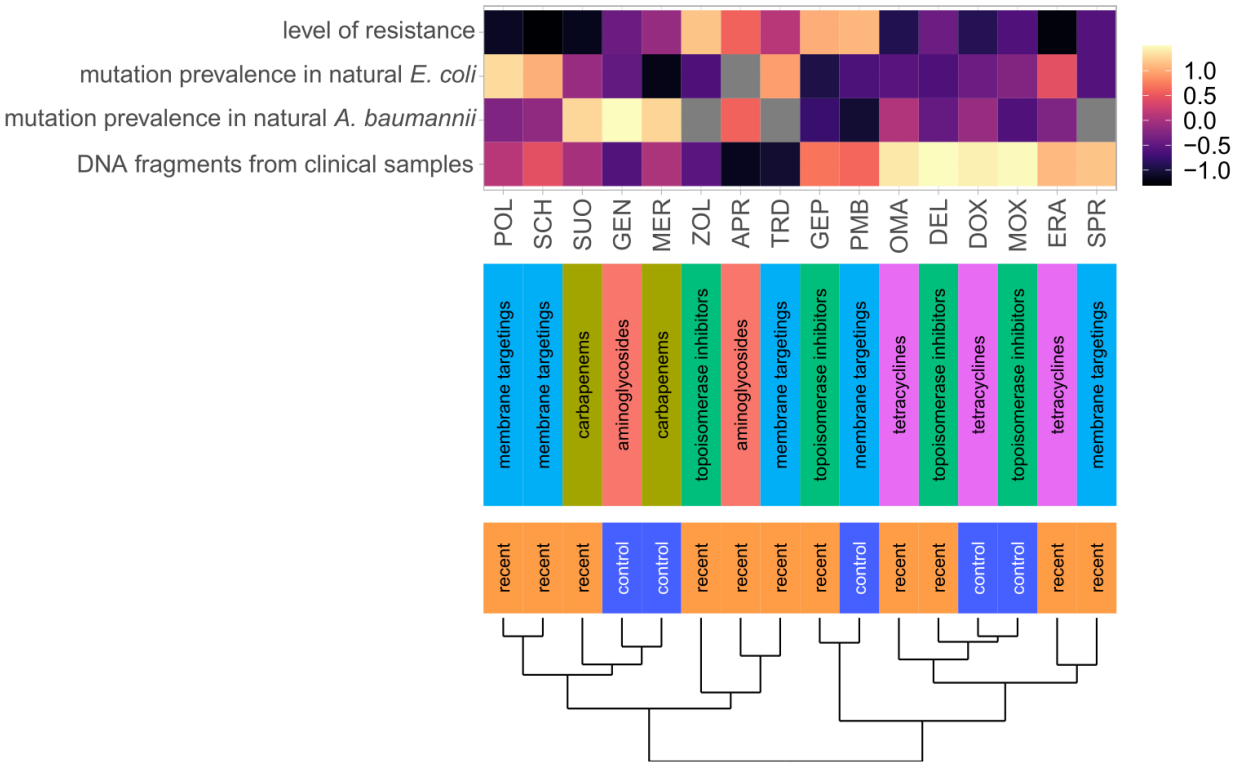

Fig 7. Resisto-plane for each antibiotic studied in this work. The heatmap shows various types of metrics for each antibiotic studied throughout the work. The scale-transformed metric values for each antibiotic are as follows: i) level of resistance, that is the median of all MIC values across each adapted bacterial strains, ii) mutation prevalence in natural *E. coli* and *A. baumannii* strains, that is the fraction of such laboratory observed adaptive mutations that are already present in natural *E. coli* and *A. baumannii* strains, respectively, and iii) DNA fragments from clinical samples, that is the number of unique DNA fragments identified from the clinical metagenomics library. Grey color denotes missing value, due to initial resistance in the studied species. The panels below the heatmap denote the generation and the class the given antibiotic belongs to. Antibiotic clustering (bottom panel) was based on calculating euclidean distance of metric values and using the complete hierarchical clustering method.

Supplementary Figures

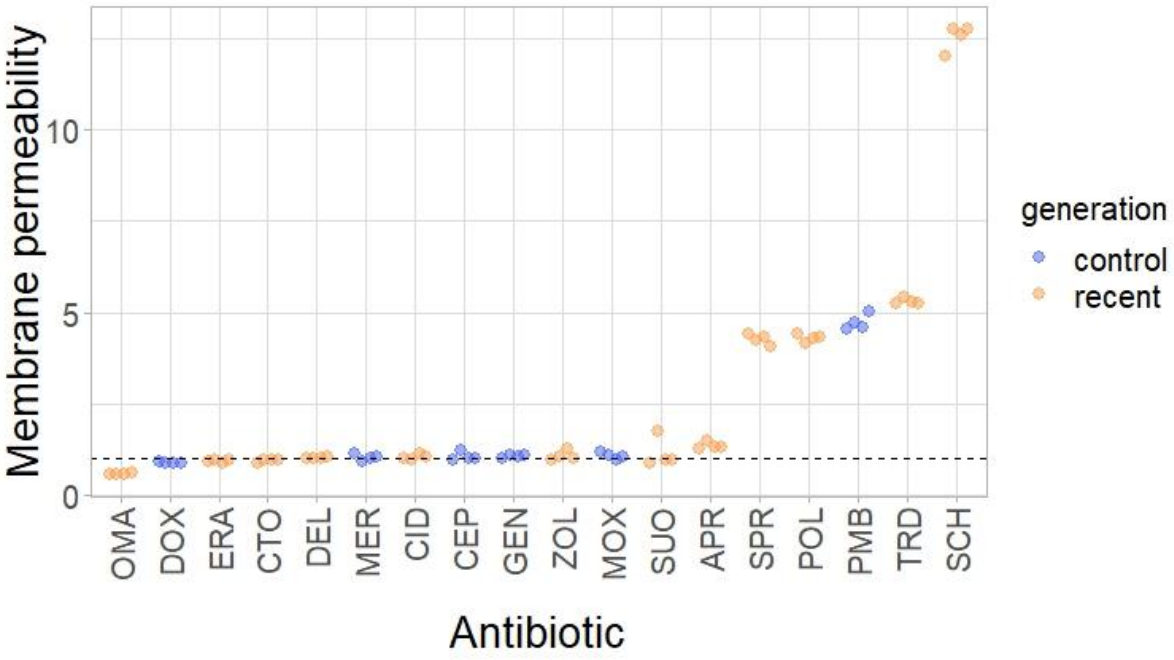

Supplementary Fig 1. Outer membrane permeabilization induced by the antibiotic was detected by a fluorescent probe (1-N-phenylnaphthylamine, i.e., NPN) uptake (four replicates per treatment). *E. coli* ATCC25922 (EC-SEN) were exposed to different antibiotics treatment (at a concentration of 4×MIC) and the intracellular accumulation of the probe was normalized to that of the untreated control. The fluorescence intensity of NPN gradually increases due to damage to the bacterial outer membrane by SCH, TRD, POL, SPR and PMB. The dashed line indicates the normalized untreated control. For antibiotic abbreviations, see Table 1.

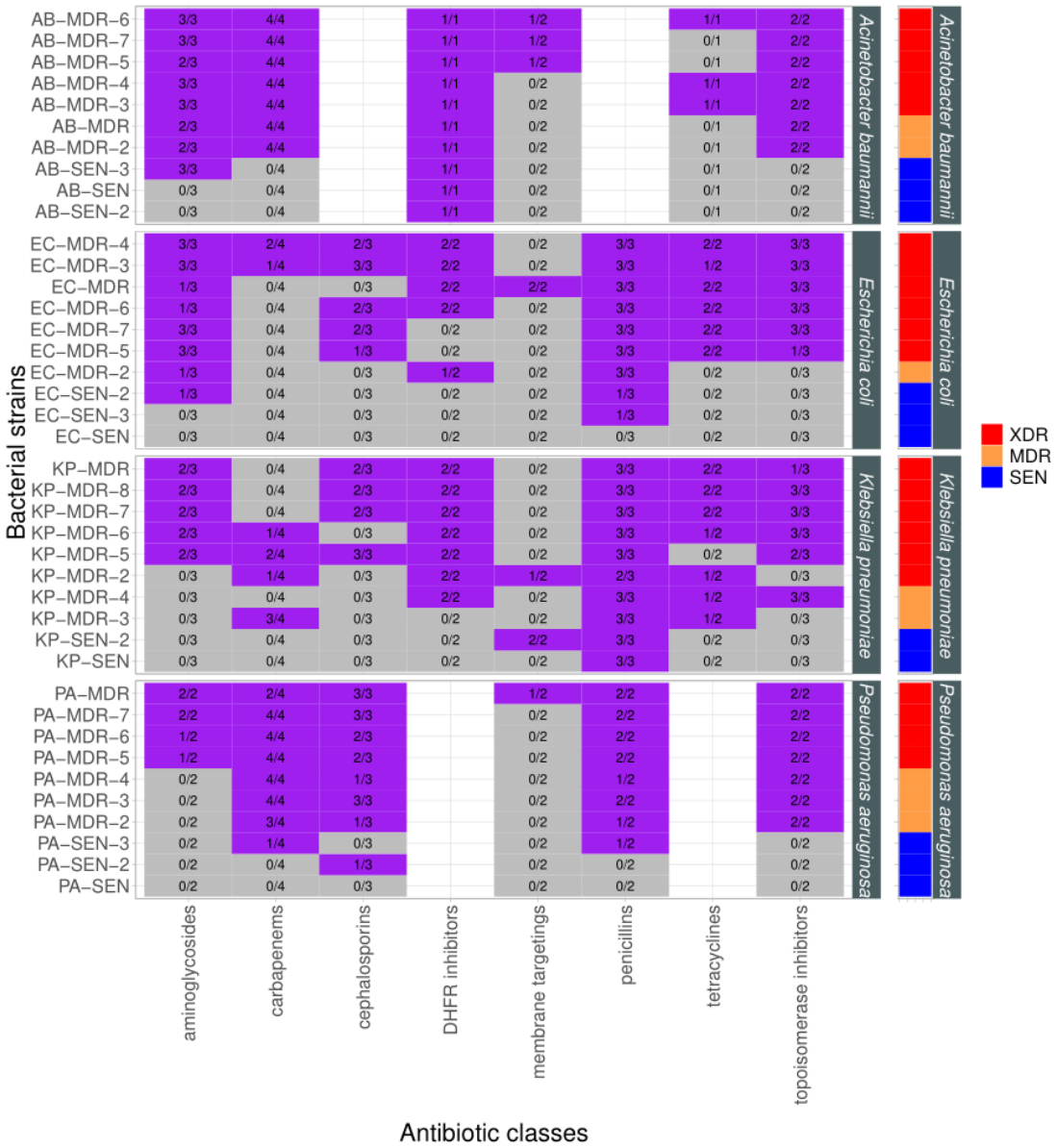

Supplementary Fig 2. The heatmap shows the resistance profile of 40 bacterial strains against 8 different antibiotic classes. Strains resistant and sensitive to a given antibiotic class (based on clinical breakpoints) are represented by purple and gray, respectively. The numbers correspond to the number of drugs a strain is resistant to out of the number of drugs tested. The right panel classifies the strains based on their resistance profile as sensitive (SEN), multidrug-resistant (MDR), or extremely drug-resistant (XDR). Strains are classified as MDR, if being resistant to 3 or 4 antibiotic classes and XDR if being resistant to 5 or more antibiotic classes, respectively[100]. For strain abbreviations, see Supplementary Table 2.

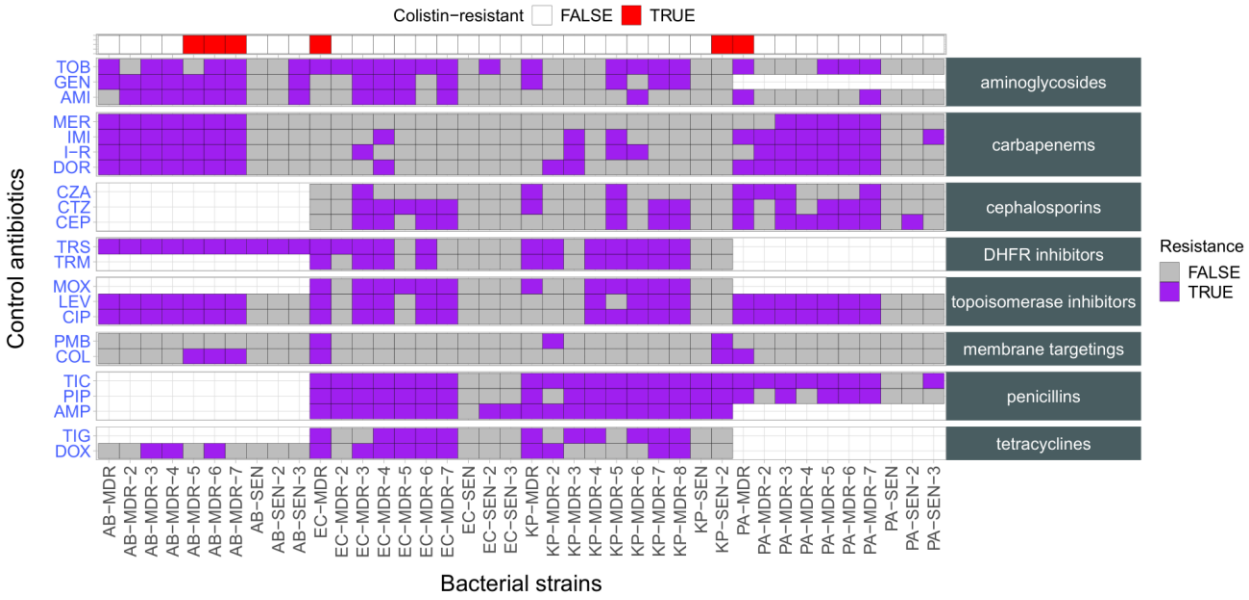

Supplementary Fig 3. The heatmap shows the resistance profile of 40 bacterial strains against control drugs. Antibiotics are grouped by the antibiotic classes they belong to. Bacterials strains are ordered by the fraction of resistance against control antibiotics. Strains resistant and sensitive to a given antibiotic are represented by purple and gray, respectively. Resistance is defined as having an MIC value greater than the clinical breakpoint in a given species. Accordingly, missing values indicate the absence of clinical breakpoints in certain combinations of species and antibiotics. Strains that are colistin-resistant are indicated in the top panel. For abbreviations, see Table 1 and Supplementary Table 2.

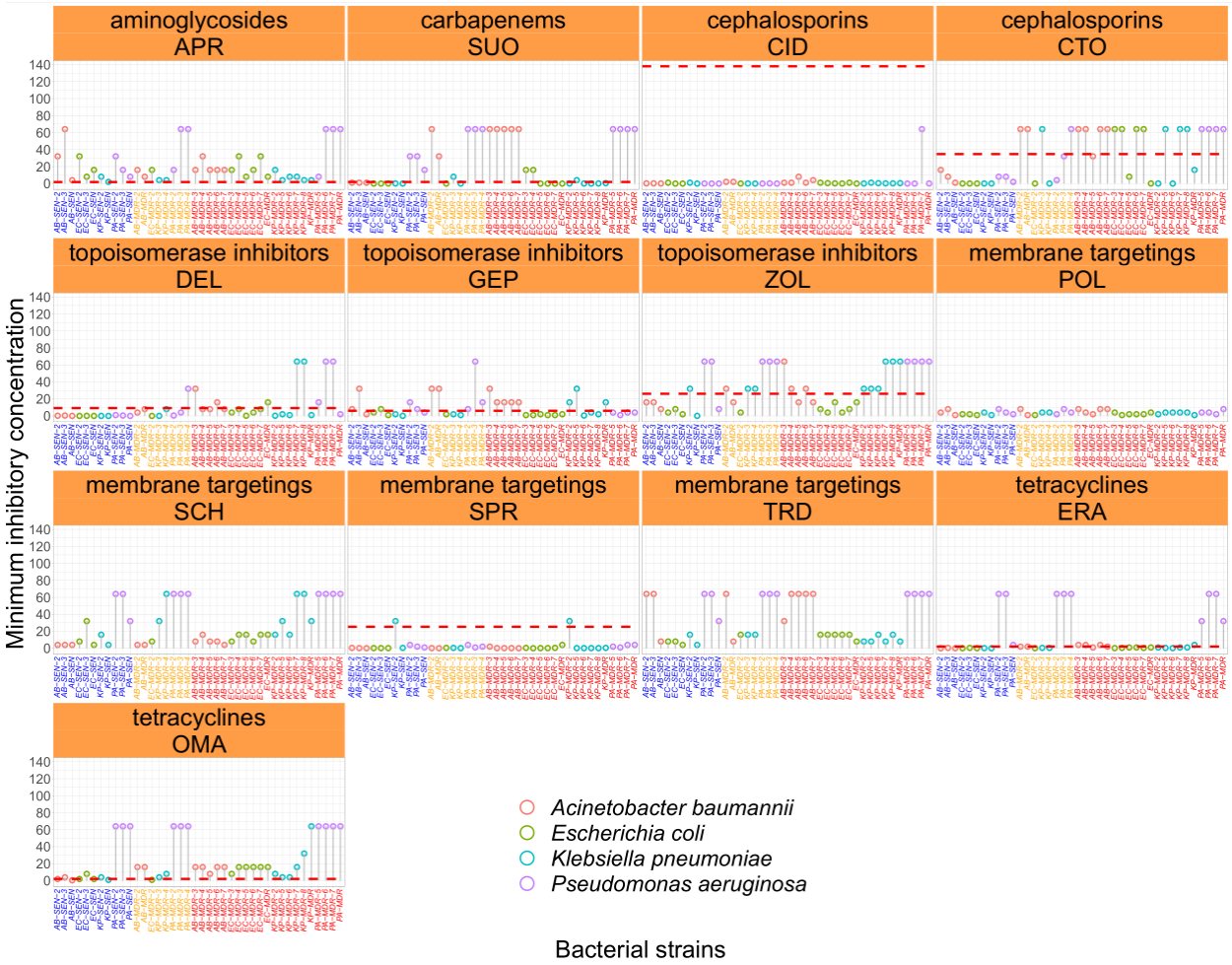

Supplementary Fig 4. The figure shows the antibiotic susceptibility of 40 strains to 'recent' antibiotics. Blue, orange, and red labels indicate sensitive (SEN), multidrug-resistant (MDR), or extremely drug-resistant (XDR) strains, respectively. The color of the points marks the bacterial species. Dashed line indicates the estimated antibiotic specific peak-plasma concentration (see Supplementary Table 1). For abbreviations, see Table 1 and Supplementary Table 2.

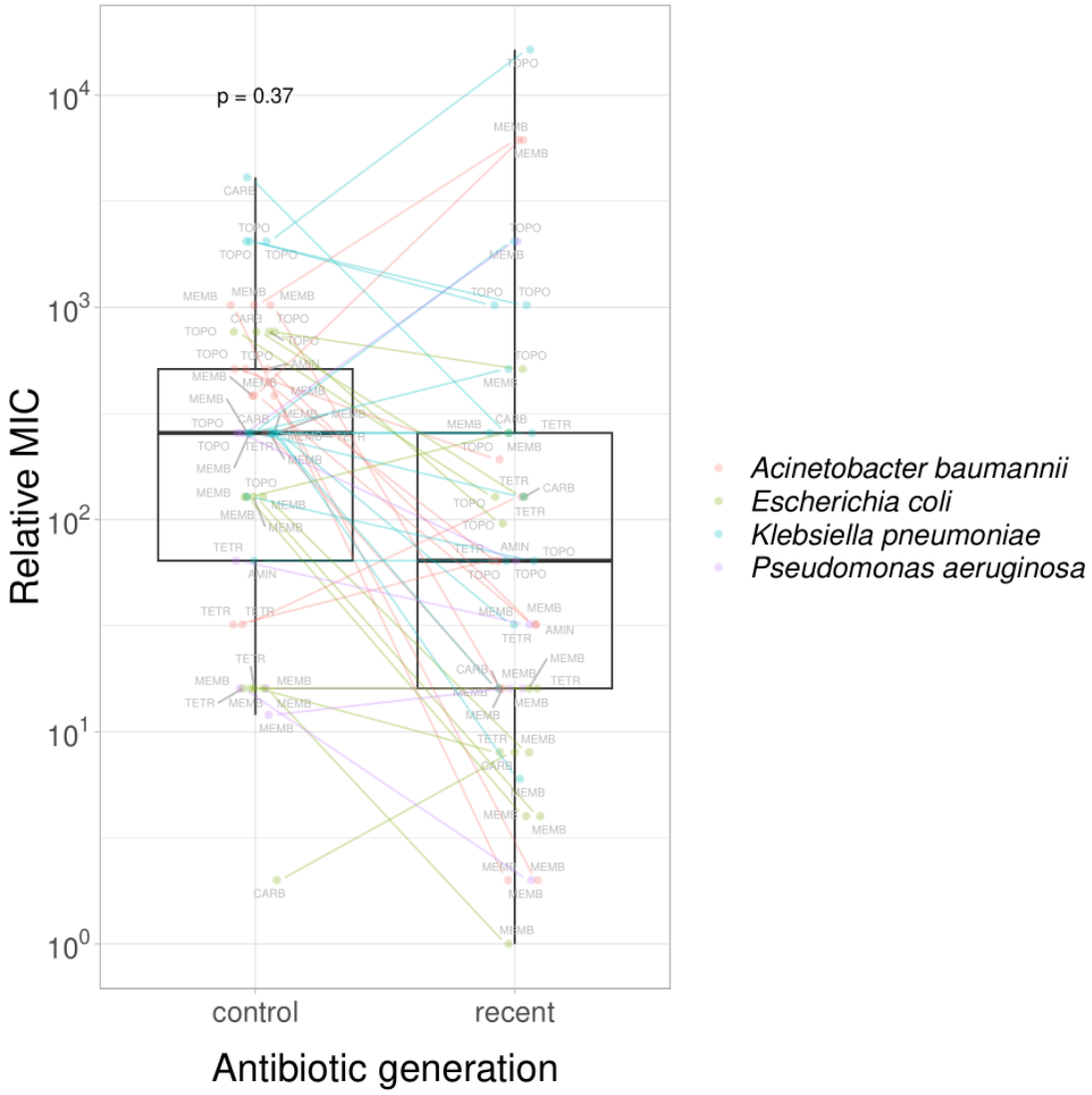

Supplementary Fig 5. Control and recent antibiotics are equally prone to resistance. The boxplot shows the relative MIC of control and recent antibiotics from adaptive laboratory evolution (ALE). The lines connect different generations of antibiotic belonging to the same antibiotic class (labels). We found no significant difference between the control and recent antibiotics (paired T-test, P = 0.37).

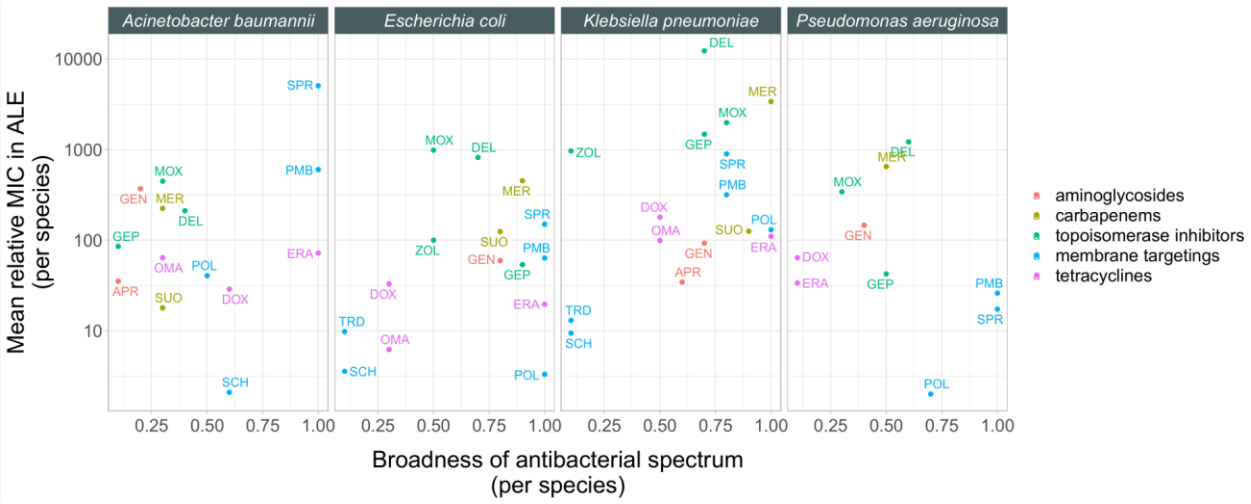

Supplementary Fig 6. No connection between the broadness of spectrum and susceptibility for resistance development. The scatterplot shows the mean relative MIC of adapted lines per species from ALE against the broadness of antibacterial spectrum per species for a given antibiotic. Broadness of spectrum was estimated for each antibiotic by calculating the fraction of strains (per species) resistant to it (using the 4 mg/L concentration as MIC cutoff). Colors indicate the class a given antibiotic belongs to. We found no correlation between the broadness of antibacterial spectrum and the level of resistance reached by ALE (Spearman's correlation, *A. baumannii*: r = 0.132, P = 0.653, *E. coli*, r = 0.188, P = 0.502, *K. pneumoniae*, r = 0.371, P = 0.174, *P. aeruginosa*, r = -0.404, P = 0.247). For abbreviations, see Table 1.

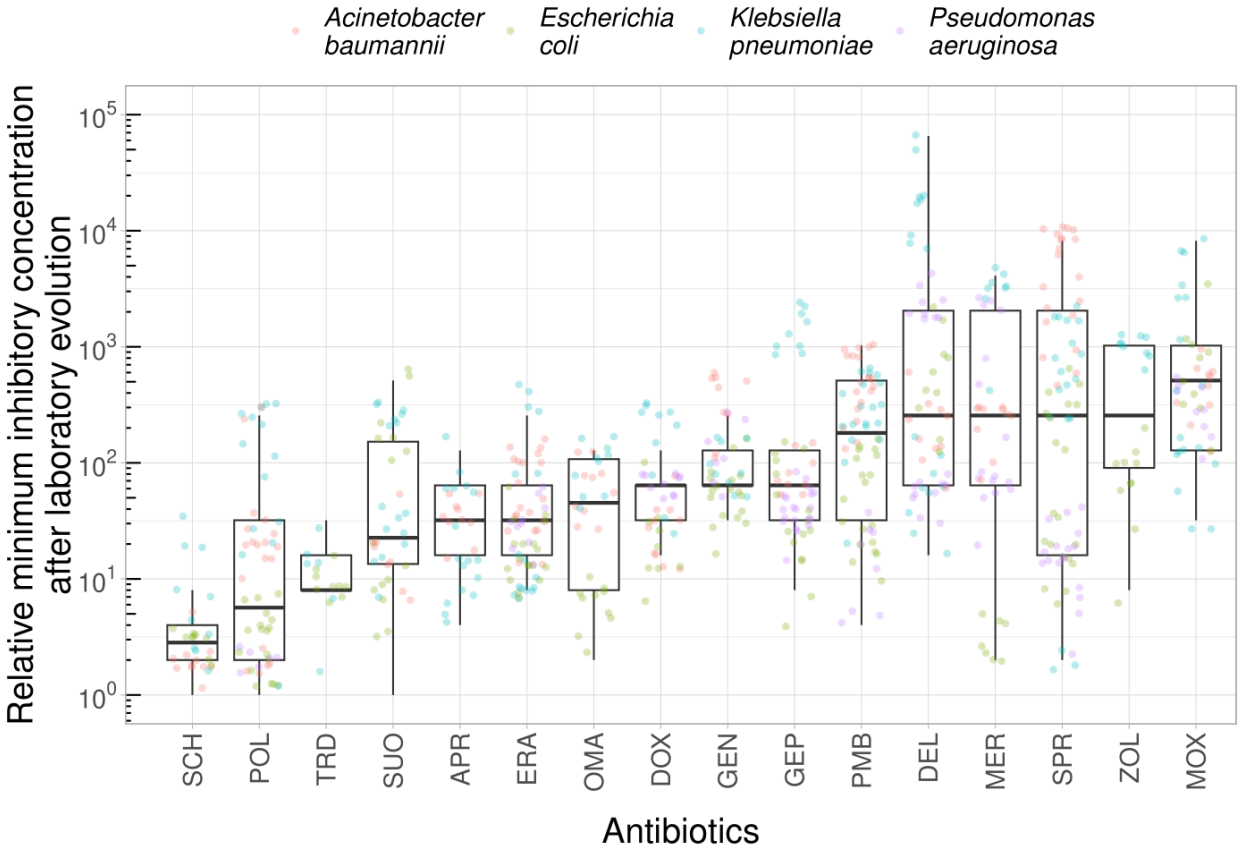

Supplementary Fig 7. Relative MIC of laboratory evolved lines across all antibiotics. Relative MIC is the MIC of the evolved line divided by the MIC of the corresponding ancestor. Each point is a laboratory evolved line, the colors indicate the bacterial species. The boxplots show the median, first and third quartiles, with whiskers showing the 5th and 95th percentiles. There is a highly significant heterogeneity in relative MIC across antibiotics (Kruskal-Wallis chi-squared = 281.03, df = 15, P < 2.2e-16). For antibiotic abbreviations, see Table 1.

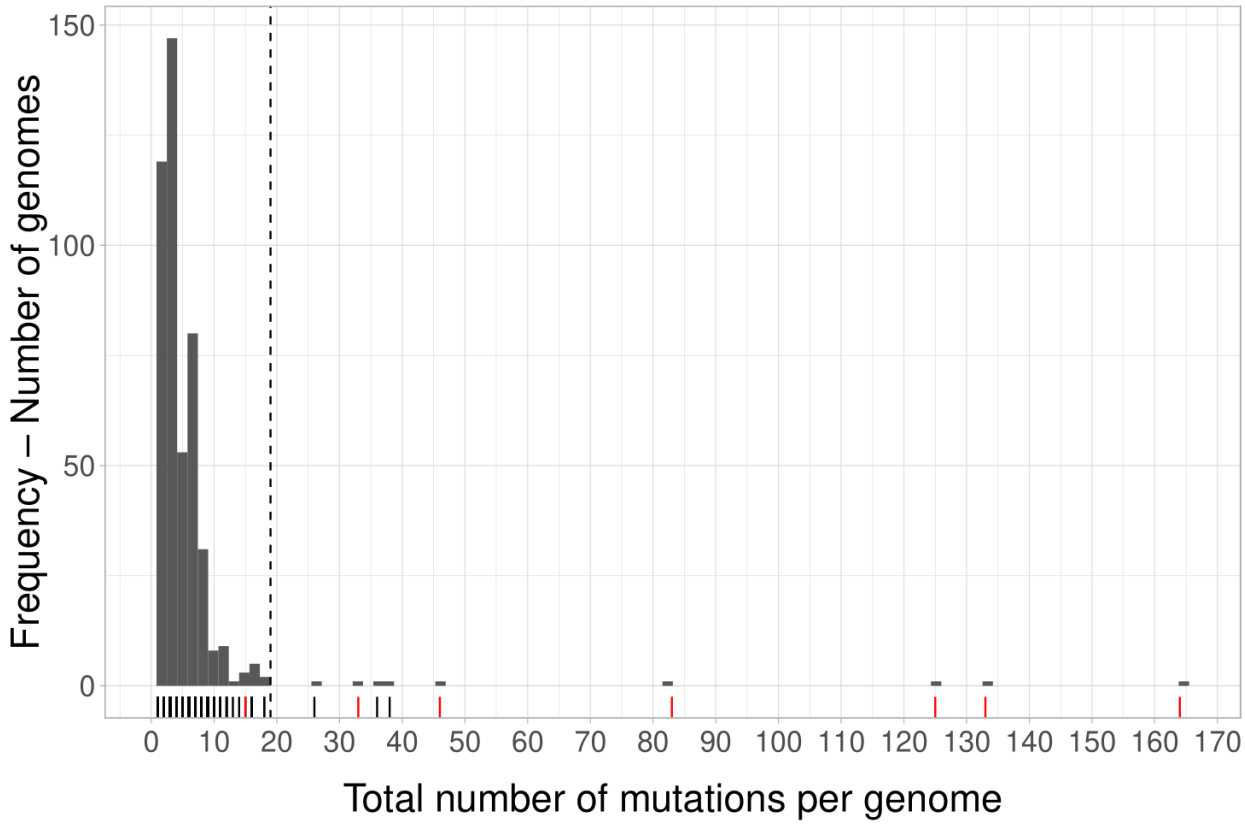

Supplementary Fig 8. The histogram shows the distribution of the total number of mutations that has accumulated during the course of laboratory evolution. Resistant lineages derived from laboratory evolution (n=332) and frequency-of-resistance (n=135) assays are depicted here. 10 resistant lineages accumulated exceptionally large numbers of mutations (>18, see Methods), 6 of which accumulated mutations in methyl-directed mismatch repair (mutL, mutS or mutY). For these two reasons these lineages are likely to be hypermutator lines, and were excluded from further analysis.

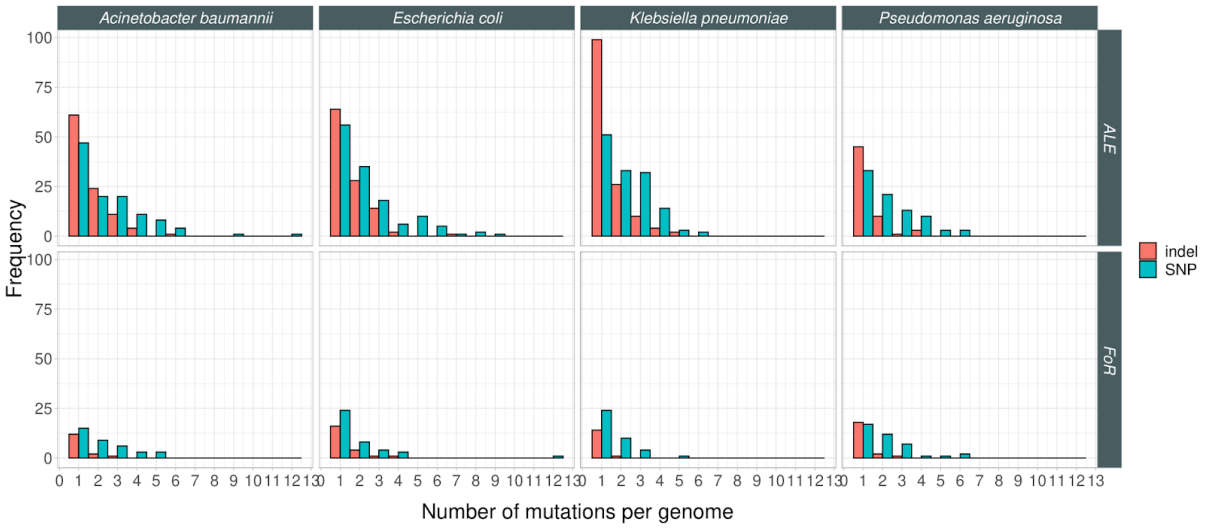

Supplementary Fig 9. Distribution of SNPs and indels in resistant lines across four bacterial species. Red and green colors denote short indels and SNPs, respectively. As expected, lines derived from short-term frequency-of-resistance assays (FoR) have accumulated fewer mutations (Wilcoxon rank sum test, $P < 2.2e-16$), when compared to lines derived from adaptive laboratory evolution (ALE).

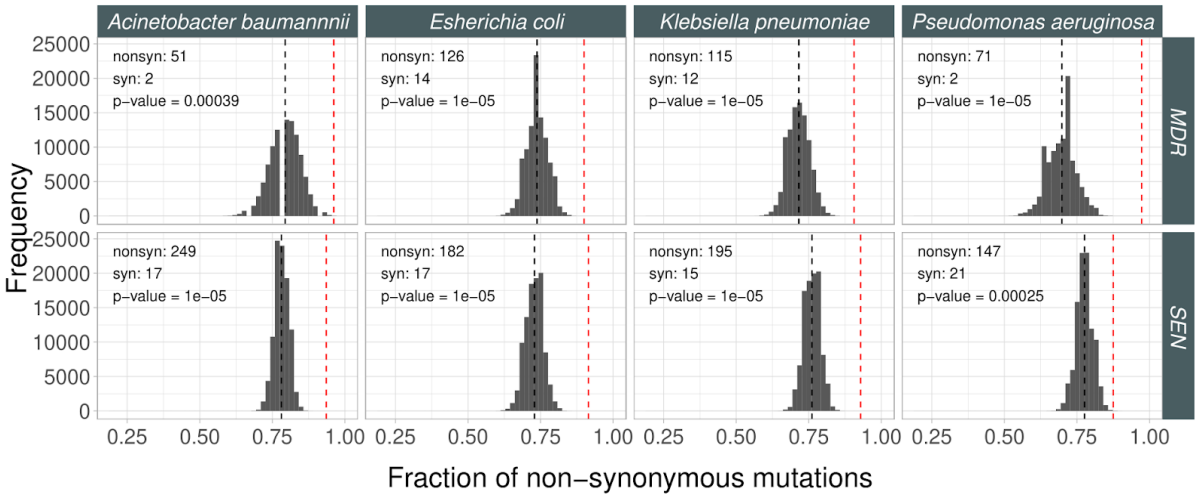

Supplementary Fig 10. Fraction of non-synonymous mutations. To assess the signatures of adaptive evolution in our genomic samples from ALE and FoR assay, we tested whether the fraction of non-synonymous mutational events within all SNPs in the coding region was higher than expected based on a purely neutral model of evolution using an established method[101]. For each bacterial strain background, we identified all SNPs in the coding regions, counted the number of non-synonymous (*nonsyn*) and synonymous (*syn*) ones and calculated the observed fraction of non-synonymous mutations (red dashed line) as follows: nonsyn / nonsyn + syn, where nonsyn and syn are the number of non-synonymous and synonymous mutations, respectively. Next, we randomly generated the same number of SNPs at random coding positions along the genome as observed in the mutation dataset. We repeated this step 5000 times, then plotted the fraction of non-synonymous mutations as histograms for each species (columns) and strain type (rows). Next, we calculated the probability (P-value) that the fraction of nonsynonymous mutations was equal to or higher in the real data than that of in the randomly generated one.

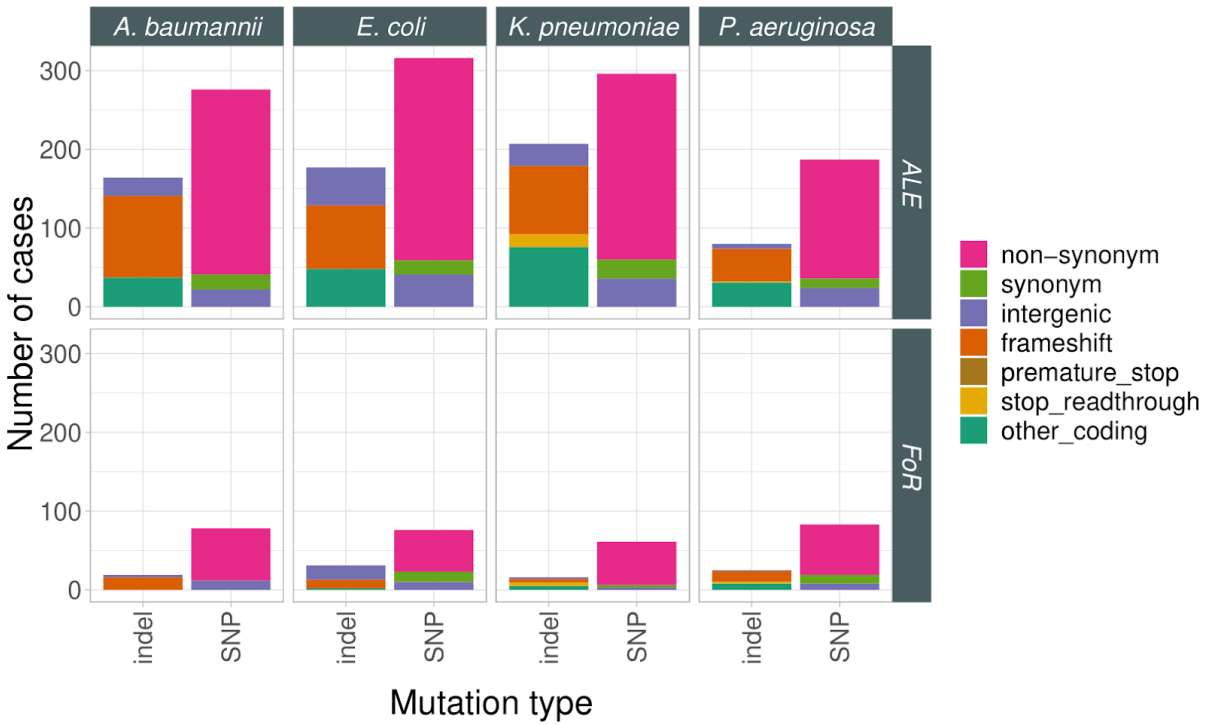

Supplementary Fig 11. Distribution of different mutational events. Top and bottom row correspond to the adapted lines originating for laboratory evolution (ALE) and frequency of resistance (FoR) assays, respectively.

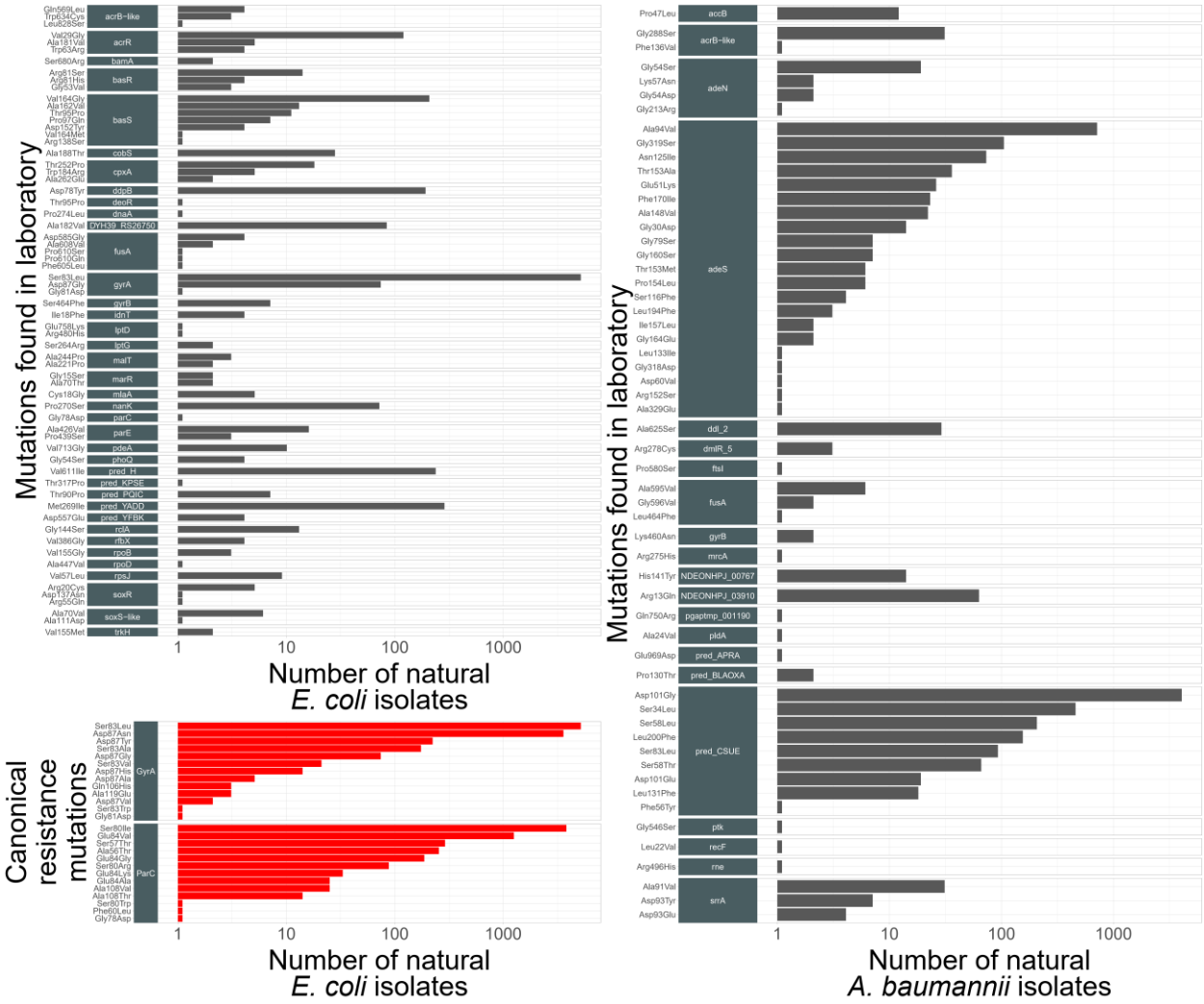

Supplementary Fig 12. Non-synonymous mutations shared by laboratory evolved lines and natural isolates of *E. coli* and *A. baumannii*. The barplot shows the number of natural isolates with the same non-synonymous mutation that arose during laboratory evolution of resistance. The corresponding genes possessing non-synonymous mutations are labelled with dark gray strips. The bottom left panel shows the number of natural strains with canonical resistance mutations (source: Pointfinder).

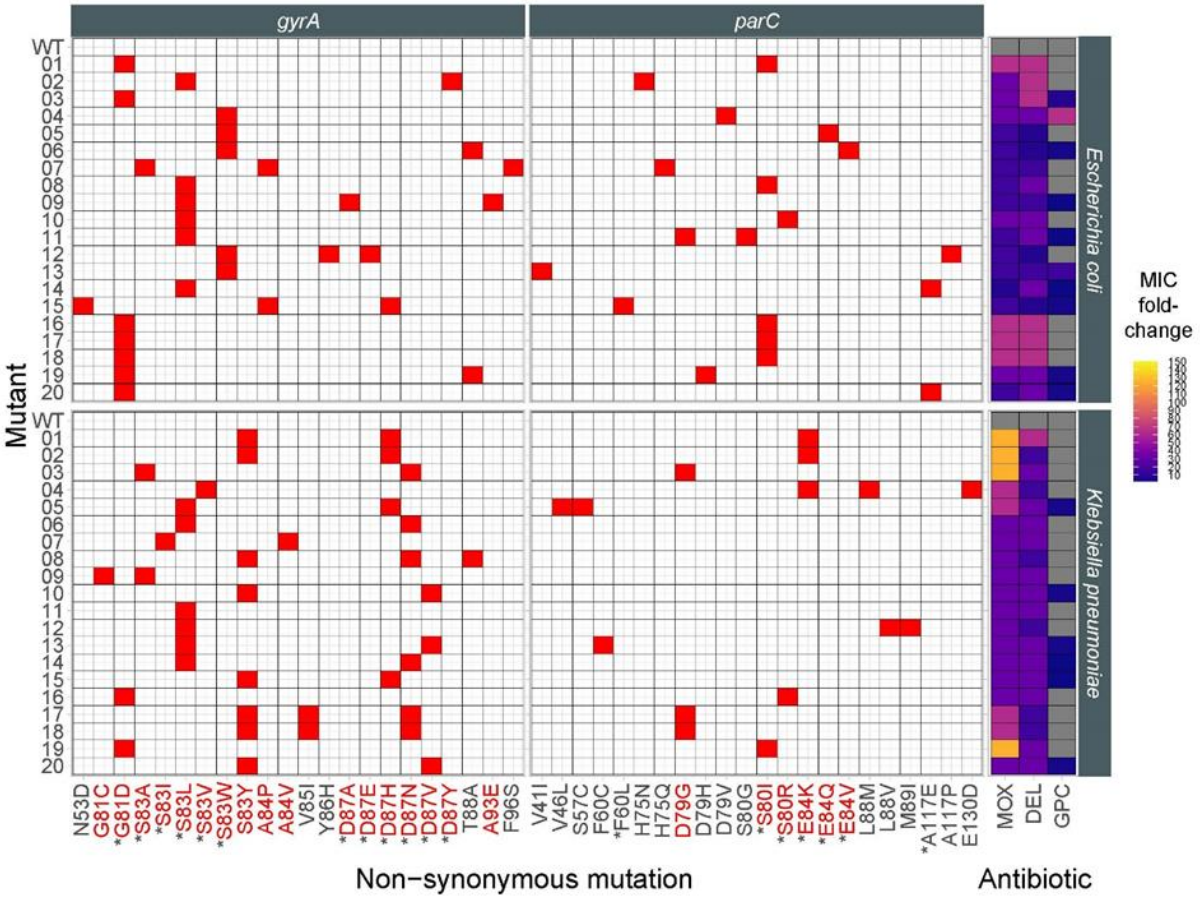

Supplementary Fig 13. Mutations and the associated cross-resistance patterns across topoisomerase inhibitors. QRDR regions of the gyrA and parC genes of *Escherichia coli* MG 1655 K-12 and *Klebsiella pneumoniae ATCC* 10031 were subjected to targeted mutagenesis (DIvERGE) and selection for moxifloxacin resistance. The figure shows the mutations carried by the 20-20 strains isolated on moxifloxacin agar plates. The heatmap on the right shows the MIC fold change of the selected mutants to topoisomerase inhibitors, including moxifloxacin (MOX), delafloxacin (DEL) and gepotidacin (GEP). Grey color indicates no change in MIC compared to the wild type. Mutations indicated with red color have been shown previously as topoisomerase resistance-conferring mutations. Asterisks indicate mutations found in the genomes of clinical E. *coli* isolates.

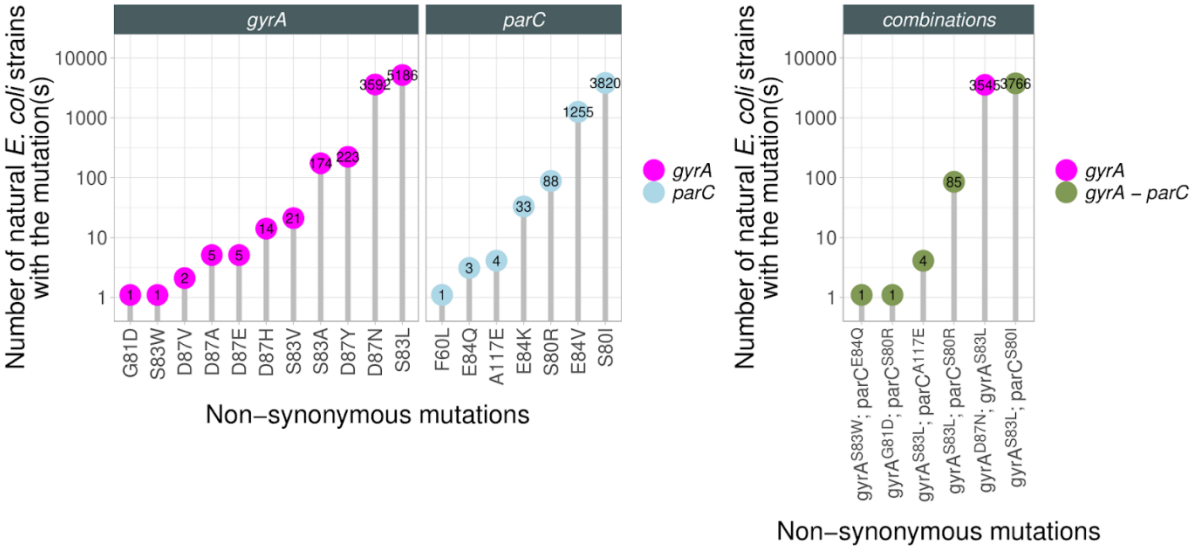

Supplementary Fig 14. Moxifloxacin resistance mutations in the genomes of natural *E.coli* isolates. The figure shows mutations generated by DIvERGE experiment in gyrA (magenta, left panel) and parC (blue, middle panel) and their frequencies across the genomes of natural *E. coli* isolates. Combination of mutations (right panel) found in the same resistant clone are also depicted here (magenta: gyrA-gyrA, green: gyrA-parC). Mutations and combinations thereof in coding sequences were searched for in a dataset of 20,786 natural *E. coli* genomes (see Methods).

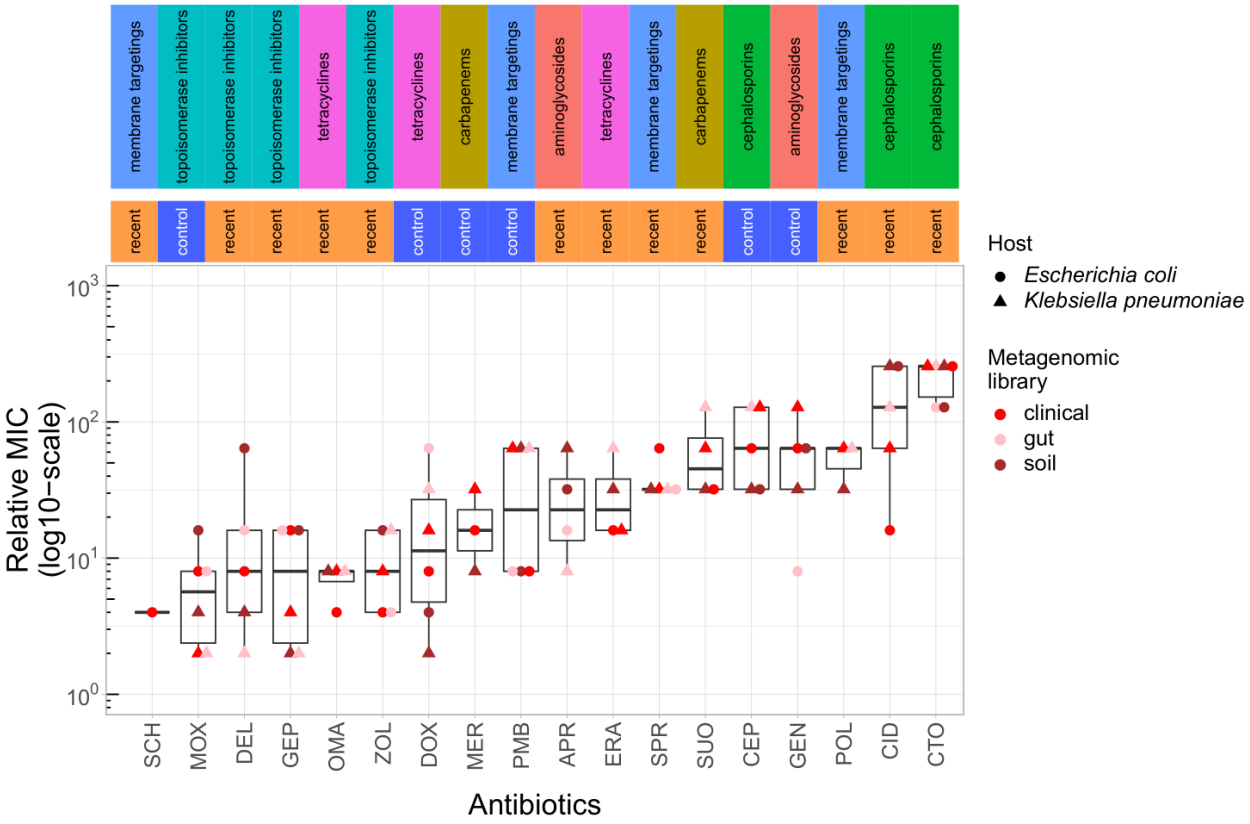

Supplementary Fig 15. Functional selection of metagenomic libraries with 18 antibiotics resulted in reduced antibiotic susceptibility in the bacterial hosts. The figure shows the MIC fold change in the bacterial host provided by the DNA fragments associated with a given metagenomic library. Only resistant populations or populations with a relative MIC > 1 are depicted here. We observed a substantial, up to 256-fold variation in the resistance level across antibiotics (Kruskal-Wallis chi-squared = 1168.5, df = 18, P < 2.2e-16), whereas no significant difference was observed between the median relative MICs of recent antibiotics and their corresponding control antibiotic(paired T-test, t = -0.08746, df = 12, P = 0.9317). Boxplots show the median, first and third quartiles, with whiskers showing the 5th and 95th percentiles. For abbreviations, see Table 1.

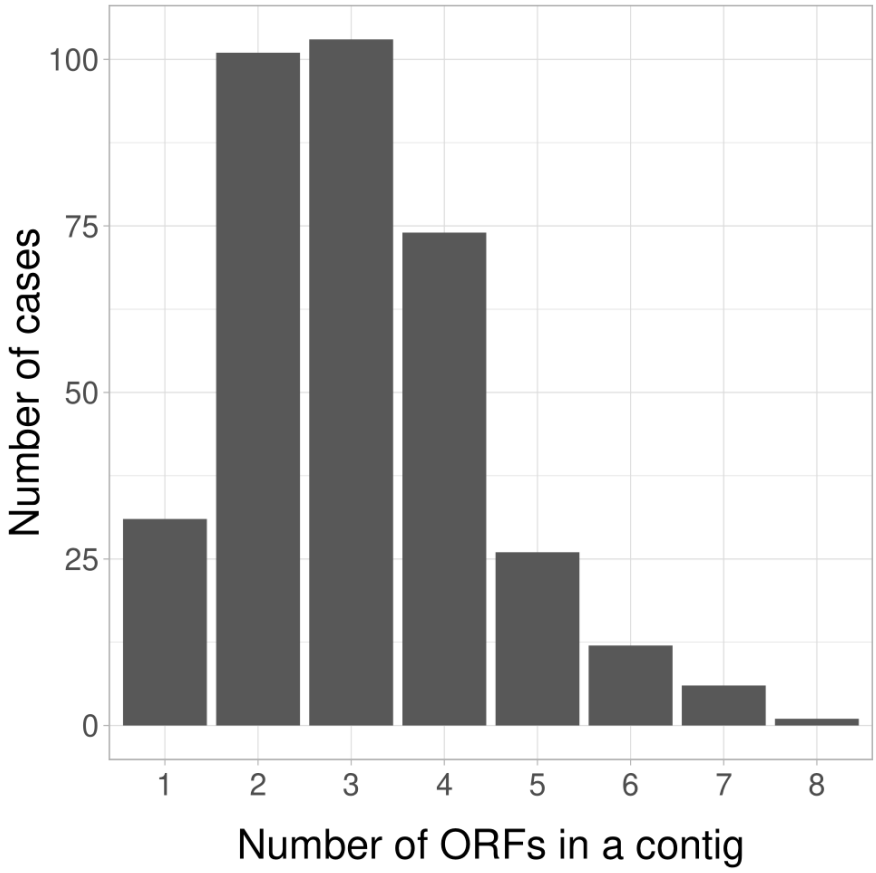

Supplementary Fig 16. Most DNA fragments carry more than one predicted ORF. The barplot shows the distribution of contigs with different numbers of ORFs.

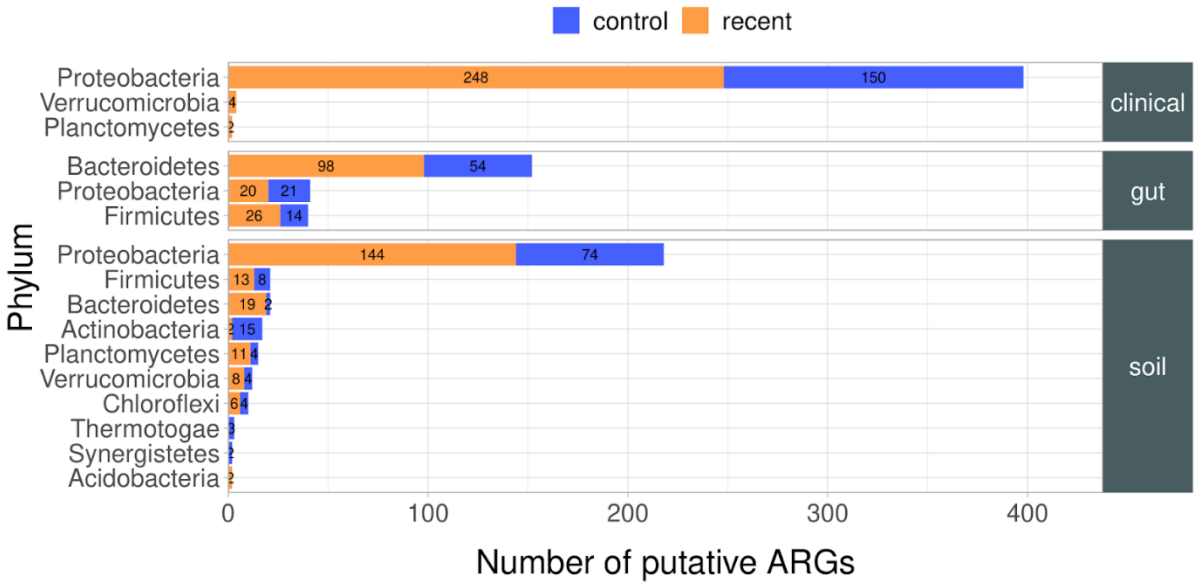

Supplementary Fig 17. Phylogenetic origin of ARGs. The barplot shows the number of ARGs originating from various phyla. Blue and orange bars denote the number of ARGs detected in control and recent antibiotics, respectively.

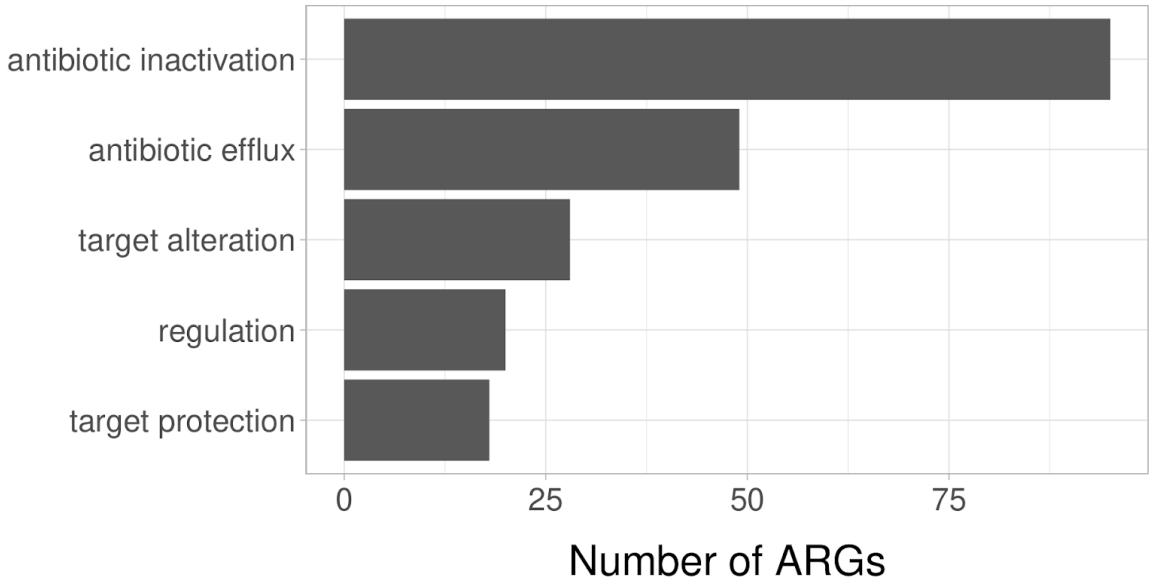

Supplementary Fig 18. Prevalence of resistance mechanisms for ARGs. The barplot shows the number of ARGs linked to various resistance mechanisms and/or gene regulation.

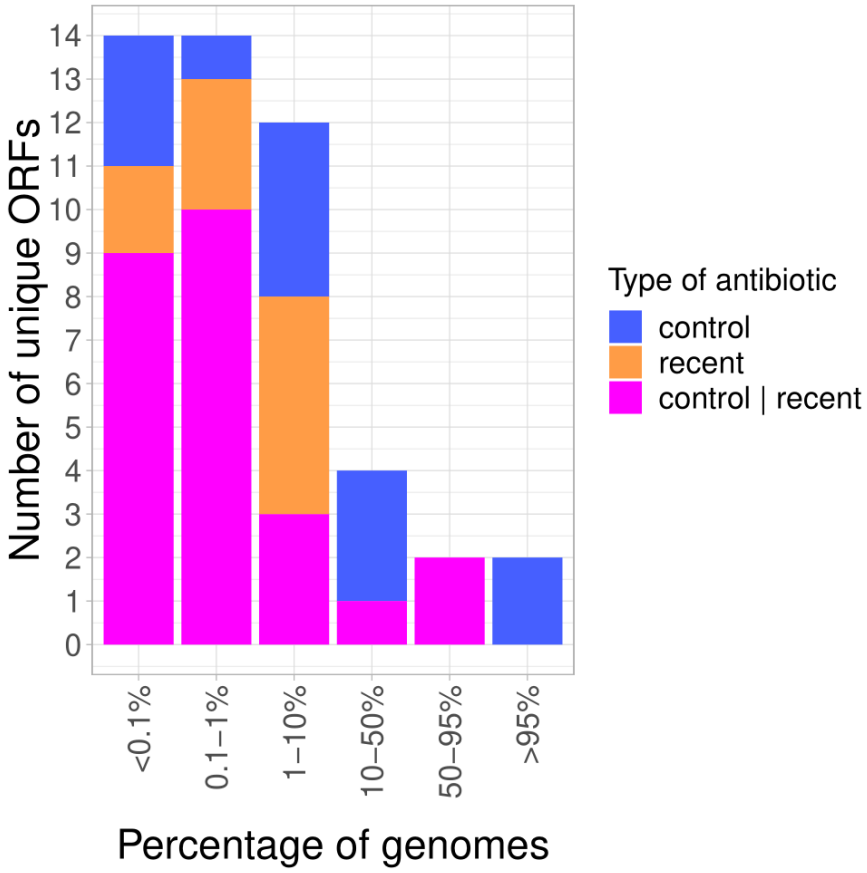

Supplementary Fig 19. Most putative ARGs are present in only a small fraction of the investigated genomes. The barplot shows the distribution of putative ARGs, detected either against control (blue), recent (orange) or both types of antibiotics (magenta), in the investigated genomes of natural *E. coli* isolates.

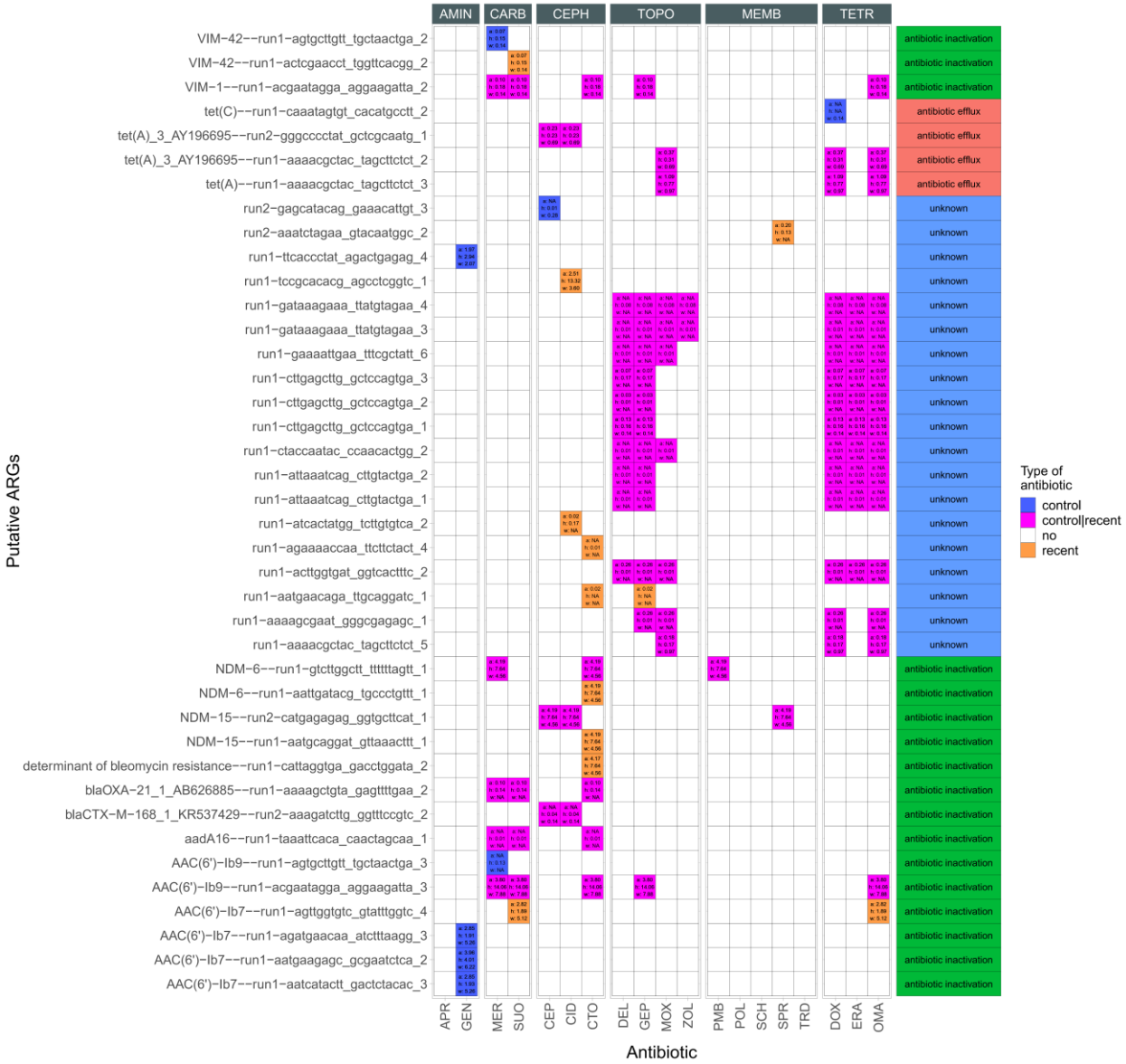

Supplementary Fig 20. Various putative ARGs could confer resistance to multiple antibiotics. The heatmap shows the distribution of putative ARGs found in natural habitats across antibiotics. Numbers within a cell indicate the number of isolates across habitats (*a*, *h* and *w* denote agriculture, human and wild-animal, respectively). The right panel shows the identified resistance mechanism, if any, for each putative ARGs. ARGs where no sequence similarity was found are labeled with a unique identifier, whereas those that share sequence similarity with known resistance genes (present in either CARD or ResFinder) are labeled with the corresponding gene name.

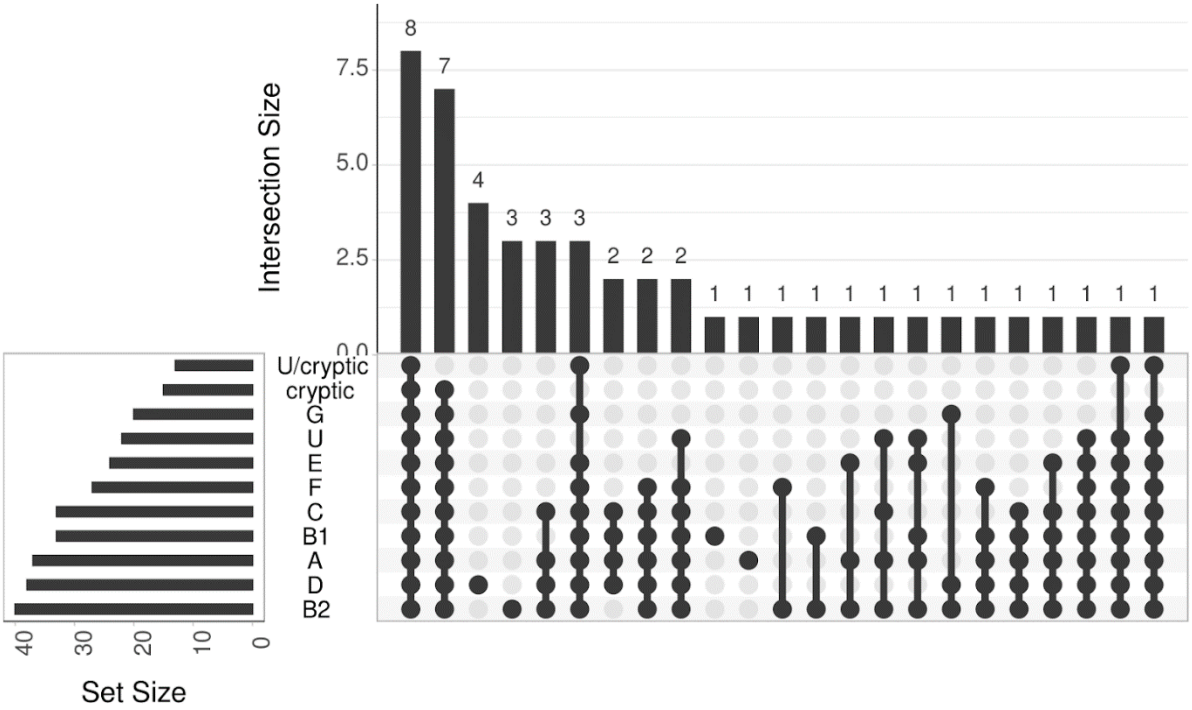

Supplementary Fig 21. Phylogenetic origin of putative ARGs. The figure shows the overlap of putative ARGs across different phylogroups of *E. coli*. The plot shows 48 putative ARGs detected in at least one *E. coli* genome. Letters on the left (A, B1, B2, D, E, F, G, U, U/cryptic, and cryptic) denote phylogroups, according to a previous study[26].

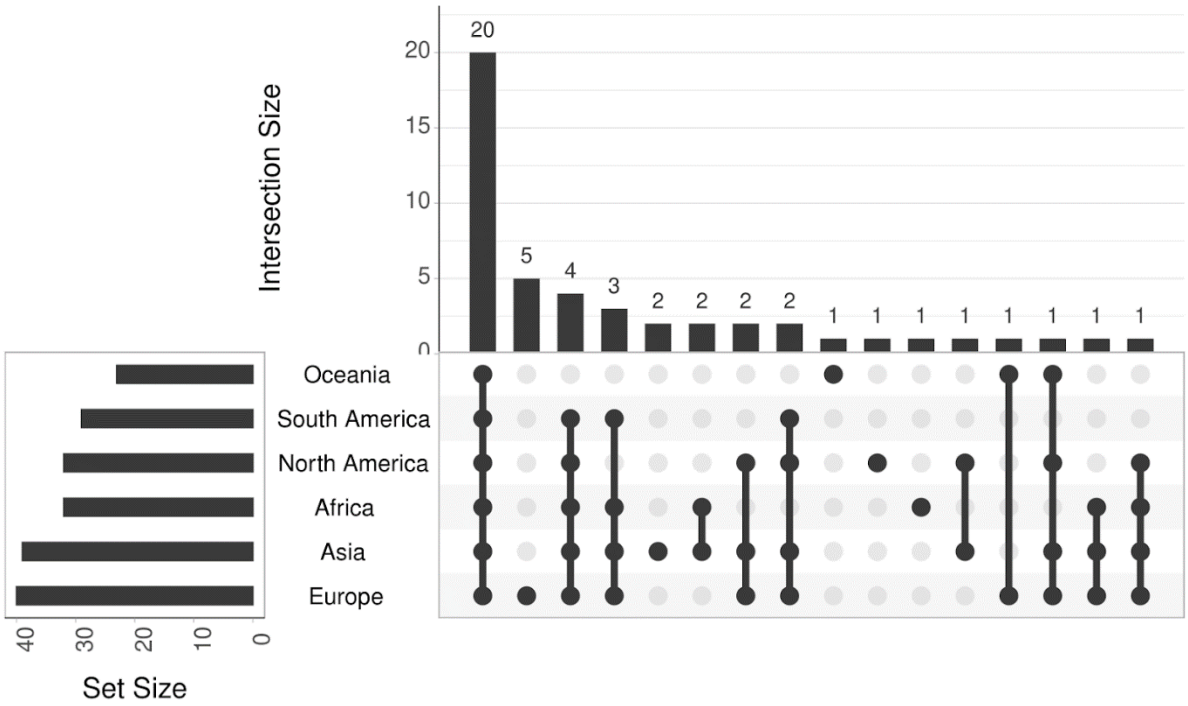

Supplementary Fig 22. Geographical origin of putative ARGs. The figure shows the overlap of putative ARGs across *E. coli* from different continents.

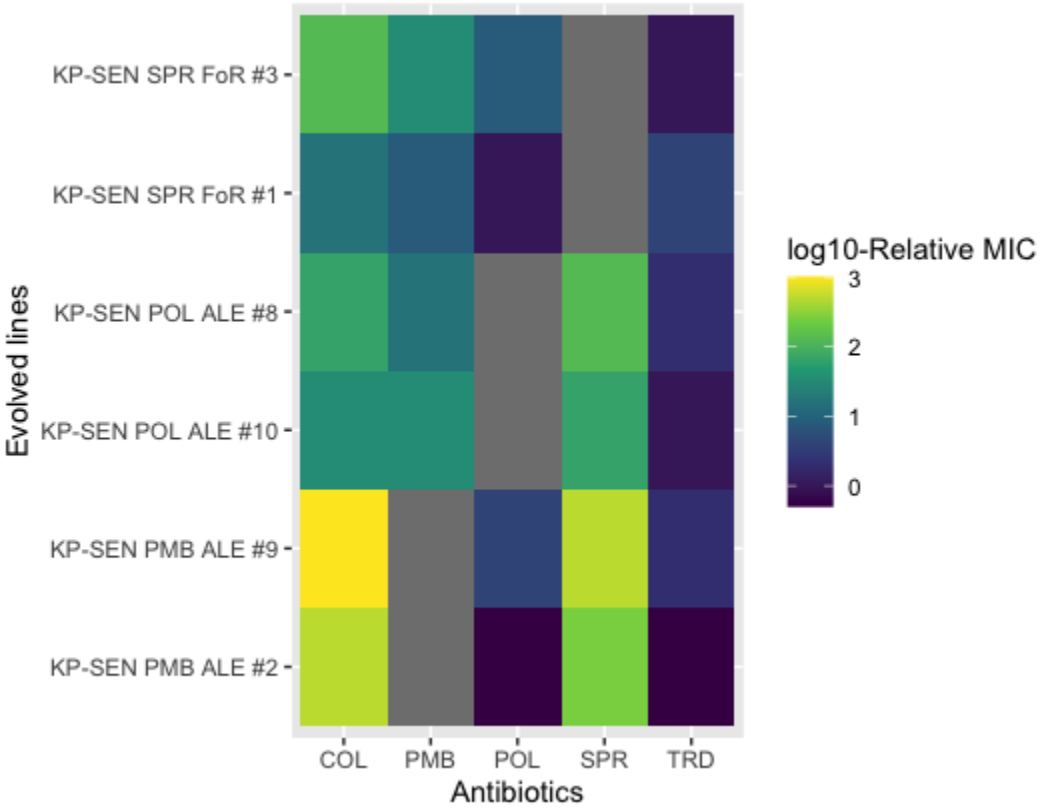

Supplementary Fig 23. Cross-resistance panel of the laboratory evolved KP-SEN lines. The heatmap shows the cross-resistance profile of 6 laboratory evolved KP-SEN lines, all of which display increased virulence in a *Galleria mellonella* infection model. The lines were evolved against one antibiotic (indicated in the name of the line) either using frequency of resistance assay (FoR), or with adaptive laboratory evolution (ALE). The color scale can be seen on the right and was projected after taking the $\log_{10}$ of the relative MIC values compared to the ancestor KP-SEN. Gray color indicates antibiotics the tested line was adapted to. For abbreviation see Table 1 and Supplementary Table 2.

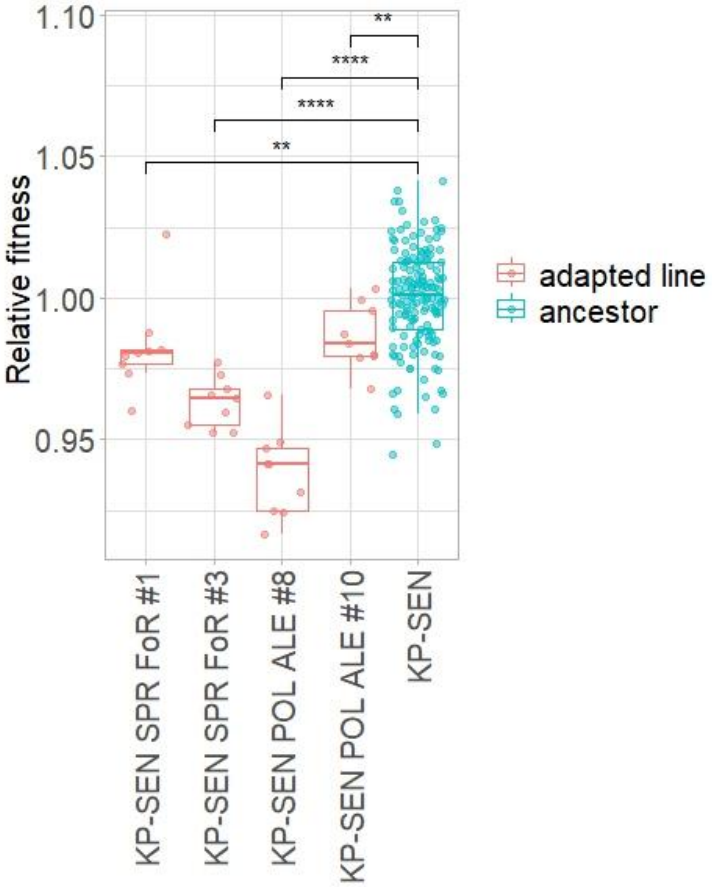

Supplementary Fig 24. ***In vitro* fitness of SPR206- and POL7306-resistant lines.** Fitness was determined by measuring the growth of evolved lines and the ancestor strain in antibiotic-free medium. The area under the growth curve was used as a measure of fitness and normalized to the ancestor strain. KP-SEN SPR FoR #1 and KP-SEN SPR FoR #3 represent two SPR206-resistant lines, while KP-SEN POL ALE #8 and KP-SEN POL ALE #10 indicate two POL7306-resistant lines. KP-SEN refers to the antibiotic-sensitive ancestor strain (*K. pneumoniae* ATCC 10031). Measurements were conducted in 9 biological replicates. Boxplots show the median, first and third quartiles, with whiskers showing the 5th and 95th percentiles. P-values were calculated using the Wilcoxon rank sum test (** and **** indicates $P < 0.005$ and $P < 5e\text{-}06$, respectively). For abbreviations, see Supplementary Table 2.

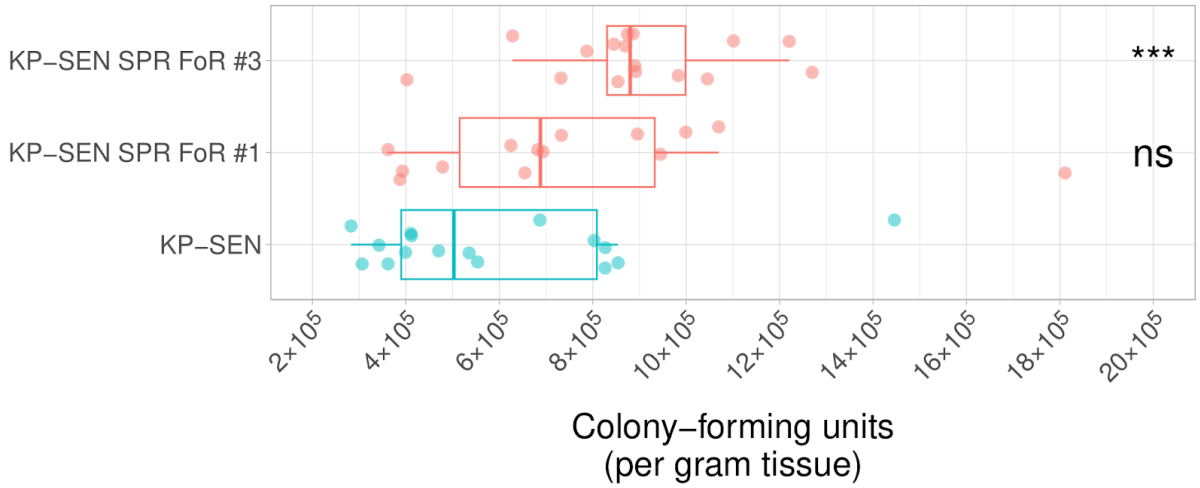

Supplementary Fig 25. *K. pneumoniae* SPR206-resistant lines show increased wound colonization capacity in mice. The figure shows the colonization capacity of antibiotic sensitive (green, KP-SEN, i.e. *K. pneumoniae* ATCC 10031) and SPR206-resistant *K. pneumoniae* lines (red, SPR FoR #1 and KP-SEN SPR FoR #3) in the murine thigh wound infection model. Bacterial colonization was quantified by determining the number of colony-forming units per gram tissue after homogenizing the infected calves. Experiments were performed in 7 biological replicates. Boxplots show the median, first and third quartiles, with whiskers showing the 5th and 95th percentiles. P-values were calculated using the Wilcoxon rank sum test (*** and ns indicates $P < 0.001$ and P = not significant, respectively). For abbreviations, see Supplementary Table 2.

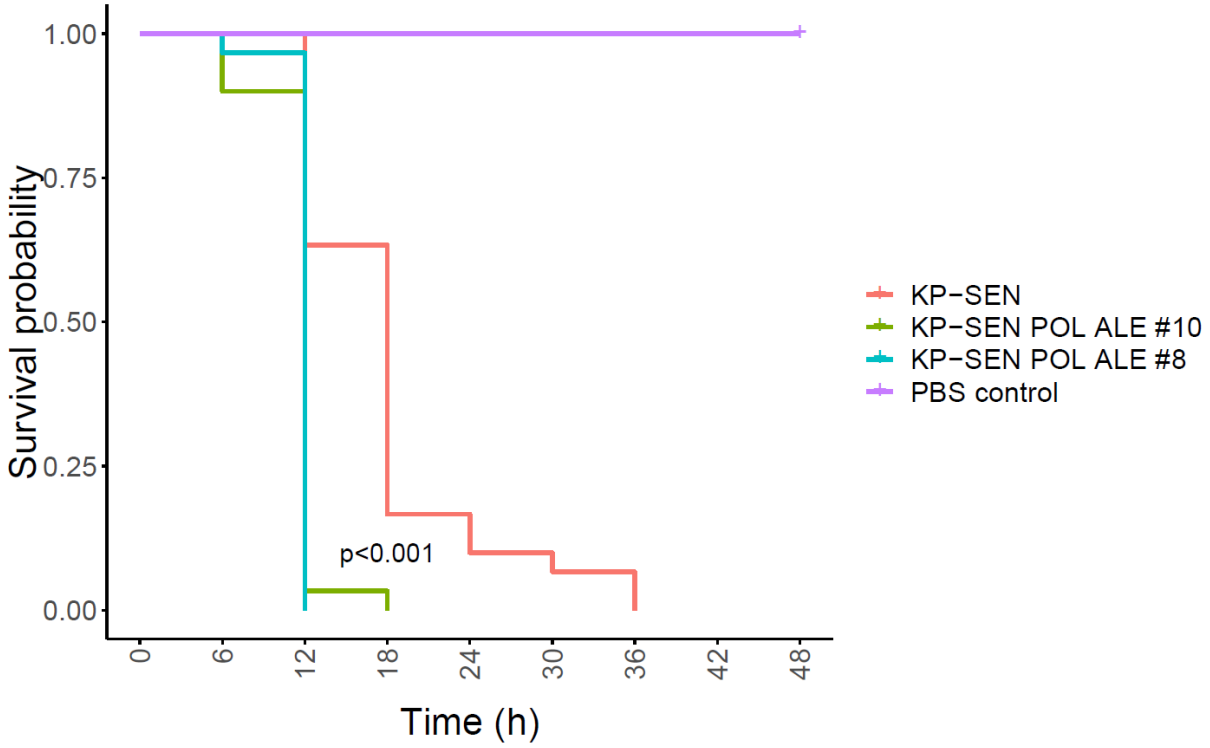

Supplementary Fig 26. *In vivo* virulence of POL7306-resistant lines in *Galleria mellonella* infection model. Kaplan-Meier survival curve depicts the survival probabilities for animals infected with the ancestor (KP-SEN, i.e. *K.pneumoniae* ATCC 10031) and the corresponding POL7306-resistant lines (POL ALE #8 and POL ALE #10). The resistant lines display significantly elevated virulence compared to the wild type (P<0.001 for both line #8 and #10. P-values were calculated using standard log-rank tests). Experiments were performed in three biological replicates, with 10 animals per treatment group, hence each curve represents 30 animals. For abbreviations, see Supplementary Table 2.

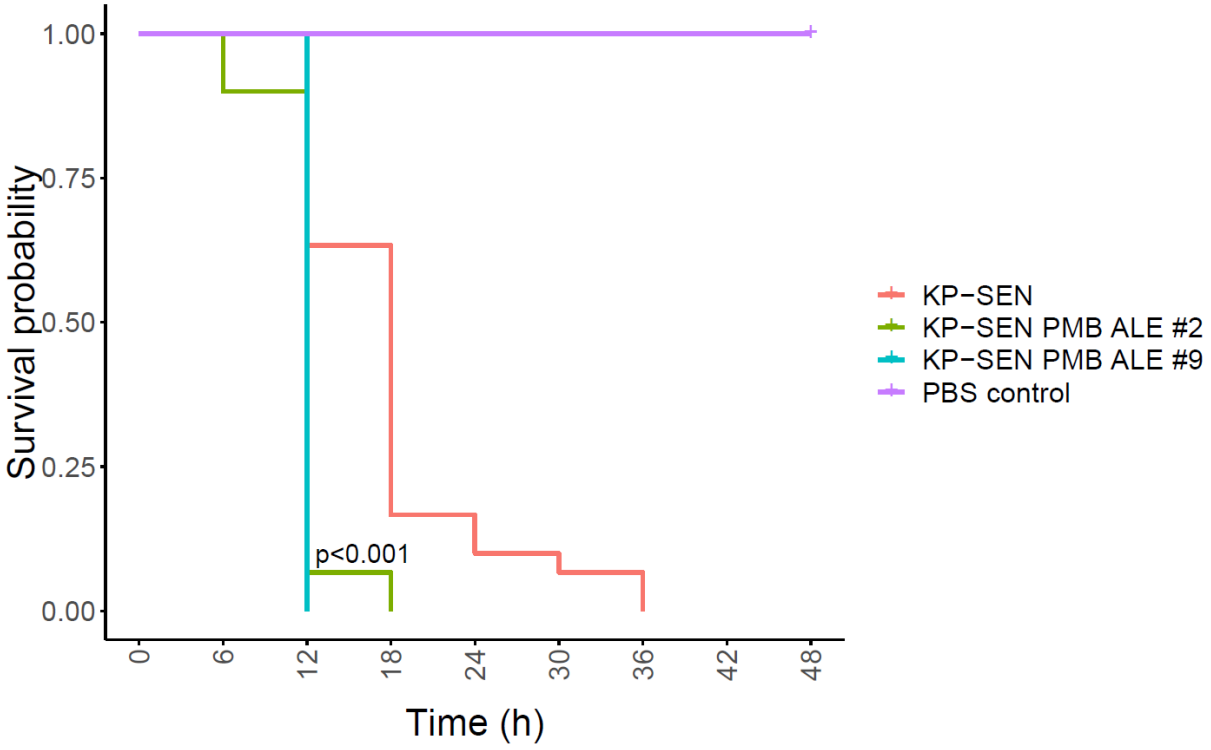

Supplementary Fig 27. *In vivo* virulence of Polymyxin-B-resistant lines in *Galleria mellonella* infection model. Kaplan-Meier survival curve depicting the survival probabilities for animals infected with the ancestor (KP-SEN, i.e. *K.pneumoniae* ATCC10031) and two Polymyxin-B-resistant lines (PMB ALE #2 and ALE #9). The resistant lines display significantly elevated virulence compared to the ancestor ($P < 0.001$ for both line ALE #2 and ALE #9. P-values were calculated using a standard log-rank test). Experiments were performed in three biological replicates, with 10 animals per treatment group, hence each curve represents 30 animals. For abbreviations, see Supplementary Table 2.

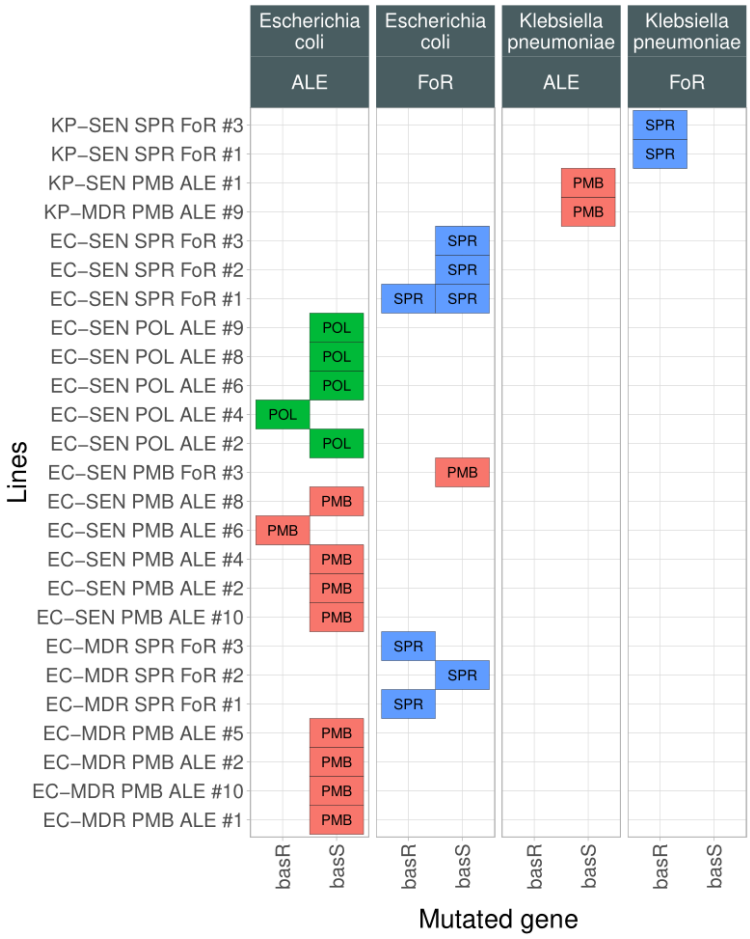

Supplementary Fig 28. *BasS* and *basR* are commonly mutated genes in lines adapted to peptide-based antibiotics, including Polymyxin-B (PMB), SPR206 (SPR) and Pol7306 (POL). The heatmap shows the mutant lines with non-synonymous mutations in *basS* and *basR*. ALE indicates lines derived from adaptive laboratory evolution, while FOR indicates lines derived from frequency-of-resistance assays. For abbreviations, see Supplementary Table 2.

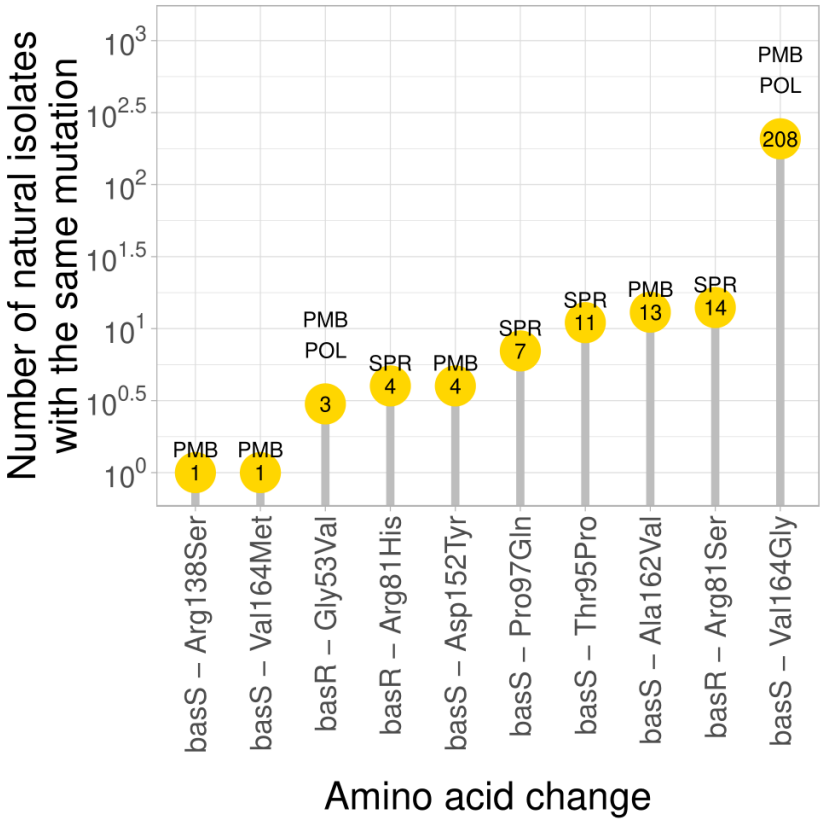

Supplementary Fig 29 Specific amino acid substitutions in *basS* and *basR* shared by laboratory evolved lines adapted to peptide-based antibiotics and natural isolates. For abbreviations, see Table 1.

References

1. Antimicrobial Resistance Collaborators. Global burden of bacterial antimicrobial resistance in 2019: a systematic analysis. *Lancet* **399**, 629–655 (2022).
2. O'Neill, J. Tackling Drug-Resistant Infections Globally: Final Report and Recommendations https://amr-review.org/sites/default/files/160525_Final%20paper_with%20cover.pdf (2016).
3. Miethke, M. *et al.* Towards the sustainable discovery and development of new antibiotics. *Nat Rev Chem* **5**, 726–749 (2021).
4. Payne, D. J., Gwynn, M. N., Holmes, D. J. & Pompliano, D. L. Drugs for bad bugs: confronting the challenges of antibacterial discovery. *Nat Rev Drug Discov* **6**, 29–40 (2007).
5. Spellberg, B., Powers, J. H., Brass, E. P., Miller, L. G. & Edwards, J. E. Trends in antimicrobial drug development: implications for the future. *Clin Infect Dis* **38**, 1279–1286 (2004).
6. O'Dwyer, K. *et al.* Bacterial resistance to leucyl-tRNA synthetase inhibitor GSK2251052 develops during treatment of complicated urinary tract infections. *Antimicrob Agents Chemother* **59**, 289–298 (2015).
7. Werth, B. J. *et al.* Dalbavancin exposure in vitro selects for dalbavancin-non-susceptible and vancomycin-intermediate strains of methicillin-resistant Staphylococcus aureus. *Clin Microbiol Infect* **27**, 910.e1-910.e8 (2021).
8. Al Janabi, J., Tevell, S., Sieber, R. N., Stegger, M. & Söderquist, B. Emerging resistance in Staphylococcus epidermidis during dalbavancin exposure: a case report and in vitro analysis of isolates from prosthetic joint infections. *J Antimicrob Chemother* **78**, 669–677 (2023).
9. Sommer, M. O. A., Munck, C., Toft-Kehler, R. V. & Andersson, D. I. Prediction of antibiotic resistance: time for a new preclinical paradigm? *Nat Rev Microbiol* **15**, 689–696 (2017).
10. World Health Organization. 2021 antibacterial agents in clinical and preclinical development: an overview and analysis https://www.who.int/publications-detail-redirect/9789240047655 (2021).
11. Lewis, K. The Science of Antibiotic Discovery. *Cell* **181**, 29–45 (2020).
12. Al-Tawfiq, J. A. *et al.* Antibiotics in the pipeline: a literature review (2017-2020). *Infection* **50**, 553–564 (2022).
13. Theuretzbacher, U., Outterson, K., Engel, A. & Karlén, A. The global preclinical antibacterial pipeline. *Nat Rev Microbiol* **18**, 275–285 (2020).
14. Ling, L. L. *et al.* A new antibiotic kills pathogens without detectable resistance. *Nature* **517**, 455–459 (2015).
15. Nyerges, A. *et al.* Rational design of balanced dual-targeting antibiotics with limited resistance. *PLOS Biology* **18**, e3000819 (2020).
16. Luria, S. E. & Delbrück, M. Mutations of Bacteria from Virus Sensitivity to Virus Resistance. *Genetics* **28**, 491–511 (1943).
17. Bell, G. & MacLean, C. The Search for 'Evolution-Proof' Antibiotics. *Trends in Microbiology* **26**, 471–483 (2018).
18. Nyerges, Á. *et al.* A highly precise and portable genome engineering method allows comparison of mutational effects across bacterial species. *Proceedings of the National Academy of Sciences* **113**, 2502–2507 (2016).
19. Jolivet-Gougeon, A. *et al.* Bacterial hypermutation: clinical implications. *J Med Microbiol* **60**, 563–573 (2011).
20. Lázár, V. *et al.* Genome-wide analysis captures the determinants of the antibiotic cross-resistance interaction network. *Nat Commun* **5**, 4352 (2014).
21. Yoshida, H., Bogaki, M., Nakamura, M. & Nakamura, S. Quinolone resistance-determining region in the DNA gyrase gyrA gene of Escherichia coli. *Antimicrob Agents Chemother* **34**, 1271–1272 (1990).
22. Nyerges, Á. *et al.* Directed evolution of multiple genomic loci allows the prediction of antibiotic resistance. *Proceedings of the National Academy of Sciences* **115**, E5726–E5735 (2018).
23. Apjok, G. *et al.* Characterization of antibiotic resistomes by reprogrammed bacteriophage-enabled functional metagenomics in clinical strains. *Nat Microbiol* **8**, 410–423 (2023).
24. George, A. M., Hall, R. M. & Stokes, H. W. Multidrug resistance in Klebsiella pneumoniae: a novel gene, ramA, confers a multidrug resistance phenotype in Escherichia coli. *Microbiology (Reading)* **141 (Pt 8)**, 1909–1920 (1995).
25. Luo, C. *et al.* Genome sequencing of environmental Escherichia coli expands understanding of the ecology and speciation of the model bacterial species. *Proc Natl Acad Sci U S A* **108**, 7200–7205 (2011).

26. Pursey, E., Dimitriu, T., Gaze, W. H., Westra, E. R. & Houte, S. van. Modelling the distribution of antimicrobial resistance genes across geography, climate, host species and phylogroup in 16,000 E. coli genomes. 2022.08.05.22278465 Preprint at https://doi.org/10.1101/2022.08.05.22278465 (2022).
27. Perron, G. G., Zasloff, M. & Bell, G. Experimental evolution of resistance to an antimicrobial peptide. *Proc Biol Sci* **273**, 251–256 (2006).
28. Andersson, D. I., Hughes, D. & Kubicek-Sutherland, J. Z. Mechanisms and consequences of bacterial resistance to antimicrobial peptides. *Drug Resist Updat* **26**, 43–57 (2016).
29. Ramarao, N., Nielsen-Leroux, C. & Lereclus, D. The insect Galleria mellonella as a powerful infection model to investigate bacterial pathogenesis. *J Vis Exp* e4392 (2012) doi:10.3791/4392.
30. Oelschlaeger, T. A. & Tall, B. D. Invasion of cultured human epithelial cells by Klebsiella pneumoniae isolated from the urinary tract. *Infect Immun* **65**, 2950–2958 (1997).
31. Hsu, C.-R. *et al.* Klebsiella pneumoniae translocates across the intestinal epithelium via Rho GTPase- and phosphatidylinositol 3-kinase/Akt-dependent cell invasion. *Infect Immun* **83**, 769–779 (2015).
32. Gunn, J. S., Ryan, S. S., Van Velkinburgh, J. C., Ernst, R. K. & Miller, S. I. Genetic and functional analysis of a PmrA-PmrB-regulated locus necessary for lipopolysaccharide modification, antimicrobial peptide resistance, and oral virulence of Salmonella enterica serovar typhimurium. *Infect Immun* **68**, 6139–6146 (2000).
33. Eriksson, S., Lucchini, S., Thompson, A., Rhen, M. & Hinton, J. C. D. Unravelling the biology of macrophage infection by gene expression profiling of intracellular Salmonella enterica. *Mol Microbiol* **47**, 103–118 (2003).
34. Jangra, M. *et al.* Tridecaptin M, a New Variant Discovered in Mud Bacterium, Shows Activity against Colistin- and Extremely Drug-Resistant Enterobacteriaceae. *Antimicrob Agents Chemother* **63**, e00338-19 (2019).
35. Zhao, X., Yin, Z., Breukink, E., Moll, G. N. & Kuipers, O. P. An Engineered Double Lipid II Binding Motifs-Containing Lantibiotic Displays Potent and Selective Antimicrobial Activity against Enterococcus faecium. *Antimicrob Agents Chemother* **64**, e02050-19 (2020).
36. Solomkin, J. *et al.* Assessing the Efficacy and Safety of Eravacycline vs Ertapenem in Complicated Intra-abdominal Infections in the Investigating Gram-Negative Infections Treated With Eravacycline (IGNITE 1) Trial: A Randomized Clinical Trial. *JAMA Surg* **152**, 224–232 (2017).
37. Karlowsky, J. A. *et al.* In Vitro Activity of Sulopenem, an Oral Penem, against Urinary Isolates of Escherichia coli. *Antimicrob Agents Chemother* **63**, e01832-18 (2019).
38. Brown, P. *et al.* Design of Next Generation Polymyxins with Lower Toxicity: The Discovery of SPR206. *ACS Infect. Dis.* **5**, 1645–1656 (2019).
39. Jangir, P. K. *et al.* The evolution of colistin resistance increases bacterial resistance to host antimicrobial peptides and virulence. *eLife* **12**, e84395 (2023).
40. Ma, P. *et al.* Genetic determinants facilitating the evolution of resistance to carbapenem antibiotics. *Elife* **10**, e67310 (2021).
41. Papkou, A., Hedge, J., Kapel, N., Young, B. & MacLean, R. C. Efflux pump activity potentiates the evolution of antibiotic resistance across S. aureus isolates. *Nat Commun* **11**, 3970 (2020).
42. Arcilla, M. S. *et al.* Dissemination of the mcr-1 colistin resistance gene. *The Lancet Infectious Diseases* **16**, 147–149 (2016).
43. Hackel, M. A. *et al.* Reproducibility of broth microdilution MICs for the novel siderophore cephalosporin, cefiderocol, determined using iron-depleted cation-adjusted Mueller-Hinton broth. *Diagn Microbiol Infect Dis* **94**, 321–325 (2019).
44. Koch, A. E. & Burchall, J. J. Reversal of the antimicrobial activity of trimethoprim by thymidine in commercially prepared media. *Appl Microbiol* **22**, 812–817 (1971).
45. Helander, I. M. & Mattila-Sandholm, T. Fluorometric assessment of gram-negative bacterial permeabilization. *J Appl Microbiol* **88**, 213–219 (2000).
46. Wiegand, I., Hilpert, K. & Hancock, R. E. W. Agar and broth dilution methods to determine the minimal inhibitory concentration (MIC) of antimicrobial substances. *Nat Protoc* **3**, 163–175 (2008).
47. Spohn, R. *et al.* Integrated evolutionary analysis reveals antimicrobial peptides with limited resistance. *Nat Commun* **10**, 4538 (2019).
48. Bódi, Z. *et al.* Phenotypic heterogeneity promotes adaptive evolution. *PLOS Biology* **15**, e2000644 (2017).
49. Brouwers, R. *et al.* Stability of β-lactam antibiotics in bacterial growth media. *PLOS ONE* **15**, e0236198 (2020).
50. Li, H. & Durbin, R. Fast and accurate short read alignment with Burrows-Wheeler transform. *Bioinformatics* **25**, 1754–1760 (2009).

51. Garrison, E. & Marth, G. Haplotype-based variant detection from short-read sequencing. Preprint at https://doi.org/10.48550/arXiv.1207.3907 (2012).
52. Garrison, E., Kronenberg, Z. N., Dawson, E. T., Pedersen, B. S. & Prins, P. A spectrum of free software tools for processing the VCF variant call format: vcflib, bio-vcf, cyvcf2, hts-nim and slivar. *PLOS Computational Biology* **18**, e1009123 (2022).
53. Robinson, J. T. *et al.* Integrative genomics viewer. *Nat Biotechnol* **29**, 24–26 (2011).
54. Törönen, P. & Holm, L. PANNZER—A practical tool for protein function prediction. *Protein Science* **31**, 118–128 (2022).
55. Törönen, P., Medlar, A. & Holm, L. PANNZER2: a rapid functional annotation web server. *Nucleic Acids Res* **46**, W84–W88 (2018).
56. Emms, D. M. & Kelly, S. OrthoFinder: phylogenetic orthology inference for comparative genomics. *Genome Biol* **20**, 238 (2019).
57. Emms, D. M. & Kelly, S. OrthoFinder: solving fundamental biases in whole genome comparisons dramatically improves orthogroup inference accuracy. *Genome Biol* **16**, 157 (2015).
58. Chen, I.-M. A. *et al.* The IMG/M data management and analysis system v.6.0: new tools and advanced capabilities. *Nucleic Acids Research* **49**, D751–D763 (2021).
59. Moradigaravand, D. *et al.* Prediction of antibiotic resistance in Escherichia coli from large-scale pan-genome data. *PLOS Computational Biology* **14**, e1006258 (2018).
60. Johnson, J. R. *et al.* Accessory Traits and Phylogenetic Background Predict Escherichia coli Extraintestinal Virulence Better Than Does Ecological Source. *The Journal of Infectious Diseases* **219**, 121–132 (2019).
61. Martin, M. Cutadapt removes adapter sequences from high-throughput sequencing reads. *EMBnet.journal* **17**, 10–12 (2011).
62. Leinonen, R., Sugawara, H., Shumway, M., & on behalf of the International Nucleotide Sequence Database Collaboration. The Sequence Read Archive. *Nucleic Acids Research* **39**, D19–D21 (2011).
63. Prjibelski, A., Antipov, D., Meleshko, D., Lapidus, A. & Korobeynikov, A. Using SPAdes De Novo Assembler. *Current Protocols in Bioinformatics* **70**, e102 (2020).
64. Manni, M., Berkeley, M. R., Seppey, M., Simão, F. A. & Zdobnov, E. M. BUSCO Update: Novel and Streamlined Workflows along with Broader and Deeper Phylogenetic Coverage for Scoring of Eukaryotic, Prokaryotic, and Viral Genomes. *Molecular Biology and Evolution* **38**, 4647–4654 (2021).
65. Hyatt, D. *et al.* Prodigal: prokaryotic gene recognition and translation initiation site identification. *BMC Bioinformatics* **11**, 119 (2010).
66. Buchfink, B., Xie, C. & Huson, D. H. Fast and sensitive protein alignment using DIAMOND. *Nat Methods* **12**, 59–60 (2015).
67. Katoh, K. & Standley, D. M. MAFFT Multiple Sequence Alignment Software Version 7: Improvements in Performance and Usability. *Molecular Biology and Evolution* **30**, 772–780 (2013).
68. Fick, J. *et al.* Contamination of surface, ground, and drinking water from pharmaceutical production. *Environ Toxicol Chem* **28**, 2522–2527 (2009).
69. Ando, H., Lemire, S., Pires, D. P. & Lu, T. K. Engineering Modular Viral Scaffolds for Targeted Bacterial Population Editing. *Cell Syst* **1**, 187–196 (2015).
70. Yosef, I., Goren, M. G., Globus, R., Molshanski-Mor, S. & Qimron, U. Extending the Host Range of Bacteriophage Particles for DNA Transduction. *Mol Cell* **66**, 721-728.e3 (2017).
71. Kintses, B. *et al.* Phylogenetic barriers to horizontal transfer of antimicrobial peptide resistance genes in the human gut microbiota. *Nat Microbiol* **4**, 447–458 (2019).
72. Szybalski, W. Genetic studies on microbial cross resistance to toxic agents. IV. Cross resistance of Bacillus megaterium to forty-four antimicrobial drugs. *Appl Microbiol* **2**, 57–63 (1954).
73. Alcock, B. P. *et al.* CARD 2020: antibiotic resistome surveillance with the comprehensive antibiotic resistance database. *Nucleic Acids Research* **48**, D517–D525 (2020).
74. Bortolaia, V. *et al.* ResFinder 4.0 for predictions of phenotypes from genotypes. *Journal of Antimicrobial Chemotherapy* **75**, 3491–3500 (2020).
75. Altschul, S. F., Gish, W., Miller, W., Myers, E. W. & Lipman, D. J. Basic local alignment search tool. *Journal of Molecular Biology* **215**, 403–410 (1990).
76. Fu, L., Niu, B., Zhu, Z., Wu, S. & Li, W. CD-HIT: accelerated for clustering the next-generation sequencing data. *Bioinformatics* **28**, 3150–3152 (2012).
77. O'Leary, N. A. *et al.* Reference sequence (RefSeq) database at NCBI: current status, taxonomic expansion, and functional annotation. *Nucleic Acids Research* **44**, D733–D745 (2016).
78. R: The R Project for Statistical Computing. https://www.r-project.org/.

79. Grenié, M., Berti, E., Carvajal-Quintero, J., Winter, M. & Sagouis, A. *Harmonizing taxon names in biodiversity data: a review of tools, databases, and best practices*. (2021). doi:10.32942/osf.io/e3qnz.
80. Chamberlain, S. *et al.* ropensci/taxizedb: taxizedb v0.3.1. (2023) doi:10.5281/zenodo.7797082.
81. Chamberlain, S., Arendsee, Z. & Stirling, T. taxizedb: Tools for Working with 'Taxonomic' Databases. (2023).
82. Smillie, C. S. *et al.* Ecology drives a global network of gene exchange connecting the human microbiome. *Nature* **480**, 241–244 (2011).
83. Galata, V., Fehlmann, T., Backes, C. & Keller, A. PLSDB: a resource of complete bacterial plasmids. *Nucleic Acids Res* **47**, D195–D202 (2019).
84. Clermont, O., Christenson, J. K., Denamur, E. & Gordon, D. M. The Clermont Escherichia coli phylo-typing method revisited: improvement of specificity and detection of new phylo-groups. *Environ Microbiol Rep* **5**, 58–65 (2013).
85. Waters, N. R., Abram, F., Brennan, F., Holmes, A. & Pritchard, L. Easy phylotyping of Escherichia coli via the EzClermont web app and command-line tool. *Access Microbiol* **2**, acmi000143 (2020).
86. Natural Earth - Free vector and raster map data at 1:10m, 1:50m, and 1:110m scales. https://www.naturalearthdata.com/.
87. Warringer, J. & Blomberg, A. Automated screening in environmental arrays allows analysis of quantitative phenotypic profiles in Saccharomyces cerevisiae. *Yeast* **20**, 53–67 (2003).
88. Hasenbrink, G. *et al.* Analysis of the mKir2.1 channel activity in potassium influx defective Saccharomyces cerevisiae strains determined as changes in growth characteristics. *FEBS Lett* **579**, 1723–1731 (2005).
89. Dunai, A. *et al.* Rapid decline of bacterial drug-resistance in an antibiotic-free environment through phenotypic reversion. *eLife* **8**, e47088 (2019).
90. Lenski, R. E. & Travisano, M. Dynamics of adaptation and diversification: a 10,000-generation experiment with bacterial populations. *Proc Natl Acad Sci U S A* **91**, 6808–6814 (1994).
91. Bhaumik, K. N. *et al.* Rationally designed foldameric adjuvants enhance antibiotic efficacy via promoting membrane hyperpolarization. *Mol. Syst. Des. Eng.* **7**, 21–33 (2022).
92. Reddy, S. & Austin, F. Adhesion and Invasion Assay Procedure Using Caco-2 Cells for Listeria monocytogenes. *Bio Protoc* **7**, e2267 (2017).
93. Franken, N. A. P., Rodermond, H. M., Stap, J., Haveman, J. & van Bree, C. Clonogenic assay of cells in vitro. *Nat Protoc* **1**, 2315–2319 (2006).
94. Velkov, T., Bergen, P. J., Lora-Tamayo, J., Landersdorfer, C. B. & Li, J. PK/PD models in antibacterial development. *Curr Opin Microbiol* **16**, 573–579 (2013).
95. Tan, C. M. *et al.* Restoring methicillin-resistant Staphylococcus aureus susceptibility to β-lactam antibiotics. *Sci Transl Med* **4**, 126ra35 (2012).
96. DeRyke, C. A., Banevicius, M. A., Fan, H. W. & Nicolau, D. P. Bactericidal activities of meropenem and ertapenem against extended-spectrum-beta-lactamase-producing Escherichia coli and Klebsiella pneumoniae in a neutropenic mouse thigh model. *Antimicrob Agents Chemother* **51**, 1481–1486 (2007).
97. Scangarella-Oman, N. E. *et al.* Microbiological Analysis from a Phase 2 Randomized Study in Adults Evaluating Single Oral Doses of Gepotidacin in the Treatment of Uncomplicated Urogenital Gonorrhea Caused by Neisseria gonorrhoeae. *Antimicrob Agents Chemother* **62**, e01221-18 (2018).
98. Martin, J. K. *et al.* A Dual-Mechanism Antibiotic Kills Gram-Negative Bacteria and Avoids Drug Resistance. *Cell* **181**, 1518-1532.e14 (2020).
99. Dias, C. & Rauter, A. P. Membrane-targeting antibiotics: recent developments outside the peptide space. *Future Med Chem* **11**, 211–228 (2019).
100. Magiorakos, A.-P. *et al.* Multidrug-resistant, extensively drug-resistant and pandrug-resistant bacteria: an international expert proposal for interim standard definitions for acquired resistance. *Clin Microbiol Infect* **18**, 268–281 (2012).
101. Barrick, J. E. *et al.* Genome evolution and adaptation in a long-term experiment with Escherichia coli. *Nature* **461**, 1243–1247 (2009).

Acknowledgments:

The authors thank Adrienn Kobl for her help with the visual elements of Fig. 1. Fig 1. was created using BioRender, owning a full licence to publish.

Funding: This work was supported by:

The National Laboratory of Biotechnology Grant 2022-2.1.1-NL-2022-00008 (CP, BK, BP)
National Research Development and Innovation Office 'Élvonal' Programme KKP 126506 (CP)
National Research, Development and Innovation Office 'Élvonal' program KKP KH125616 (BP)
The National Laboratory for Health Security RRF-2.3.1-21-2022-00006 (BP)
The European Union's Horizon 2020 research and innovation programme under grant agreement no. 739593 (BK, BP, MM)
National Research, Development and Innovation Office grant FK-135245 (BK)
János Bolyai Research Fellowship from the Hungarian Academy of Sciences (BO/352/20) (BK)
New National Excellence Program of the Ministry of Human Capacities (UNKP-20-5-SZTE-654 and UNKP-21- 5-SZTE-579) (BK)
Proof of Concept grant of the Eötvös Loránd Research Network (ELKH-PoC-2022-034) (B K)
The New National Excellence Program of the Ministry for Culture and Innovation - ÚNKP-22-2-SZTE-220 (MSCz)
The National Academy of Scientist Education under the sponsorship of the Hungarian Ministry of Culture and Innovation (VI/1697-4/2022/FÁFIN) (MSCz, BDV)
The Janos Bolyai Research Fellowship from the Hungarian Academy of Sciences BO/779/20 (ZF)
The New National Excellence Program of the Ministry of Human Capacities Bolyai +, UNKP-22-5-SZTE-551 (ZF)
The National Research, Development and Innovation Office, Hungary (NKFIH) grant PD, grant number 131839 (EA)
The National Research, Development and Innovation Office, Hungary (NKFIH) grant FK-142312 (MM)
The National Research, Development and Innovation Office, Hungary (NKFIH) grant FK-131961 (SJ)
The New National Excellence Program of the Ministry of Human Capacities Bolyai +, ÚNKP-22-5-SZTE-578-Bolyai+ (SJ)
The Janos Bolyai Research Fellowship from the Hungarian Academy of Sciences bo_656_20 (SJ)
The Lister Institute for Preventative Medicine (SvH)
The National Research, Development, and Innovation Office (PharmaLab, RRF-2.3.1-21-2022-00015 and TKP-31-8/PALY-2021) (LH)
Grant no. TKP2021-EGA-28 by the Ministry of Innovation and Technology of Hungary from the National Research, Development and Innovation Fund, NKFIH K 123952, LP2018-15/2018, and ELKH 2001007 (AG, CGP, ZS)

Author contributions:

Conceptualization: LD, MSCz, PSz, ZF, BK, BP, CP
Methodology: LD, MSCz, PSz, ZF, DB, GG, SJ, AD, MSz, TSári, TStirling, BMV, EA, CC, MM, MZsE, GJ, SvH, EP, CGP, ZS, LP, LH, AG, BK, BP, CP
Software: GG, TStirling, BMV, EA, CC, MM, GJ, SvH, EP
Validation: LD, MSCz, PSz, ZF, DB, GG, SJ, AD, MSz, TSári, TStirling, BMV, EA, CC, MM, MZsE, GJ, SvH, EP, CGP, ZS, LP
Formal analysis: LD, MSCz, PSz, ZF, DB, EM, TV, LS, BDV, GG, SJ, AD, MSz, TStirling, BMV, EA, CC, MM, GJ, SvH, EP, CGP, ZS
Investigation: LD, MSCz, PSz, DB, EM, TV, LS, BDV, SJ, AD, MSz, CGP, ZS
Resources: AD, TSári, MZsE, LP, LH, AG, BK, BP, CP
Data Curation: LD, MSCz, PSz, ZF, GG, TStirling, BMV, EA, CC, MM, GJ, SvH, EP
Writing - Original Draft: LD, MSCz, PSz, ZF, DB, GG, SJ, AD, MSz, TStirling, BMV, EA, MM, CGP, ZS, BK, BP, CP
Writing - Review & Editing: LD, MSCz, PSz, ZF, AD, AG, BK, BP, CP
Visualization: LD, MSCz, PSz, ZF, GG, TStirling, BMV, EA, CC, MM
Supervision: LH, AG, BK, BP, CP
Project administration: AD, BK, BP, CP
Funding acquisition: BK, BP, CP

Competing interests:

Authors declare that they have no competing interests.

Data and materials availability:

All data are available in the main text or the supplementary information. Illumina reads and Nanopore contigs for this study have been deposited in the European Nucleotide Archive (ENA) at EMBL-EBI under accession number PRJEB63210 (https://www.ebi.ac.uk/ena/browser/view/PRJEB63210).

Supplementary Information

Supplementary Note